

QUANTUM PHASE TRANSITIONS IN MAGNETIC SYSTEMS:  
APPLICATION OF COUPLED CLUSTER METHOD

DISSERTATION

zur Erlangung des akademischen Grades

doctor rerum naturalium

(Dr. rer. nat. )

der Fakultät für Naturwissenschaften  
der Otto-von-Guericke-Universität Magdeburg

vorgelegt von

Diplomphysiker Rachid Darradi

Magdeburg, 27. Oktober 2008

QUANTUM PHASE TRANSITIONS IN MAGNETIC SYSTEMS:  
APPLICATION OF COUPLED CLUSTER METHOD

DISSERTATION

zur Erlangung des akademischen Grades

doctor rerum naturalium  
(Dr. rer. nat. )

genehmigt durch die Fakultät für Naturwissenschaften  
der Otto-von-Guericke-Universität Magdeburg

von **Diplomphysiker Rachid Darradi**

geboren am 25. November 1970  
in Khouribga (Marokko)

Gutachter: Prof. Dr. Johannes Richter  
PD Dr. Andreas Honecker

eingereicht am: 27.10.2008  
verteidigt am: 26.01.2009

## DEDICATION

*This work is dedicated to my family, who supported me with their love, care and prayers.*



## ACKNOWLEDGMENTS

First of all, I would like to express my deepest gratitude to my supervisor, Professor Johannes Richter for providing me an opportunity to work with him on number of interesting and challenging physical questions. His professional guidance, inspirational help, constructive criticism, and continuous support helped me to finish my work successfully. Really, without his guidance this work would not have been accomplished.

I would like to thank Dr. Damian Farnell and Dr. Sven Krüger for their timely help, valuable discussions and encouragement. I am also highly indebted to the Rechenzentrum of the University Magdeburg and in particular to Dr. Jörg Schulenburg for assistance in numerical calculations.

I am grateful to Professor Raymond Bishop for giving me the chance of an educational visit at the University of Manchester and due to this educational visit, I was able to develop new ideas for my research work.

I would like to acknowledge the University of Magdeburg for financial support and Germany Research Foundation (Deutsche Forschungsgemeinschaft) for financial support (No. Ri614/14-1, Ri615/12-1, and No. Ih13/7-1).

I would like to thank my colleagues Reimar Schmidt, Dr. Dirk Schmalfuß, Ronald Zinke and Moritz Härtel for their good cooperation, many stimulating coffee breaks, and useful discussions. Special thanks to our secretary Silvia Simon for all her patience with me.

Finally, I must give immense thanks to my parents, my sisters, my brothers, and of course my wife and my children for their love, and moral support.



# CONTENTS

<b>Dedication</b>	<b>iii</b>
<b>Acknowledgments</b>	<b>v</b>
<b>List of Figures</b>	<b>xi</b>
<b>List of Tables</b>	<b>xvii</b>
<b>1. Introduction</b>	<b>1</b>
<b>2. Many-Body Method: The coupled cluster method (CCM)</b>	<b>7</b>
2.1. The CCM ground-state formalism . . . . .	7
2.2. The CCM for quantum spin lattices . . . . .	9
2.2.1. Choice of CCM model state . . . . .	9
2.2.2. Commutation relations and the high-order general- $s$ CCM formalism . . . . .	10
2.2.3. Hierarchical approximation schemes . . . . .	11
2.2.4. The ket-state equations . . . . .	13
2.2.5. The bra-state equations . . . . .	14
2.3. The excited-state formalism . . . . .	15
2.4. Calculation of physical quantities using CCM . . . . .	17
2.4.1. Ground state energy and Sublattice magnetization . . . . .	17
2.4.2. Spin stiffness . . . . .	18
2.4.3. Generalized susceptibilities . . . . .	18
2.5. Extrapolation Schemes . . . . .	19
2.6. The CCM for the pure Heisenberg antiferromagnet on square and cubic lattice . . . . .	20
<b>3. Quantum phase transitions in 2D unfrustrated Heisenberg antiferromagnet - <math>J</math>-<math>J'</math> model</b>	<b>23</b>
3.1. Introduction . . . . .	23
3.2. The Model . . . . .	24
3.3. Influence of Ising-anisotropy . . . . .	25
3.3.1. Variational mean-field approach . . . . .	25
3.3.2. Coupled cluster method . . . . .	26
3.3.3. Exact diagonalization . . . . .	28
3.3.4. Phase diagram . . . . .	29

3.4.	Influence of the spin quantum number . . . . .	30
3.4.1.	Variational mean-field approach (MFA) . . . . .	30
3.4.2.	Coupled cluster method . . . . .	33
3.4.3.	Exact diagonalization . . . . .	36
3.4.4.	Phase diagram . . . . .	36
<b>4.</b>	<b>The quantum ground state phase diagram of the Shastry-Sutherland model</b>	<b>39</b>
4.1.	Model . . . . .	40
4.2.	The classical ground state . . . . .	40
4.3.	The quantum ground state . . . . .	41
4.4.	The plaquette valence bond order in the nonmagnetic phase . . . . .	47
4.5.	Conclusions . . . . .	47
<b>5.</b>	<b>Spin stiffness of quantum Heisenberg antiferromagnets</b>	<b>49</b>
5.1.	The square lattice . . . . .	51
5.2.	The triangular lattice . . . . .	52
5.3.	The cubic lattice . . . . .	54
<b>6.</b>	<b>Ground-state phases of the spin-1/2 <math>J_1</math>-<math>J_2</math> Heisenberg antiferromagnet on the square lattice</b>	<b>55</b>
6.1.	Introduction . . . . .	55
6.2.	Ground-state phase diagram . . . . .	58
6.2.1.	Ground-state energy . . . . .	58
6.2.2.	Magnetic order parameter . . . . .	59
6.2.3.	Spin stiffness . . . . .	60
6.3.	Order of the phase transition. Generalized susceptibilities . . . . .	61
6.4.	Conclusions . . . . .	69
<b>7.</b>	<b>The Quantum <math>J_1</math>-<math>J_2</math> Antiferromagnet on the Stacked Square Lattice</b>	<b>71</b>
7.1.	Introduction . . . . .	71
7.2.	Results and discussions . . . . .	72
7.3.	Conclusions . . . . .	74
<b>8.</b>	<b>The spin-1/2 and spin-1 quantum <math>J_1</math>-<math>J'_1</math>-<math>J_2</math> Heisenberg models on the square lattice</b>	<b>77</b>
8.1.	Introduction . . . . .	77
8.2.	The Model . . . . .	78
8.3.	Results and Discussion . . . . .	80
8.3.1.	Ground-state energy . . . . .	80
8.3.2.	Magnetic order parameter . . . . .	82
8.3.3.	Ground-state phase diagrams . . . . .	85
<b>9.</b>	<b>Effect of anisotropy on the ground-state magnetic ordering of the</b>	



---

<b>spin-1/2 and spin-1 frustrated <math>J_1</math>-<math>J_2</math> XXZ model on the square lattice</b>	<b>89</b>
9.1. Introduction . . . . .	89
9.2. The Model . . . . .	90
9.3. Results . . . . .	93
9.3.1. Ground-state energy . . . . .	93
9.3.2. Magnetic order parameter . . . . .	96
9.3.3. Ground-state phase diagrams . . . . .	100
9.4. Discussion and Conclusions . . . . .	102
<b>10. Summary and Outlook</b>	<b>105</b>
<b>Bibliography</b>	<b>109</b>



## LIST OF FIGURES

2.1. Illustration of fundamental configurations for square lattice antiferromagnet within the LSUB4 approximation. . . . .	13
3.1. Illustration of arrangement of bonds in the $J - J'$ model on the square lattice (Eq.(3.1)): $J$ – dashed lines; $J'$ – solid lines; A and B characterize the two sublattices of the classical Néel ground state. . . . .	24
3.2. Sublattice magnetization $M_s$ versus $J'$ obtained by CCM LSUB $n$ with $n = 2, 4, 6, 8$ for $\Delta = 1$ and its extrapolated values to $n \rightarrow \infty$ using two different extrapolation schemes, namely according to Eq. (2.43)(extrapol 1) and to Eq. (2.45) (extrapol 3). . . . .	27
3.3. Sublattice magnetization $M_s$ versus $J'$ for $\Delta = 2$ using coupled cluster method (CCM), see Chap.2. . . . .	27
3.4. Order parameter versus $J'$ for $\Delta = 2$ using exact diagonalization of finite lattices of different sizes $N$ , see text. . . . .	28
3.5. The critical points $J'_c$ versus anisotropy parameter $\Delta$ using mean-field approach (MFA), CCM with extrapolation of the order parameter (CCM I), CCM with extrapolation of the inflection points (CCM II) and exact diagonalization (ED). . . . .	29
3.6. Sublattice magnetization $M/s$ versus $J'$ calculated by the variational mean-field like approach (MFA), see text. . . . .	32
3.7. Sublattice magnetization $M/s$ versus $J'$ for spin quantum number $s = 1$ using coupled cluster method (CCM) . . . . .	34
3.8. Extrapolated sublattice magnetization $M/s$ versus $J'$ for various spin quantum numbers $s$ using coupled cluster method (CCM) . . . . .	35
3.9. Sublattice magnetization $M/s$ versus $J'$ for spin quantum number $s = 1$ using exact diagonalization of finite lattices of $N = 8, 10, 16$ , see text. . . . .	36
3.10. The critical value $J'_c$ versus spin quantum number $s$ obtained by different methods. MFA: variational mean-field approach (see Sec. 3.4.1); CCM I: coupled cluster method (extrapolation of the order parameter, see Sec. 3.3.2); CCM II: coupled cluster method (extrapolation of the inflection point, see Sec. 3.3.2); ED: exact diagonalization (see Sec. 3.4.3). . . . .	37
4.1. Lattice structure of the $\text{Cu}^{2+}$ spins closed circle of $\text{SrCu}(\text{BO}_3)_2$ . The dashed and solid lines represent the nearest-neighbor bonds $J_1$ and next-nearest-neighbor bonds $J_2$ respectively. . . . .	39

4.2.	Illustration of the Shastry-Sutherland model on the square lattice (Eq. (4.1)). The antiferromagnetic NN bonds $J_1 = 1$ and NNN bonds $J_2$ are represented by solid and dashed lines. . . . .	40
4.3.	Illustration of the Shastry-Sutherland model with antiferromagnetic NN bonds $J_1 = 1$ (solid lines) and NNN bonds $J_2$ (dashed lines), together with its classical spiral state. The spin orientations at lattice sites $n$ are given by the angles $\theta = n\phi_{cl}$ , where $n = 0, 1, 2, \dots$ , and $\phi_{cl}$ is the characteristic pitch angle of the classical spiral state. The state is shown for $\phi_{cl} = 5\pi/6$ and $n = 0, 1, \dots, 5$ . . . . .	42
4.4.	Ground-state energy versus the pitch angle $\phi$ within CCM-LSUB4 approximation for different values of $J_2$ in the range $1.55 \leq J_2 \leq 1.59$ . . .	44
4.5.	The “quantum” pitch angle $\phi_{qu}$ as a function of $J_2$ calculated within CCM-LSUB $n$ approximation with $n = 2, 4, 6$ . . . . .	45
4.6.	The energy of (i) the collinear quantum ground state as function of $J_2$ obtained by CCM-LSUB $n$ with $n = 4, 6, 8$ and its extrapolated value to $n \rightarrow \infty$ , see Eq. (2.42), and (ii) of the orthogonal-dimer state. . . . .	45
4.7.	Sublattice magnetization $M$ versus $J_2$ obtained by CCM-LSUB $n$ with $n = 4, 6, 8$ and its extrapolated values to $n \rightarrow \infty$ using two different extrapolation schemes, namely according to Eq. (2.43) (extrapol 1), Eq. (2.44) (extrapol 2) and Eq. (2.45) (extrapol 3) . . . . .	46
4.8.	the inverse susceptibility $1/\chi_p$ versus $J_2$ obtained within the CCM LSUB $n$ approximation with $n = 4, 6, 8$ and extrapolated to $n \rightarrow \infty$ using Eq. (2.43). Inset: Pattern of plaquette valence bond order. . . . .	48
5.1.	Illustration of the twisted Néel state (a: square lattice; b: triangular lattice). The twist is introduced along rows in $x$ direction. The angles at the lattice sites indicated the twist of the spins with respect to the corresponding Néel state. . . . .	50
5.2.	Extrapolation of the CCM-LSUB $n$ results for the stiffness. The points represent the CCM-LUB $n$ results and the lines correspond to the function (2.43) fitted to this data points. . . . .	51
6.1.	(a) $J_1$ - $J_2$ model; — $J_1$ ; - - $J_2$ ; (b) Néel state, (c) stripe state - columnar and (d) stripe state - row. Arrows in (b), (c) and (d) represent spins situated on the sites of the square lattice (indicated by $\bullet$ in (a)). . . . .	56
6.2.	Illustration of the twisted reference states used for the calculation of the spin stiffness $\rho_s$ . The angles at the lattice sites indicate the twist of the spins with respect to the Néel or the collinear state. (a): Twisted Néel state, the twist is introduced along rows in $x$ direction. (b): Twisted collinear state, the twist is introduced along rows in $\vec{e}_x + \vec{e}_y$ direction. . .	57

6.3.	The GS energy per spin as function of $J_2$ obtained by CCM-LSUB $n$ with $n = 4, 6, 8, 10$ and its extrapolated values to $n \rightarrow \infty$ using the extrapolation scheme of Eq. (2.42). ED results for $N = 32$ are shown by circles. . . . .	58
6.4.	Magnetic order parameter $M$ versus $J_2$ obtained by CCM-LSUB $n$ with $n = 4, 6, 8, 10$ and its extrapolated values to $n \rightarrow \infty$ using the extrapolation scheme of Eq. (2.45). . . . .	59
6.5.	The spin stiffness $\rho_s$ versus $J_2$ obtained by CCM-LSUB $n$ with $n = 4, 6, 8$ and its extrapolated values to $n \rightarrow \infty$ using the extrapolation scheme $\rho_s(n) = c_0 + c_1(1/n) + c_2(1/n)^2$ . . . . .	60
6.6.	(Color online) Illustration of perturbations (fields) $F_j$ related to generalized susceptibilities $\chi_j$ : (a) perturbation $F_1$ (6.2), (b) perturbation $F_2$ (6.3), (c) perturbation $F_3$ (6.4), (d) perturbation $F_4$ (6.5). Dark (red) [light (green)] shadows correspond to enforced [weakened] exchange couplings. . . . .	62
6.7.	The GS energy $e(\delta) - e(0)$ versus square of field strength $\delta$ for $H + \delta \hat{O}_1$ , see Eq. (6.2), for $J_2 = 0.0, 0.1, 0.2, 0.3, 0.4, 0.45$ (from top to bottom). (a): CCM results extrapolated to $n \rightarrow \infty$ using the extrapolation scheme $e(n) = a_0 + a_1(1/n)^2 + a_2(1/n)^4$ . (b): ED results for $N = 32$ . The displayed curves might be compared to the ones in Fig. 1 of Ref. [47] where corresponding series-expansion data for $e(\delta)$ are reported (however, only up to $J_2 = 0.3$ ). . . . .	64
6.8.	The coefficient $b$ of the quartic term in Eq. (6.6) obtained from a fit of the CCM data in Fig. 6.7a and the ED data in Fig. 6.7b in dependence on $J_2$ . This figure might be compared to Fig. 3 of Ref. [47]. Inset: The coefficient $b$ versus $J_2$ shown for small $J_2$ with an enlarged scale. . . . .	65
6.9.	The inverse susceptibilities (a) $1/\chi_1$ , (b) $1/\chi_2$ , (c) $1/\chi_3$ (please note the scaling factor 0.01 at the $y$ -axis), and (d) $1/\chi_4$ versus $J_2$ obtained within the CCM LSUB $n$ approximation with $n = 4, 6, 8$ and extrapolated to $n \rightarrow \infty$ using $\chi(n) = c_0 + c_1(1/n) + c_2(1/n)^2$ . . . . .	66
6.10.	The inverse susceptibilities (a) $1/\chi_1$ , (b) $1/\chi_2$ , (c) $1/\chi_3$ (please note the scaling factor 0.01 at the $y$ -axis), and (d) $1/\chi_4$ versus $J_2$ obtained within the CCM LSUB $n$ approximation with $n = 4, 6, 8$ and extrapolated to $n \rightarrow \infty$ using $\chi(n) = c_0 + c_1(1/n) + c_2(1/n)^2$ Insets: The same as in the main panels but using ED for finite lattice of $N = 16, 24, 32$ . Panel (a) might be compared to Fig. 2 of Ref. [47] and Fig. 3 of Ref. [49], panel (b) might be compared to Fig. 5 of Ref. [47], panel (c) might be compared to Fig. 6 of Ref. [47] and Fig. 3 of Ref. [50]. . . . .	67
6.11.	Susceptibilities $1/\chi_1$ (red) and $1/\chi_4$ (gray) around the critical point $J_2^{c1}$ . Bold curves correspond to the CCM curves shown in Fig. 6.10a and Fig. 6.10d. Thin lines obtained from a linear fit of the CCM data for $0 \leq J_2 \leq J_2^{c1}$ . Extrapolated (thin) lines for both inverse susceptibilities become zero at $J_2 \approx 0.47$ . . . . .	68

7.1.	Illustration of arrangement of bonds in the $J_1$ - $J_2$ model on the Stacked Square Lattice (Eq.(7.1)). . . . .	72
7.2.	The magnetic order parameter $m$ versus $J_2$ for various strengths of the interlayer coupling $J_\perp$ (with $J_1 = 1$ ). . . . .	73
7.3.	The ground-state phase diagram (where the solid lines show those values of $J_2$ for which the order parameters vanish and the dashed line represents those values of $J_2$ where the two energies calculated for the Néel and collinear reference states). Note that $J_1 = 1$ . . . . .	74
7.4.	CCM results for the energy per spin $e$ for both reference states (inset) and the order parameter $M$ for $J_\perp = 0.2$ . Both quantities are obtained by extrapolation of the 'raw' LSUB $n$ results to the limit $n \rightarrow \infty$ as explained in the text. The energies calculated with the Néel and collinear reference states become equal at $J_2 \approx 0.58$ indicating a first-order transition. For the order parameter $M$ , we take that value calculated with the reference state of lower CCM energy. . . . .	74
8.1.	(a) $J_1$ - $J'_1$ - $J_2$ model; — $J_1$ ; - - $J'_1$ ; · - · $J_2$ ; (b) Néel state, (c) stripe state - columnar and (d) stripe state - row. Arrows in (b), (c) and (d) represent spins situated on the sites of the square lattice (indicated by • in (a)). . . . .	78
8.2.	Extrapolated CCM LSUB $n$ results for the gs energy per spin, $E/N$ , for $J'_1 = 0.2, 0.4, 0.6, 0.8, 1.0$ , using the Néel and stripe states of the $s = 1/2$ $J_1$ - $J'_1$ - $J_2$ model. The LSUB $n$ results are extrapolated(according to Eq. (2.43)) in the limit $n \rightarrow \infty$ using the set $n = \{4, 6, 8, 10\}$ . The NN exchange coupling $J_1 = 1$ . . . . .	81
8.3.	Extrapolated CCM SUB $n$ - $n$ results for the gs energy per spin, $E/N$ , of the $s = 1$ $J_1$ - $J'_1$ - $J_2$ model, for $J'_1 = 0.2, 0.4, 0.6, 0.7, 0.8, 0.9, 1.0$ . The SUB $n$ - $n$ results are extrapolated(according to Eq. (2.43)) in the limit $n \rightarrow \infty$ using the set $n = \{2, 4, 6, 8\}$ . . . . .	82
8.4.	Extrapolated CCM LSUB $n$ results for the gs staggered magnetization, $M$ , for $J'_1 = 0.6, 0.65, 0.7$ for the Néel state of the $s = 1/2$ $J_1$ - $J'_1$ - $J_2$ model. (a) Results using Eq. (2.44), (b) Results using Eq. (2.45). The LSUB $n$ results are extrapolated in the limit $n \rightarrow \infty$ using the set $n = \{4, 6, 8, 10\}$ . The NN exchange coupling $J_1 = 1$ . . . . .	83
8.5.	The extrapolated CCM LSUB $n$ results for the staggered magnetization, $M$ , for $J'_1 = 0.2, 0.4, 0.6, 0.8, 1.0$ of the $s = 1/2$ $J_1$ - $J'_1$ - $J_2$ model. The LSUB $n$ results are extrapolated(according to Eq. (2.45)) in the limit $n \rightarrow \infty$ using the set $n = \{4, 6, 8, 10\}$ . The NN exchange coupling $J_1 = 1$ . . . . .	84
8.6.	Extrapolated CCM SUB $n$ - $n$ results for the gs staggered magnetisation, $M$ , of the $s = 1$ $J_1$ - $J'_1$ - $J_2$ model, for $J'_1 = 0.2, 0.4, 0.6, 0.7, 0.8, 0.9, 1.0$ . The SUB $n$ - $n$ results are extrapolated(according to Eq. (2.45)) in the limit $n \rightarrow \infty$ using the set $n = \{2, 4, 6, 8\}$ . . . . .	84

8.7.	The extrapolated CCM LSUB $n$ results for the gs phase diagram of the $s = 1/2$ $J_1$ - $J'_1$ - $J_2$ model. The LSUB $n$ results are extrapolated in the limit $n \rightarrow \infty$ using the set $n = \{4, 6, 8, 10\}$ . The NN exchange coupling $J_1 = 1$ . QTP $\equiv$ quantum triple point. . . . .	86
8.8.	Extrapolated CCM SUB $n$ - $n$ results for the gs staggered magnetisation, $M$ , of the spin-1 $J_1$ - $J'_1$ - $J_2$ model, for $J'_1 = 0.2, 0.4, 0.6, 0.7, 0.8, 0.9, 1.0$ . The SUB $n$ - $n$ results are extrapolated in the limit $n \rightarrow \infty$ using the set $n = \{2, 4, 6, 8\}$ . . . . .	87
9.1.	(a) The $J_1$ - $J_2$ XXZ Heisenberg model; — $J_1$ ; - - - $J_2$ ; (b) and (c) $z$ -aligned states for the Néel and stripe columnar phases respectively; (d) and (e) planar $x$ -aligned states for the Néel and stripe columnar phases respectively. Arrows in (b), (c), (d) and (e) represent spins situated on the sites of the square lattice [symbolized by $\bullet$ in (a)]. . . . .	90
9.2.	Extrapolated CCM LSUB $n$ results using (a) the $z$ -aligned and (b) planar $x$ -aligned states for the gs energy per spin, $E/N$ , for the Néel and stripe phases of the $s = 1/2$ $J_1^{XXZ}$ - $J_2^{XXZ}$ model. The LSUB $n$ results are extrapolated in the limit $n \rightarrow \infty$ using the sets $n = \{4, 6, 8, 10\}$ for both the $z$ -aligned states and the planar $x$ -aligned states. The NN exchange coupling $J_1 = 1$ . The meaning of the $E_{\max}$ points shown is described in the text. . . . .	94
9.3.	Extrapolated CCM SUB $n$ - $n$ results using (a) the $z$ -aligned and (b) planar $x$ -aligned states for the gs energy, $E/N$ , for the Néel and stripe phases of the $s = 1$ $J_1^{XXZ}$ - $J_2^{XXZ}$ model. The SUB $n$ - $n$ results are extrapolated to the limit $n \rightarrow \infty$ using the sets $n = \{2, 4, 6, 8\}$ for both the $z$ -aligned and planar $x$ -aligned states. . . . .	95
9.4.	Extrapolated CCM LSUB $n$ results using (a) the $z$ -aligned and (b) planar $x$ -aligned states for the gs staggered magnetization, $M$ , for the Néel and stripe phases of the $s = 1/2$ $J_1^{XXZ}$ - $J_2^{XXZ}$ model. The LSUB $n$ results are extrapolated in the limit $n \rightarrow \infty$ using the sets $n = \{4, 6, 8, 10\}$ for both the $z$ -aligned states and planar $x$ -aligned states. The NN exchange coupling $J_1 = 1$ . . . . .	97
9.5.	Extrapolated CCM LSUB $n$ results using the $z$ -aligned and planar $x$ -aligned states for the staggered magnetization versus the anisotropy $\Delta$ for the $s = 1/2$ $J_1^{XXZ}$ - $J_2^{XXZ}$ model, for the NN exchange coupling $J_1 = 1$ . The LSUB $n$ results are extrapolated in the limit $n \rightarrow \infty$ using the sets $n = \{4, 6, 8, 10\}$ for both the $z$ -aligned model states and the planar $x$ -aligned model states. . . . .	98
9.6.	Extrapolated CCM SUB $n$ - $n$ results using (a) the $z$ -aligned and (b) planar $x$ -aligned states for the gs staggered magnetization, $M$ , for the Néel and stripe phases of the spin-1 $J_1^{XXZ}$ - $J_2^{XXZ}$ model. The SUB $n$ - $n$ results are extrapolated to the limit $n \rightarrow \infty$ using the sets $n = \{2, 4, 6, 8\}$ for the $z$ -aligned states. . . . .	99

- 9.7. Extrapolated CCM LSUB $n$  results using the  $z$ -aligned and planar  $x$ -aligned states for the ground-state phase diagram of the spin-1/2  $J_1^{XXZ}$ - $J_2^{XXZ}$  model, for the NN exchange coupling  $J_1 = 1$ . The LSUB $n$  results for the staggered magnetization are extrapolated to the limit  $n \rightarrow \infty$  using the sets  $n = \{4, 6, 8, 10\}$  for both the  $z$ -aligned model states and the planar  $x$ -aligned model states.  $M_c \equiv$  magnetization critical point, defined in the text. . . . . 100
- 9.8. Extrapolated CCM SUB $n$ - $n$  results using the  $z$ -aligned and planar  $x$ -aligned states for the ground-state phase diagram of the spin-1  $J_1^{XXZ}$ - $J_2^{XXZ}$  anisotropic Heisenberg model on the square lattice, for the NN exchange coupling  $J_1 = 1$ . The SUB $n$ - $n$  results for the energy per spin and the staggered magnetization are extrapolated to the limit  $n \rightarrow \infty$  using the sets  $n = \{2, 4, 6, 8\}$  for both the  $z$ -aligned and planar  $x$ -aligned model states.  $M_c \equiv$  magnetization critical point, defined in the text.  $E_{\text{meet}}$  denotes the crossing point of the CCM energy curves for the same value of  $\Delta$  based on the Néel-ordered and collinear stripe-ordered model states. . . . . 101



## LIST OF TABLES

2.1.	Data for the spin-1/2 square-lattice pure HAFM. $N_f$ is the number of fundamental configurations for the Néel reference state, $E/N$ is the GS energy per spin and $m$ is the sublattice magnetization. The LSUB $n$ results are extrapolated using Eq. (2.42) for $E/N$ and Eq. (2.43) for $m$ .	20
2.2.	Data for the spin-1/2 simple-cubic lattice pure HAFM. $N_f$ is the number of fundamental configurations for the Néel reference state, $E/N$ is the GS energy per spin and $m$ is the sublattice magnetization. The LSUB $n$ results are extrapolated using Eq. (2.42) for $E/N$ and Eq. (2.43) for $m$ .	21
3.1.	CCM results for the ground state of the Heisenberg antiferromagnet on the square lattice with spin quantum number $s = 3/2$ and $s = 2$ using the SUB $n$ - $n$ approximation with $n = \{2, 4, 6\}$ . Note that $N_F$ indicates the number of fundamental clusters at each level of approximation. For comparison we present the results of the second-order spin wave theory (SWT) [131]. . . . .	34
4.1.	Number of fundamental GS configurations of the LSUB $n$ approximation for the Shastry-Sutherland model using the Néel state ( $\phi = 0$ ) and the spiral state ( $\phi \neq 0$ ) as the CCM reference state. . . . .	43
5.1.	Spin stiffness $\rho_s$ for the spin-1/2 HAFM on the square lattice calculated by various CCM-LSUB $n$ approximations and the result of the $n \rightarrow \infty$ extrapolation using LSUB $n$ with $n = 4, 6, 8$ . . . . .	52
5.2.	Collection of data for the spin stiffness $\rho_s$ for the spin-1/2 HAFM on the square lattice calculated by different methods. . . . .	52
5.3.	In-plane spin stiffness $\rho_s$ for the spin-1/2 HAFM on the triangular lattice calculated by various CCM-LSUB $n$ approximations and the result of the $n \rightarrow \infty$ extrapolation using LSUB $n$ with $n = 2, 3, 4, 5, 6, 7$ . . . . .	53
5.4.	Collection of data for the spin stiffness $\rho_s$ for the spin-1/2 HAFM on the triangular lattice calculated by different methods. . . . .	53
5.5.	Spin stiffness $\rho_s$ for the spin-1/2 HAFM on the cubic lattice calculated by various CCM-LSUB $n$ approximations and the result of the $n \rightarrow \infty$ extrapolation using LSUB $n$ with $n = 2, 4, 6$ . . . . .	54
8.1.	Numbers of fundamental configurations ( $N_f$ ) for $s = 1/2$ and $s = 1$ in various CCM approximations. . . . .	80

- 9.1. Numbers of fundamental configurations ( $N_f$ ) for spin-1/2 and spin-1 in various CCM approximations for the  $z$ -aligned states of the spin-1/2 and spin-1  $J_1^{XXZ}-J_2^{XXZ}$  model on the square lattice. . . . . 92
- 9.2. Numbers of fundamental configurations ( $N_f$ ) for spin-1/2 and spin-1 in various CCM approximations for the planar  $x$ -aligned states of the spin-1/2 and spin-1  $J_1^{XXZ}-J_2^{XXZ}$  model on the square lattice. . . . . 92

## CHAPTER 1

# INTRODUCTION

The study of quantum magnetism has attracted much experimental and theoretical attention over many years, for an overview, see Ref. [1]. In particular, quantum phase transitions (or zero-temperature transitions) are one of the most active fields in condensed matter physics [2, 3] because of the discovery of high temperature superconductivity in  $\text{La}_{2-x}\text{Sr}_x\text{CuO}_4$  and  $\text{YBa}_2\text{Cu}_3\text{O}_{7-x}$  [4, 5]. The pure materials are antiferromagnets and are not superconducting. The phase diagram of these materials shows that by increasing the concentration by doping, the materials can be driven from insulating to metallic behavior. While high-temperature superconductivity has raised the question of the link between the mechanism of superconductivity in the cuprates, for example, and spin fluctuations and magnetic order in one-dimensional (1D) and two-dimensional (2D) spin-half antiferromagnets, the new magnetic materials exhibit a wealth of new quantum phenomena of enormous interest in their own right.

For example, in 1D systems, the universal paradigm of Tomonaga-Luttinger liquid [6, 7] behavior has occupied a key position of interest, since Fermi liquid theory breaks down in 1D. More generally, in *all* restricted geometries the interplay between reduced dimensionality, competing interactions and strong quantum fluctuations, generates a plethora of new states of condensed matter beyond the usual states of quasiclassical long-range order (LRO). For the zero-temperature transitions thermal fluctuations are irrelevant and the transition between different quantum phases (e.g. between magnetically ordered and disordered phases) is driven purely by quantum fluctuations.

The basic model which shows strong quantum fluctuations in the antiferromagnetic case is the spin-half Heisenberg model, particularly in low dimensions. According the Mermin-Wagner theorem [8], we know that thermal fluctuations are strong enough to destroy magnetic long-range order (LRO) at any finite temperature for Heisenberg spin systems in one and two dimensions, the role of quantum fluctuations is less understood. It is now well-established that the ground-state of the Heisenberg antiferromagnet in one-dimensional does not have Néel LRO [1, 9], whereas, the pure Heisenberg antiferromagnet in two-dimensional (2d) and three-dimensional (3d) model counterparts on the square or cubic lattice, respectively, is long-range ordered (e.g., see the reviews [4, 10]). For the Heisenberg antiferromagnet (HAFM) on two-dimensional lattices the interplay of interactions and fluctuations is well balanced and the existence of semi-classical magnetic long-range order depends on the degree of competition between bonds [1, 11]. Competition between bonds in spin systems may appear in various ways. As frustration, which is present in classical as well as in quantum spin systems.

In quantum systems a direct competition between bonds also exists which may lead to local singlet formation on certain antiferromagnetic bonds (or plaquettes of four spins) if these bonds are increased in strength. By tuning the degree of competition zero-temperature order-disorder phase transitions can be realized. In contrast to frustration, which yields competition in quantum as well as in classical systems, this type of competition is present only in quantum systems.

Recent experiments on  $\text{SrCu}_2(\text{BO}_3)_2$  [12,13] and on  $\text{CaV}_4\text{O}_9$  [14,15] demonstrate the existence of gapped quantum paramagnetic ground states in (quasi-)two-dimensional Heisenberg systems, and have stimulated various theoretical studies of quantum spin lattices with competing interactions.

An example for competition without frustration is the 'melting' of semi-classical Néel order by local singlet formation in Heisenberg systems with two non-equivalent nearest-neighbor bonds like the bilayer antiferromagnet [16,17], the  $J - J'$  antiferromagnet on the square lattice [18–20] and on the depleted square (CaVO) lattice [13,21]. In the above mentioned papers [13,16–19,21] the strength of quantum fluctuations is tuned by variation of the exchange bonds  $J'$ . Alternatively, the strength of quantum fluctuations can be tuned by the anisotropy  $\Delta$  and the spin quantum number  $s$  in an XXZ model.

In the classical HAFM the geometrical frustration often leads to canted spin states which may or may not have counterparts in quantum HAFM. Such frustrated quantum magnets often have ground states that are macroscopically degenerate. This feature leads naturally to an increased sensitivity of the underlying Hamiltonian to the presence of small perturbations. The interplay between frustration and quantum fluctuations in magnetic systems may lead to unusual quantum phases [1]. A canonical model to study these effects is the frustrated spin-1/2  $J_1$ - $J_2$  antiferromagnet on the square lattice ( $J_1$ - $J_2$  model). This model has attracted a great deal of interest, see, e.g., Reefs. [22–52]. The recent discovery of several other quasi-2D materials that are realizations of the  $J_1$ - $J_2$  model, has only served to extend the theoretical interest in the model. Some of the actual magnetic compounds that can be well described by the  $s = \frac{1}{2}$   $J_1$ - $J_2$  model are  $\text{La}_2\text{CuO}_4$  [53] for small values of  $J_2/J_1$ , and  $\text{Li}_2\text{VOSiO}_4$  and  $\text{Li}_2\text{VOGeO}_4$  [54,55] for large values of  $J_2/J_1$ . Other such materials include the compounds  $\text{VOMoO}_4$  [56] and  $\text{Pb}_2\text{VO}(\text{PO}_4)_2$  [57]. The compound  $\text{VOMoO}_4$  is interesting because its exchange couplings appear to be more than an order of magnitude larger than those of  $\text{Li}_2\text{VOSiO}_4$ , even though the structures of the two compounds are closely related. Similarly, the compound  $\text{Pb}_2\text{VO}(\text{PO}_4)_2$  also has a structure closely related to that of  $\text{Li}_2\text{VOSiO}_4$ , but it appears to have a ferromagnetic NN exchange coupling ( $J_1 < 0$ ) frustrated by an antiferromagnetic NNN exchange coupling ( $J_2 > 0$ ), with  $|J_2/J_1| \approx 1.5$ . By contrast, although all of the other compounds mentioned above are also examples of quasi-2D frustrated spin-1/2 magnets, they have NN and NNN exchanges that are both antiferromagnetic.

For the past few decades, a great deal of attention has also been devoted to magnetic materials with spin-1 ions, such as the linear chain systems including  $\text{CsNiCl}_3$  [58] with a weak axial anisotropy,  $\text{CsFeBr}_3$  [59] with a strong planar anisotropy and the complex

materials NENP ( $\text{Ni}(\text{C}_2\text{H}_8\text{N}_2)_2\text{NO}_2(\text{ClO}_4)$ ) [60] with a weak planar anisotropy and NENC ( $\text{Ni}(\text{C}_2\text{H}_8\text{N}_2)_2\text{Ni}(\text{CN}_4)$ ) [61] with a strong planar anisotropy; as well as the 2D Heisenberg antiferromagnet  $\text{K}_2\text{NiF}_4$  [62]. The spin gaps observed in  $\text{CsNiCl}_3$  and NENP are believed to be examples of the integer-spin gap behaviour predicted by Haldane [63, 64]; whereas half-odd-integer spin systems are gapless. Another new spin-gapped material is the 2D triangular lattice antiferromagnet  $\text{NiGa}_2\text{S}_4$  [65] which, it has been argued [66, 67], may be a “spin nematic” [68]. It is clear, therefore, that the theoretical study of 2D spin-1 quantum magnets is worthy of pursuit.

In this context we note the recent discovery of superconductivity with a transition temperature at  $T_c \approx 26$  K in the layered iron-based compound  $\text{LaOFeAs}$ , when doped by partial substitution of the oxygen atoms by fluorine atoms [69],  $\text{La}[\text{O}_{1-x}\text{F}_x]\text{FeAs}$ , with  $x \approx 0.05\text{--}0.11$ . This has been followed by the rapid discovery of superconductivity at even higher values of  $T_c$  ( $\gtrsim 50$  K) in a broad class of similar doped quaternary oxypnictide compounds. Enormous interest has thereby been engendered in this class of materials. Of particular relevance to the present work are the very recent first-principles calculations [70] showing that the undoped parent precursor material  $\text{LaOFeAs}$  is well described by the spin-1  $J_1\text{--}J_2$  model on the square lattice with  $J_1 > 0$ ,  $J_2 > 0$ , and  $J_2/J_1 \approx 2$ . Broadly similar conclusions have also been reached by other authors [71].

There has also been considerable discussion in recent years as to whether the quantum phase transition between the quasiclassical Néel phase and the magnetically disordered (intermediate paramagnetic) phase in the spin-1/2  $J_1\text{--}J_2$  model on the 2D square lattice is first-order or of continuous second-order type. A particularly intriguing suggestion by Senthil *et al.* [72, 73] is that there is a second-order phase transition in the model between the Néel state and the intermediate disordered state (which these authors argue is a VBS state), which is not described by a Ginzburg-Landau-type critical theory, but is rather described in terms of a deconfined quantum critical point. Such direct second-order quantum phase transitions between two states with different broken symmetries, and which are hence characterized by two seemingly independent order parameters, are difficult to understand within the standard critical theory approach of Ginzburg and Landau, as we indicate below.

Thus, the competition between two such distinct kinds of quantum order associated with different broken symmetries would lead generically in the Ginzburg-Landau scenario to one of only three possibilities: (i) a first-order transition between the two states, (ii) an intermediate region of co-existence between both phases with both kinds of order present, or (iii) a region of intermediate phase with neither of the orders of these two phases present. A direct second-order transition between states of different broken symmetries is only permissible within the standard Ginzburg-Landau critical theory if it arises by an accidental fine-tuning of the disparate order parameters to a multicritical point. Thus, for the spin-1/2  $J_1\text{--}J_2$  model on the 2D square lattice and its quantum phase transition suggested by Senthil *et al.*, [72, 73] it would require the completely accidental coincidence (or near coincidence) of the point where the magnetic order parameter (i.e., the staggered magnetization) vanishes for the Néel phase

with the point where the dimer order parameter vanishes for the VBS phase. Since each of these phases has a different broken symmetry (viz., spin-rotation symmetry for the Néel phase and the lattice symmetry for the VBS phase), one would naively expect that each transition is described by its own independent order parameter (i.e., the staggered magnetization for the Néel phase and the dimer order parameter for the VBS phase) and that the two transitions should hence be mutually independent.

By contrast, the “deconfined” type of quantum phase transition postulated by Senthil *et al.* [72, 73] permits direct second-order quantum phase transitions between such states with different forms of broken symmetry. In their scenario the quantum critical points still separate phases characterized by order parameters of the conventional (i.e., in their language, “confining”) kind, but their proposed new critical theory involves fractional degrees of freedom (viz., spinons for the spin-1/2  $J_1$ - $J_2$  model on the 2D square lattice) that interact via an emergent gauge field. For our specific example the order parameters of both the Néel and VBS phases discussed above are represented in terms of the spinons, which themselves become “deconfined” exactly at the critical point. The postulate that the spinons are the fundamental constituents of both order parameters then affords a natural explanation for the direct second-order phase transition between two states of the system that otherwise seem very different on the basis of their broken symmetries.

We note, however, that the deconfined phase transition theory of Senthil *et al.* [72, 73] is still the subject of controversy. Other authors believe that the phase transition in the spin-1/2  $J_1$ - $J_2$  model on the 2D square lattice from the Néel phase to the intermediate magnetically-disordered phase need not be due to a deconfinement of spinons. For example, Sirker *et al.* [47] have argued on the basis of both spin-wave theory and numerical results from series expansion analyses, that this transition is more likely to be a (weakly) first-order transition between the Néel phase and a VBS phase with columnar dimerization. Other authors have also proposed other, perhaps less radical, mechanisms to explain such second-order phase transitions (if they exist) and their seeming disagreement (except by accidental fine tuning) with Ginzburg-Landau theory. What seems clearly to be a minimal requirement is that the order parameters of the two phases with different broken symmetry should be related in some way. Thus, a Ginzburg-Landau-type theory can only be preserved if it contains additional terms in the effective theory that represent interactions between the two order parameters. For example, just such an effective theory has been proposed for the 2D spin-1/2  $J_1$ - $J_2$  model on the square lattice by Sushkov *et al.*, [50] and further discussed by Sirker *et al.* [47].

Another example model of a frustrated HAFM is the Shastry-Sutherland [74] type models used in understanding the physical properties of  $\text{SrCu}(\text{BO}_3)_2$  [14, 75] (see e.g., Chap. 4: Fig. 4.1). This system is a magnetic insulator with dimer singlet phase, which realized due to the strong antiferromagnetic couplings for dimer bonds. In the classical limit ( $S \rightarrow \infty$ ), the ground state is the Néel ordered if  $J_1/J_2 \geq 1$  and is helically ordered (see e.g., Chap. 4: Fig. 4.3) otherwise. Recently, new interesting results on the magnetization process of  $\text{SrCu}(\text{BO}_3)_2$  have been observed. In particular, the plateaus

at  $1/5$ ,  $1/6$ ,  $1/7$ ,  $1/9$ , and  $2/9$  of the saturated magnetization have been reported [76], in addition to the previously established plateaus at  $1/3$ ,  $1/4$ , and  $1/8$  [14].

The theoretical treatment of the frustrated quantum antiferromagnets is far from being trivial. Though, surprisingly, one can find exact GS's of a simple product nature in some exceptional cases, [74, 77–79] many of the standard many-body methods, such as quantum Monte Carlo techniques, may fail or become computationally infeasible to implement if frustration is present. Other methods, such as density-matrix renormalization group (DMRG) is essentially restricted to low-dimensional systems, at least for the present. Hence, there is considerable interest in any method that can deal with frustrated spin systems in any number of dimensions, including magnetic systems with incommensurate spiral GS's. A method fulfilling this requirement is the coupled cluster method (CCM). This approach, introduced many years ago by Coester and Kümmel, [80, 81] is one of the most universal and most powerful methods of quantum many-body theory (and for a review of which see, e.g., Ref. [22]). The CCM has previously been applied to various quantum spin systems with much success. [18, 20, 42, 82–95] The application to frustrated spin systems was started in the 1990's, [86, 87] and has been developed in more recent years to the point where it has become a powerful tool in this field by including higher orders of approximations in a well-defined truncation scheme. [18, 20, 42, 90, 93, 94]. Note, that The CCM is also extended to models of strongly interacting electrons on lattices, such as the Hubbard model [96].

This thesis is organized as follows. In Chap. 2 we present a general description of the CCM methodology. The ket and bra state formalisms are given, and the form of the ground-state energy equation, along with the characteristic CCM similarity transform, is described. We also illustrate the CCM for quantum spin lattices. Finally, we report (as a benchmark test) high-order CCM results for standard unfrustrated lattices in  $d = 2, 3$  and compare them with other accurate methods. In Chap. 3 we study the Influence of Ising-anisotropy and the spin quantum number  $s$  on the zero-temperature phase transition in the square lattice spin- $1/2$   $J$ - $J'$  model. In Chap. 4 we report on a CCM treatment of the 2d Shastry-Sutherland model. In Chap. 5 we calculate the spin stiffness for the the spin- $\frac{1}{2}$  HAFM with nearest-neighbor interaction on the cubic, the square, and on the triangular lattices and compare our results with available data in the literature. In Chap. 6 we investigate GS phase diagram for spin-half  $J_1$ - $J_2$  model on the square lattice, we also discuss the nature of the phase transition between the semiclassical Néel phase and the quantum paramagnetic phase. In Chap. 7 contains a discussion of the GS ordering of a stacked frustrated square-lattice HAFM (the quasi-2d  $J_1$ - $J_2$  model). In Chap. 8 we study the phase diagram of the 2D  $J_1$ - $J'_1$ - $J_2$  spin- $1/2$  and spin-1 Heisenberg model. The effect of the coupling  $J'_1$  on the Néel and stripe states is investigated. Finally, in Chap. 9 we study the zero-temperature phase diagram of the 2D quantum spin- $1/2$  and spin-1 frustrated  $J_1$ - $J_2$  XXZ model on the square lattice. In particular, we examined the effects of the anisotropy  $\Delta$  on the  $z$ -aligned Néel and (collinear) stripe states, as well as on the  $xy$ -planar-aligned Néel and collinear stripe states.





## CHAPTER 2

# MANY-BODY METHOD: THE COUPLED CLUSTER METHOD (CCM)

### 2.1. THE CCM GROUND-STATE FORMALISM

In this section , we firstly describe the general ground-state CCM formalism [80,81,97], and then we apply it to the different models. The exact ket and bra ground-state energy eigenvectors,  $|\Psi\rangle$  and  $\langle\tilde{\Psi}|$ , of a many-body system described by a Hamiltonian  $H$ ,

$$H|\Psi\rangle = E_g|\Psi\rangle ; \quad \langle\tilde{\Psi}|H = E_g\langle\tilde{\Psi}| , \quad (2.1)$$

are parametrised within the single-reference CCM as follows:

$$\begin{aligned} |\Psi\rangle &= e^S|\Phi\rangle \quad ; \quad S = \sum_{I \neq 0} \mathcal{S}_I C_I^+ , \\ \langle\tilde{\Psi}| &= \langle\Phi|\tilde{S}e^{-S} \quad ; \quad \tilde{S} = 1 + \sum_{I \neq 0} \tilde{\mathcal{S}}_I C_I^- . \end{aligned} \quad (2.2)$$

The starting point for the CCM calculation is the choice of a normalized reference or model state  $|\Phi\rangle$ , together with a set of (mutually commuting) multi-configurational creation operators  $\{C_I^+\}$  and the corresponding set of their Hermitian adjoints destruction counterparts  $\{C_I \equiv (C_I^+)^\dagger\}$ . Thus,  $|\Phi\rangle$  plays the role of a vacuum state with respect to a suitable set of many-body creation operators  $\{C_I^+\}$ ,

$$\langle\Phi|C_I^+ = 0 = C_I|\Phi\rangle \quad \forall I \neq 0 , \quad [C_I^+ , C_J^+] = 0 = [C_I , C_J] , \quad (2.3)$$

with  $C_0^+ \equiv 1$ , the identity operator. The operators  $C_I^+$  ( $C_I$ ) are defined over a complete set of many-body configurations denoted by the set of set-indices  $\{I\}$ . These operators are complete in the many-body Hilbert(or Fock) space,

$$1 = |\Phi\rangle\langle\Phi| + \sum_{I \neq 0} \frac{C_I^+|\Phi\rangle\langle\Phi|C_I^-}{\langle\Phi|C_I^-C_I^+|\Phi\rangle} . \quad (2.4)$$

We note that although the manifest hermiticity,

$$\langle\tilde{\Psi}|^\dagger = |\Psi\rangle/\langle\Psi|\Psi\rangle ,$$

is lost in these parametrisations, the intermediate normalisation condition

$$\langle \tilde{\Psi} | \Psi \rangle = \langle \Phi | \Psi \rangle = \langle \Phi | \Phi \rangle \equiv 1$$

is explicitly imposed. The ground-state version of the CCM is now completely specified by the set of parameters  $\{\mathcal{S}_I, \tilde{\mathcal{S}}_I\}$ , and in particular an arbitrary expectation value  $\bar{A}$  may be written in the CCM as:

$$\bar{A} \equiv \langle \tilde{\Psi} | A | \Psi \rangle = \langle \Phi | \tilde{S} e^{-S} A e^S | \Phi \rangle = \bar{A} \left( \{\mathcal{S}_I, \tilde{\mathcal{S}}_I\} \right) . \quad (2.5)$$

The correlation coefficients  $\{\mathcal{S}_I, \tilde{\mathcal{S}}_I\}$  are regarded independent (variational) parameters, although formally we have the relation:

$$\langle \Phi | \tilde{S} = \frac{\langle \Phi | e^{S^\dagger} e^S}{\langle \Phi | e^{S^\dagger} e^S | \Phi \rangle} . \quad (2.6)$$

We note that the exponentiated form of the ground-state CCM parametrisation of eq.(2.2) ensures the correct counting of the independent and excited correlated many-body clusters with respect to  $|\Phi\rangle$  which are present in the exact ground state  $|\Psi\rangle$ . It also ensures the exact incorporation of the Goldstone linked-cluster theorem, which itself guarantees the size-extensivity of all relevant extensive physical quantities [22].

The CCM correlation operators,  $S$  and  $\tilde{S}$ , contain the correlation coefficients,  $\mathcal{S}_I$  and  $\tilde{\mathcal{S}}_I$ , which have to be calculated. Once known, all GS properties of the many-body system can clearly be found in terms of them. To find the GS correlation coefficients  $\mathcal{S}_I$  and  $\tilde{\mathcal{S}}_I$ , we simply require that the GS energy expectation value  $\bar{H} = \langle \tilde{\Psi} | H | \Psi \rangle$  is a minimum with respect to the entire set  $\{\mathcal{S}_I, \tilde{\mathcal{S}}_I\}$ , which leads to the GS CCM ket-state and bra-state equations

$$\delta \bar{H} / \delta \tilde{\mathcal{S}}_I = 0 \Rightarrow \langle \Phi | C_I^- e^{-S} H e^S | \Phi \rangle = 0, \quad \forall I \neq 0 ; \quad (2.7)$$

$$\delta \bar{H} / \delta \mathcal{S}_I = 0 \Rightarrow \langle \Phi | \tilde{S} e^{-S} [H, C_I^+] e^S | \Phi \rangle = 0, \quad \forall I \neq 0 . \quad (2.8)$$

We note the important Hellmann-Feynman theorem is preserved in all such approximations [22].

The nested commutator expansion of the similarity-transformed Hamiltonian,

$$\tilde{H} \equiv e^{-S} H e^S = H + [H, S] + \frac{1}{2!} [[H, S], S] + \dots , \quad (2.9)$$

the fact that all of the individual components of  $S$  in the sum in eq. (2.2) commute with each other, by construction, so that each element of  $S$  in the parametrisation (2.2) is linked directly to the Hamiltonian in each of the terms in eq. (2.9). Thus, each of the coupled equations (2.7) is of linked-cluster type. Furthermore, each of these

equations is of finite length when expanded, since the otherwise infinite series of eq. (2.9) will always terminate at a finite order, provided (as is usually the case) only that each term in the second-quantised form of the Hamiltonian  $H$  contains a finite number of single-body destruction operators, defined with respect to the reference (vacuum) state  $|\Phi\rangle$ . Therefore, the CCM parametrisation naturally leads to a workable scheme which can be efficiently implemented computationally.

## 2.2. THE CCM FOR QUANTUM SPIN LATTICES

### 2.2.1. Choice of CCM model state

The starting point for the CCM calculation is the choice of a normalized reference or model state  $|\Phi\rangle$ . Our choice should usually be guided by any physical insight available to us concerning the system or, more specificl, that particular phase of it which is under consideration. For spin systems, an appropriate choice for the CCM model state  $|\Phi\rangle$  is often a classical spin state, in which the most general situation is that each spin can point in an arbitrary direction.

The appropriate reference state - classical ground state, e.g.

- Néel state  $|\Phi\rangle = |\downarrow\uparrow\downarrow\uparrow\downarrow\uparrow\downarrow\uparrow\cdots\rangle$
- spiral or canted state  $|\Phi\rangle = |\uparrow \nearrow \rightarrow \searrow \downarrow \swarrow \leftarrow \nwarrow \uparrow \nearrow \cdots\rangle$

To treat each site equivalently we perform a rotation of the local axis of the spins such that all spins in the reference state align in the same direction, namely along the negative  $z$  axis, such that we have  $|\Phi\rangle = |\downarrow\rangle|\downarrow\rangle|\downarrow\rangle\cdots$ . We define a set of multi-spin creation operators  $C_I^+ = s_i^+, s_i^+ s_j^+, s_i^+ s_j^+ s_k^+, \dots$ .

The choice of the  $C_I^+$  ensures that  $\langle\Phi|C_I^+ = 0 = C_I|\Phi\rangle$ , where  $C_I = s_i^-, s_i^- s_j^-, s_i^- s_j^- s_k^-, \dots$  is the Hermitian adjoint of  $C_I^+$ .

In order to make the spin  $s_i$  to be aligned along the negative  $z$  axis one has to perform a rotation of the respective spin by an appropriate angle  $\delta_i$ . This rotation is equivalent to the canonical transformations,

$$s_i^x = \cos \delta_i \tilde{s}_i^x + \sin \delta_i \tilde{s}_i^z; \quad s_i^y = \tilde{s}_i^y; \quad s_i^z = -\sin \delta_i \tilde{s}_i^x + \cos \delta_i \tilde{s}_i^z. \quad (2.10)$$

A similar rotation about the  $y$ -axis by an angle  $\delta_j$  is performed for the spin  $s_j$ . Thus we get for the transformation of the scalar product of the two spins,  $s_i \cdot s_j \rightarrow (s_i \cdot s_j)_\varphi$ , where

$$\begin{aligned} (s_i \cdot s_j)_\varphi &\equiv \cos \varphi [\tilde{s}_i^x \tilde{s}_j^x + \tilde{s}_i^z \tilde{s}_j^z] + \sin \varphi [\tilde{s}_i^x \tilde{s}_j^z - \tilde{s}_i^z \tilde{s}_j^x] + \tilde{s}_i^y \tilde{s}_j^y \\ &= \frac{1}{4} [\cos \varphi + 1] (\tilde{s}_i^+ \tilde{s}_j^- + \tilde{s}_i^- \tilde{s}_j^+) + \frac{1}{4} [\cos \varphi - 1] (\tilde{s}_i^+ \tilde{s}_j^+ + \tilde{s}_i^- \tilde{s}_j^-) \\ &+ \frac{1}{2} \sin \varphi [\tilde{s}_i^+ \tilde{s}_j^z - \tilde{s}_i^z \tilde{s}_j^+ + \tilde{s}_i^- \tilde{s}_j^z - \tilde{s}_i^z \tilde{s}_j^-] + \cos \varphi \tilde{s}_i^z \tilde{s}_j^z. \end{aligned} \quad (2.11)$$

The angle  $\varphi \equiv \delta_j - \delta_i$  is the angle between the two spins, and  $s^\pm \equiv s^x \pm is^y$  are the spin-raising and spin-lowering operators. Note that this product of two spins after the rotation depends not only on the angle between them, but also on the sign of this angle. In case of the Néel model state ( $\Phi = 0$ ), the angle between any neighbouring spins is  $\pi$ , and hence eq. (2.11) becomes

$$s_i \cdot s_j \rightarrow -\frac{1}{2}[\tilde{s}_i^+ \tilde{s}_j^+ + \tilde{s}_i^- \tilde{s}_j^-] - \tilde{s}_i^z \tilde{s}_j^z. \quad (2.12)$$

### 2.2.2. Commutation relations and the high-order general- $s$ CCM formalism

In this section we present a new formalism and results for high-order ground-state CCM calculations for general spin quantum number,  $s$ , based on a model state in which all spins on the crystallographic lattice point downwards along the local  $z$ -axes. A large part of the new formalism relies on the new “high-order” CCM operators defined by

$$\begin{aligned} F_k &\equiv \sum_l \sum_{i_2, \dots, i_l} l \mathcal{S}_{k, i_2, \dots, i_l} s_{i_2}^+ \cdots s_{i_l}^+ \\ G_{k, m} &\equiv \sum_{l>1} \sum_{i_3, \dots, i_l} l(l-1) \mathcal{S}_{k, m, i_3, \dots, i_l} s_{i_3}^+ \cdots s_{i_l}^+ \\ M_{k, m, n} &\equiv \sum_{l>2} \sum_{i_4, \dots, i_l} l(l-1)(l-2) \mathcal{S}_{k, m, n, i_4, \dots, i_l} s_{i_4}^+ \cdots s_{i_l}^+ \\ N_{k, m, n, p} &\equiv \sum_{l>3} \sum_{i_5, \dots, i_l} l(l-1)(l-2)(l-3) \mathcal{S}_{k, m, n, p, i_5, \dots, i_l} s_{i_5}^+ \cdots s_{i_l}^+, \end{aligned} \quad (2.13)$$

and also their commutation relations with the single-spin operators in order to determine the similarity transforms of various operators, such as the Hamiltonian for example. In order to determine these commutation relations we firstly remind ourselves that the ket-state correlation operator  $S$  is given by eq. (2.2) with  $C_I^+ \equiv s_{i_1}^+ s_{i_2}^+ \cdots s_{i_l}^+$  and  $\mathcal{S}_I \equiv \mathcal{S}_{i_1, i_2, \dots, i_l}$ , and hence

$$S = \sum_l \sum_{i_1, i_2, \dots, i_l} \mathcal{S}_{i_1, i_2, \dots, i_l} s_{i_1}^+ s_{i_2}^+ \cdots s_{i_l}^+, \quad (2.14)$$

where each of the indices  $\{i_1, i_2, \dots, i_l\}$  runs over all lattice sites with the condition that there can be no more than  $2s$  of them at any particular lattice site. The usual spin commutation relations of the spin operators also apply,

$$[s_l^+, s_{l'}^-] = 2s_l^z \delta_{l, l'} \quad ; \quad [s_l^z, s_{l'}^\pm] = \pm s_l^\pm \delta_{l, l'}. \quad (2.15)$$

We also note that the commutation of a given operator with  $S$  must be distributive, such that

$$[s_k^\alpha, S] = \sum_l \sum_{i_1, i_2, \dots, i_l} \mathcal{S}_{i_1, i_2, \dots, i_l} \left\{ [s_k^\alpha, s_{i_1}^+] s_{i_2}^+ \cdots s_{i_l}^+ + s_{i_1}^+ [s_k^\alpha, s_{i_2}^+] s_{i_3}^+ \cdots s_{i_l}^+ \right. \\ \left. + \cdots + s_{i_1}^+ s_{i_2}^+ \cdots [s_k^\alpha, s_{i_l}^+] \right\}, \quad (2.16)$$

where  $\alpha = \{z, +, -\}$ . To calculate the commutator  $[s_k^\alpha, S]$  in eq. (2.17), we use the basic commutation relations of eq.(2.16) we thus have

$$[s_k^+, S] = 0 \\ [s_k^z, S] = \sum_l \sum_{i_2, \dots, i_l} l \mathcal{S}_{k, i_2, \dots, i_l} s_{i_2}^+ \cdots s_{i_l}^+ s_k^+ = F_k s_k^+ \\ [s_k^-, S] = -2 \sum_l \sum_{i_3, i_4, \dots, i_l} \sum_{n=1}^{l-1} \mathcal{S}_{k, k, i_3, \dots, i_l} s_{i_3}^+ s_{i_4}^+ \cdots s_{i_l}^+ s_k^+ \\ -2 \sum_l \sum_{i_2, i_3, \dots, i_l} l \mathcal{S}_{k, i_2, \dots, i_l} s_{i_2}^+ s_{i_3}^+ \cdots s_{i_l}^+ s_k^z = -G_{k, k} s_k^+ - 2F_k s_k^z. \quad (2.17)$$

By using eq. (2.17) the commutation relations between the single-operators and the  $F_k$ ,  $F_k^2$ ,  $G_{k, m}$ , and  $M_{k, m, n}$  operators can also be written in the following compact forms,

$$[s_k^z, F_m] = G_{k, m} s_k^+, \\ [s_k^z, G_{m, n}] = M_{k, m, n} s_k^+, \\ [s_k^z, F_m^2] = 2F_m G_{k, m} s_k^+, \\ [s_k^-, F_m] = -2G_{k, m} s_k^z - M_{k, k, m} s_k^+, \\ [s_k^-, F_m^2] = -2G_{k, m}^2 s_k^+ - 2F_m M_{k, k, m} s_k^+ - 4F_m G_{k, m} s_k^z, \\ [s_k^z, M_{m, n, p}] = N_{k, m, n, p} s_k^+, \\ [s_k^-, G_{m, n}] = -2M_{k, m, n} s_k^z - N_{k, k, m, n} s_k^+. \quad (2.18)$$

We note that for the case  $s = 1/2$  the operator  $G_{k, k} = 0$  because ‘‘double occupancy’’ of the lattice site  $k$  is prohibited in this case.

### 2.2.3. Hierarchical approximation schemes

By analogy to Eq. (2.2), which define the general form for the ket-state and bra-state correlation operators  $S$  and  $\tilde{S}$  respectively, we rewrite these two operators for quantum

spin systems as:

$$\begin{aligned}
S &= \sum_{I \neq 0} \alpha_I C_I^+ = \sum_{l=1}^{\infty} A_l \\
\text{with } A_l &\equiv \sum_{i_1, i_2, \dots, i_l} [i_1, i_2, \dots, i_l] s_{i_1}^+ s_{i_2}^+ \cdots s_{i_l}^+ \\
\tilde{S} &= 1 + \sum_{I \neq 0} \tilde{\alpha}_I C_I^- = \sum_{l=1}^{\infty} \tilde{A}_l \\
\text{with } \tilde{A}_l &\equiv \sum_{i_1, i_2, \dots, i_l} [i_1, i_2, \dots, i_l] s_{i_1}^- s_{i_2}^- \cdots s_{i_l}^- .
\end{aligned} \tag{2.19}$$

The CCM formalism is exact if we take into account all possible multi-spin configurations in the correlation operators  $S$  and  $\tilde{S}$ . However, in general, this is impossible to do in practice for a quantum many-body system. Hence, it is necessary to use approximation schemes in order to truncate the expansions of  $S$  and  $\tilde{S}$  in eq. (2.2) in any practical calculation. The three most commonly employed schemes have been:

$$\text{SUB}_n : S = \sum_{l=1}^n A_l .$$

- In this scheme all correlations involving only  $n$  or fewer spins are retained, but no further restriction is made concerning their spatial separation on the lattice. The SUB $n$  scheme has been used by CCM [83, 84, 97] for quantum spin systems.
- The SUB $n$ - $m$  sub-approximation, in which all SUB $n$  correlations spanning a range of no more than  $m$  adjacent lattice sites are retained.
- The localized LSUB $m$  scheme, which take in to account all possible many-body cluster configurations  $I = i_1, i_2, \dots, i_l$  in all different localised regions of  $m$  contiguous sites on the lattice.

$$\text{LSUB}_n : I \in \text{SUB}_n \text{ with } K(I) < n$$

$$K(I) = K(i_1, i_2, \dots, i_l) = \underbrace{\max}_{a, b=1 \dots l} d(i_a, i_b), \quad d(i, j) = |x_j - x_i| + |y_j - y_i| .$$

For  $s = 1/2$  the LSUB $m$  scheme is equivalent to the SUB $n$ - $m$  sub-approximation [88, 89, 98] that means  $n = m$ . In the case of quantum number  $s > 1/2$  we have  $n = 2 \cdot s \cdot m$ . We note that only the LSUB $m$  and SUB $n$ - $m$  scheme are adopted throughout this thesis.

The first step in the practical implementation of the CCM at the LSUB $m$  level of approximation is to enumerate all fundamental configurations  $\{i_1, i_2, \dots, i_l\}$  with  $n < m$ , which are retained at the LSUB $m$  level. To find all possible fundamental configurations which are different under the point and space group symmetries of both the lattice and the Hamiltonian, we use the lattice symmetries. The numbers of fundamental configurations may be further reduced by the use of additional conservation laws. For example, in the case of the Néel state  $|\uparrow\downarrow\uparrow\downarrow \cdots\rangle$ , the Hamiltonian commutes with the total uniform magnetization,  $s_T^z = \sum_k s_k^z$  (the sum on  $k$  runs over all

lattice sites). the GS lies in the  $s_T^z = 0$  subspace, and hence we exclude configuration with an odd number of spins or with unequal numbers of spins on the two equivalent sublattices. For the spiral state we cannot apply this property because it is not an eigenstate of  $s_T^z$ . For pure square lattice, this restriction, for example, reduces the number of the fundamental configurations retained in the LSUB4 approximation to 7 if the z-axis Néel model state is employed in the CCM calculations, and see Fig.(7.1). The lowest order LSUB $m$  scheme is the LSUB2 (i.e, SUB2-2) approximation in which

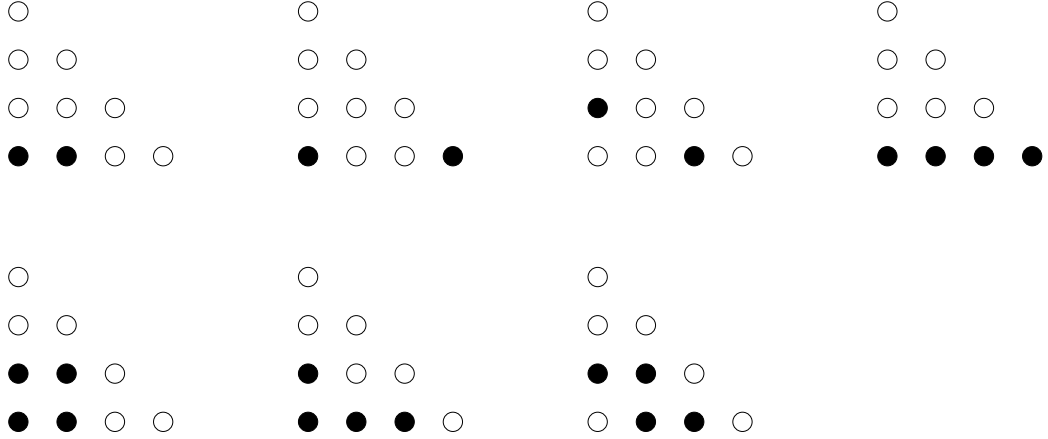


**Figure 2.1.:** Illustration of fundamental configurations for square lattice antiferromagnet within the LSUB4 approximation.

only a single nearest-neighbour, two-body term is retained in  $S$ . We note that the Hamiltonian of Eq.(2.20) includes products of the spin operators which contain even numbers of these spin operators only

$$H = \sum_{i,j} J_{ij} \mathbf{s}_i \cdot \mathbf{s}_j , \quad (2.20)$$

where  $J_{ij} = 1$  for NN bonds, and  $J_{ij} = 0$  otherwise. This means that the ground state contains only even numbers of spin flips with relation to the model state.

#### 2.2.4. The ket-state equations

According to Eq.(2.7), we now determine the CCM ket-state equations for the configuration  $j_1, j_2, \dots, j_l$  in spin systems as

$$\langle \Phi | s_{j_1}^- s_{j_2}^- \dots s_{j_l}^- e^{-S} H e^S | \Phi \rangle = 0 , \quad (2.21)$$

where  $s_{j_1}^- s_{j_2}^- \dots s_{j_l}^-$  is the Hermitian conjugate of the corresponding multi-spin correlation string  $s_{j_1}^+ s_{j_2}^+ \dots s_{j_l}^+$ .

In practice we clearly need an approximation scheme (e.g LSUB $n$ ) to truncate the

expansion of  $S$  in eq. (2.14) to some finite subset of the full set of multi-spin configuration  $\{j_1, j_2, \dots, j_l\}$ . We note that we use lattice symmetries and, where possible, any exact conservation laws for a given fundamental configuration in  $C_I^-$  in order to pattern-match with the terms within  $\tilde{H}|\Phi\rangle$  and thus determine the  $I$ -th CCM ket-state equation. The CCM ket-state equations can be determined in two steps, the first is to calculate the similarity-transformed Hamiltonian,  $\hat{H} = e^{-S}He^S$ , which acts on the reference state  $|\Phi\rangle$  can be performed straightforwardly by making use of the relations  $s^-|\Phi\rangle = 0$  and  $s^z|\Phi\rangle = -\frac{1}{2}|\Phi\rangle$ . The goal here is to completely eliminate  $s^z$  and  $s^-$ , and thus retain the creation operators only, by utilising the commutation relations of the spin operators see eq. (2.15). The similarity-transformed single spin operators can be expressed as:

$$\begin{aligned} e^{-S}s_k^+e^S &\equiv \hat{s}_k^+ = s_k^+ \\ e^{-S}s_k^ze^S &\equiv \hat{s}_k^z = s_k^z + F_k s_k^+ \\ e^{-S}s_k^-e^S &\equiv \hat{s}_k^- = s_k^- - 2F_k s_k^z - G_{kk}s_k^+ - (F_k)^2 s_k^+. \end{aligned} \quad (2.22)$$

using eq. (2.22), we can now determine the different kinds of two-spin interaction terms in the similarity transformed Hamiltonian and their application on the model state  $|\Phi\rangle$  for example we calculate for  $s = 1/2$  ( $k \neq m$ )

$$\begin{aligned} \hat{s}_k^- \hat{s}_m^- |\Phi\rangle &= [(2G_{km}^2 + 4F_k F_m G_{km} + F_k^2 F_m^2) s_k^+ s_m^+ \\ &\quad - (2G_{km} F_m + F_k F_m^2) s_m^+ - (2G_{km} F_k + F_k^2 F_m) s_k^+ \\ &\quad + G_{km} + F_k F_m] |\Phi\rangle \\ \hat{s}_k^+ \hat{s}_m^- |\Phi\rangle &= (-F_m^2 s_k^+ s_m^+ + F_m s_k^+) |\Phi\rangle \\ \hat{s}_k^- \hat{s}_m^+ |\Phi\rangle &= (-F_k^2 s_k^+ s_m^+ + F_k s_m^+) |\Phi\rangle \\ \hat{s}_k^+ \hat{s}_m^+ |\Phi\rangle &= s_k^+ s_m^+ |\Phi\rangle \\ \hat{s}_k^z \hat{s}_m^z |\Phi\rangle &= [(G_{km} + F_k F_m) s_k^+ s_m^+ - \frac{1}{2} F_k s_k^+ - \frac{1}{2} F_m s_m^+ + \frac{1}{4}] |\Phi\rangle \\ \hat{s}_k^+ \hat{s}_m^z |\Phi\rangle &= (F_m s_k^+ s_m^+ - \frac{1}{2} s_k^+) |\Phi\rangle \\ \hat{s}_k^z \hat{s}_m^+ |\Phi\rangle &= (F_k s_k^+ s_m^+ - \frac{1}{2} s_m^+) |\Phi\rangle \\ \hat{s}_k^z \hat{s}_m^- |\Phi\rangle &= [(-F_k F_m^2 - 2F_m G_{km}) s_k^+ s_m^+ + (G_{km} + F_k F_m) s_k^+ + \frac{1}{2} F_m^2 s_m^+ - \frac{1}{2} F_m] |\Phi\rangle \\ \hat{s}_k^- \hat{s}_m^z |\Phi\rangle &= [(-F_k^2 F_m - 2F_k G_{km}) s_k^+ s_m^+ + (G_{km} + F_k F_m) s_m^+ + \frac{1}{2} F_k^2 s_k^+ - \frac{1}{2} F_k] |\Phi\rangle. \end{aligned} \quad (2.23)$$

The second step is to select all terms in Eq.(2.23) which containing creation operators  $\hat{s}^+$  with indices corresponding precisely to the indices  $j_1, j_2, \dots, j_l$  of the  $\hat{s}^-$  operators in eq.(2.21). By using the orthonormality relation  $\langle \Phi | s_m^+ s_k^- | \Phi \rangle = \delta_{mk}$  one get all terms of the ket-state equations for the configuration  $j_1, j_2, \dots, j_l$

### 2.2.5. The bra-state equations

In order to compute a general ground-state physical quantity such as the magnetic order parameter, we need to calculate both the ket-state correlation coefficients  $\{\mathcal{S}_I\}$  and



the bra-state correlation coefficients  $\{\tilde{\mathcal{S}}_I\}$  which can be determined by eq.(2.5). However, the form of the bra-state equations is slightly cumbersome to use, and a simpler way to calculate it is to use the following new set of CCM correlation coefficients

$$\left. \begin{aligned} x_I &= \mathcal{S}_I \\ \tilde{x}_I &= \frac{N_B}{N} \tilde{\mathcal{S}}_I A_I \nu_I (n_I!) \end{aligned} \right\} , \quad (2.24)$$

where  $A_I$  is a normalisation factor given by  $A_I \equiv \langle \Phi | (s_{i_1}^- s_{i_2}^- \cdots s_{i_l}^-) (s_{i_1}^+ s_{i_2}^+ \cdots s_{i_l}^+) | \Phi \rangle$ , where  $N_B$  is the total number of Bravais lattice sites, and where  $\nu_I$  is a symmetry factor dependent purely on the point-group symmetries (and not the translational symmetries) for the crystallographic lattice in question and for fundamental configuration  $r$ . We note that  $n_I$  is the number of spin operators and that  $N_F$  such fundamental configurations. The CCM bra-state operator may be rewritten as

$$\tilde{\mathcal{S}} \equiv 1 + N \sum_{I=1}^{N_F} \frac{\tilde{x}_I}{A_I} C_I^- , \quad (2.25)$$

such that

$$\bar{H} = E(x_1, x_2, \dots) + N \sum_I^{N_F} \tilde{x}_I K_I(x_1, x_2, \dots) . \quad (2.26)$$

Note that  $K_I(x_1, x_2, \dots)$  is the  $r$ -th CCM ket-state equation defined by eq. (2.21). The CCM ket-state equations are easily rederived by taking the partial derivative of  $\bar{H}/N$  with respect to  $\tilde{x}_I$ , where

$$0 = \frac{\partial(\bar{H}/N)}{\partial \tilde{x}_I} \equiv K_I(x_1, x_2, \dots) . \quad (2.27)$$

We now take the partial derivative of  $\bar{H}/N$  with respect to  $x_I$  such that the bra-state equations take on a particularly simple form, given by

$$\frac{\partial(\bar{H}/N)}{\partial x_I} = \frac{\partial(E/N)}{\partial x_I} + \sum_{J=1}^{N_F} \tilde{x}_J \frac{\partial K_J}{\partial x_I} = 0 . \quad (2.28)$$

This equation is easily solved computationally, once the CCM ket-state equations have been determined and solved, and the numerical values of the coefficients  $\{\tilde{x}_I\}$  may thus be obtained.

### 2.3. THE EXCITED-STATE FORMALISM

We now turn our attention to the CCM parametrization of the excited state developed by Emrich [99] which may be utilised in order to perform high-order CCM calculations for the excited state [89] of quantum spin systems of general spin quantum number. We

note however that no excited-state results are presented in this thesis. The excited-state wave function,  $|\Psi_e\rangle$ , is determined in Emrich's formalism [99] by linearly applying an excitation operator  $X^e$  to the ket-state wave function of eq. (2.2), such that

$$|\Psi_e\rangle = X^e |\Psi\rangle = X^e e^S |\Phi\rangle . \quad (2.29)$$

By analogy with the ground-state formalism, the excited-state correlation operator is given by,

$$X^e = \sum_{I \neq 0} \mathcal{X}_I^e C_I^+ , \quad (2.30)$$

where the set  $\{C_I^+\}$  of multi-spin creation operators may differ from those used in the ground-state parametrisation in eq. (2.2), if the excited state has different quantum numbers than the ground state. We note that equation (2.30) implies the overlap relation  $\langle \Phi | \Psi_e \rangle = 0$ . Using the Schrödinger equation,  $H|\Psi_e\rangle = E_e|\Psi_e\rangle$ , we find

$$\epsilon_e X^e |\Phi\rangle = e^{-S} [H, X^e] e^S |\Phi\rangle , \quad (2.31)$$

where  $\epsilon_e \equiv E_e - E_g$  is the difference between the excited-state energy ( $E_e$ ) and the ground-state energy ( $E_g$ ). By applying  $\langle \Phi | C_I^-$  to eq. (2.31) we find that

$$\langle \Phi | C_I^- e^{-S} [H, X^e] e^S |\Phi\rangle = \epsilon_e \mathcal{X}_I^e \quad \forall I \neq 0 , \quad (2.32)$$

which is a generalized set of eigenvalue equations with eigenvalues  $\epsilon_e$  and corresponding eigenvectors  $\mathcal{X}_I^e$ . Analogously to the ground-state case, we define the excited-state operators.

$$\begin{aligned} P_k &\equiv \sum_l \sum_{i_2, \dots, i_l} l \mathcal{X}_{k, i_2, \dots, i_l}^e s_{i_2}^+ \cdots s_{i_l}^+ \\ Q_{k,m} &\equiv \sum_{l>1} \sum_{i_3, \dots, i_l} l(l-1) \mathcal{X}_{k, m, i_3, \dots, i_l}^e s_{i_3}^+ \cdots s_{i_l}^+ . \end{aligned} \quad (2.33)$$

By choosing the model state as the Néel state we find for the terms in Eq.(2.12)

$$\begin{aligned} e^{-S} [s_k^- s_m^-, X]_- e^S |\Phi\rangle &= [(4F_k F_m Q_{km} + 4G_{km} Q_{km} + 2F_k^2 P_m F_m + 2P_k F_k F_m^2 \\ &\quad + 4P_k F_m G_{km} + 4F_k P_m G_{km}) s_k^+ s_m^+ \\ &\quad - (2F_k Q_{km} + 2P_k G_{km} + F_k^2 P_m + 2P_k F_k F_m) s_k^+ \\ &\quad - (2Q_{km} F_m + 2G_{km} P_m + P_k F_m^2 + 2F_k F_m P_m) s_m^+ \\ &\quad + Q_{km} + F_k P_m + P_k F_m] |\Phi\rangle \\ e^{-S} [s_k^+ s_m^+, X]_- e^S |\Phi\rangle &= 0 \\ e^{-S} [s_k^z s_m^z, X]_- e^S |\Phi\rangle &= [(Q_{km} + F_k P_m + P_k F_m) s_k^+ s_m^+ - \frac{1}{2} P_k s_k^+ - \frac{1}{2} P_m s_m^+] |\Phi\rangle . \end{aligned} \quad (2.34)$$

For Heisenberg antiferromagnetic systems the ground state lies in the sector  $s_T^z = 0$ . By contrast, the lowest-lying excited states lie in the  $s_T^z = \pm 1$ , and the number

of such fundamental configurations for the excited state at a given level of LSUB $n$  approximation is labelled by  $N_{f_e}$ . In order to determine the excited-state eigenvalue equations we must firstly fully determine and solve the ground ket-state equations in order to obtain numerical values for the set  $\{\mathcal{S}\}$  which are then used as input to the eigenvalue problem of equation (2.32). Finally, the interested reader is referred to Ref. [89] for a full account of applications of high-order CCM calculations to the limiting spin-half case of the XXZ model for the linear chain, the square lattice, and the cubic lattice.

## 2.4. CALCULATION OF PHYSICAL QUANTITIES USING CCM

### 2.4.1. Ground state energy and Sublattice magnetization

The ground state energy at the stationary point has the simple form

$$E_g = E_g(\{\mathcal{S}_I\}) = \langle \Phi | e^{-S} H e^S | \Phi \rangle , \quad (2.35)$$

which also follows simple by projecting the ground state ket equation (2.1) with  $\langle \Phi | e^{-S}$ . We note that this bi-variational formulation does not lead to an upper bound for  $E_g$  when the summations for  $S$  and  $\tilde{S}$  in Eq. (2.2) are truncated in specific approximations, since the exact hermiticity between  $\langle \tilde{\Psi} |$  and  $|\Psi\rangle$  will thereby be lost.

In order to discuss the phase transition further it is necessary to consider the degree of quantum order inherent in the CCM wave functions obtained at the various LSUB $n$  levels of approximation, and based on both model state. The simplest such order parameter is the sublattice magnetization, which is defined as the average over the entire lattice of  $s^z$  in the local (rotated) spin coordinates, or, equivalent over a single sublattice of the corresponding unrotated component of the spin in the original global coordinates. By using the CCM parametrization of eq.(2.2) we find,

$$M = -\frac{1}{N} \sum_{k=1}^N \langle \tilde{\Psi} | s_k^z | \Psi \rangle = -\frac{1}{N} \sum_{k=1}^N \langle \Phi | \tilde{S} e^{-S} s_k^z e^S | \Phi \rangle , \quad (2.36)$$

where  $s_k^z$  is in the local coordinates of each sublattice. In the notation of eq.(2.19), and eq.(2.14) we find,

$$\begin{aligned} -\langle \Phi | \tilde{S} e^{-S} s_k^z e^S | \Phi \rangle &= -\langle \Phi | \tilde{S} (s_k^z + F_k s_k^+) | \Phi \rangle = \frac{1}{2} - \langle \Phi | \tilde{S} F_k s_k^+ | \Phi \rangle \\ \sum_{k=1}^N \langle \Phi | \tilde{S} F_k s_k^+ | \Phi \rangle &= \sum_{k=1}^{\infty} n(n!) \sum_{i_1 \dots i_n} \tilde{S}_{i_1 \dots i_n} \mathcal{S}_{i_1 \dots i_n} \\ \implies M &= \frac{1}{2} - \frac{1}{N} \sum_{k=1}^{\infty} n(n!) \sum_{i_1 \dots i_n} \tilde{S}_{i_1 \dots i_n} \mathcal{S}_{i_1 \dots i_n} . \end{aligned} \quad (2.37)$$

The sum in eq.(2.37) may be rewritten in terms of the independent correlation coefficients  $\tilde{\mathcal{X}}_I$  and  $\mathcal{X}_I$  associated with the  $N_F$  fundamental configurations of a given LSUB $n$  approximation, which were introduced in Sec. (2), to give the LSUB $n$  estimate for  $M$ ,

$$M = \frac{1}{2} - \sum_{r=1}^{N_F} n_I (n_I!)^2 \nu_I \tilde{\mathcal{X}}_I \mathcal{X}_I = \frac{1}{2} - \sum_{r=1}^{N_F} n_I (n_I!) \tilde{x}_I x_I, \quad (2.38)$$

where  $n_I$  is the number of spin flips with respect to  $|\Phi\rangle$  for the  $r$ th fundamental configuration, and where we have introduced the notation  $x_I \equiv \mathcal{X}_I$  and  $\tilde{x}_I \equiv (n_I!) \nu_I \tilde{\mathcal{X}}_I$ .

#### 2.4.2. Spin stiffness

The spin stiffness  $\rho_s$  [31, 100–110] can be calculated by imposing a twist on the order parameter of a magnetically long-range ordered system along a given direction, i.e.,

$$\frac{E(\theta)}{N} = \frac{E(\theta=0)}{N} + \frac{1}{2} \rho_s \theta^2 + \mathcal{O}(\theta^4), \quad (2.39)$$

where  $E(\theta)$  is the GS energy as a function of the twist angle  $\theta$ , and  $N$  is the number of sites. To calculate the spin stiffness within CCM(e.g.Chap.5) we need to calculate the ground state energy for Néel state ( $\theta = 0$ ) and for small value of the parameter  $\theta$  for example ( $\theta = 10^{-4}$ ) then we use the numerical differentiation of  $E(\theta)$

$$\begin{aligned} E_0''(\theta) &= [e(\theta - h) - 2E_0(\theta) + e(\theta + h)]/h^2 \quad \text{three - points formula} \\ E_0''(\theta) &= [-e(\theta - 2h) + 16e(\theta - h) - 30E_0(\theta) \\ &\quad + 16e(\theta + h) - e(\theta + 2h)]/12h^2 \quad \text{five - points formula} \end{aligned} \quad (2.40)$$

where  $E(\theta)$  is the ground state energy,  $\theta = 0$  and  $h = 0.0001$

#### 2.4.3. Generalized susceptibilities

Within the CCM technique the general susceptibility [23, 25, 26, 47, 49, 50]

$$\chi = - \left. \frac{\partial^2 e}{\partial \delta^2} \right|_{\delta=0}, \quad (2.41)$$

can be evaluated by adding to the Hamiltonian  $H$  a term  $F = \delta \hat{O}$ , where  $\hat{O}$  is an operator that breaks some symmetry of  $H$  and the coefficient  $\delta$  gives the strength of the field. After we calculate the energy per site  $e(\delta)$  for  $H + F$ , then we use the Eq.(2.40).

## 2.5. EXTRAPOLATION SCHEMES

Since the LSUB $n$  approximation becomes exact in the limit  $n \rightarrow \infty$ , it is useful to extrapolate the 'raw' LSUB $n$  results to the limit  $n \rightarrow \infty$ . Although an exact scaling theory for the LSUB $n$  results is not known, there is some empirical experience [18, 42, 88, 89, 93] indicating how the physical quantities for spin models might scale with  $n$ . For the GS energy we employ [18, 89]

$$E(n) = a_0 + a_1 \frac{1}{n^2} + a_2 \left( \frac{1}{n^2} \right)^2 . \quad (2.42)$$

Furthermore, we note that it may be useful to discard the LSUB2 results for the extrapolation, because generally they fit poorly to the asymptotic behavior [89]. For the order parameter, the stiffness, and the generalized susceptibilities one utilizes [89, 95] an extrapolation law with leading power  $1/n$ , i.e.,

$$A(n) = b_0 + b_1 \frac{1}{n} + b_2 \left( \frac{1}{n} \right)^2 . \quad (2.43)$$

However, there is some experience that when applied to systems showing an order-disorder quantum phase transition this kind of extrapolation tends to overestimate the parameter region where magnetic LRO exists, i.e. to yield too large critical values for the exchange parameter driving the transition. [18, 91, 93, 95] The reason for such behavior might derive from the change of the scaling near a critical point. Hence, in addition to the extrapolation rule of Eq. (2.43) for the order parameter  $m$ , we also use a leading 'power-law' extrapolation [89, 93, 95] given by

$$m(n) = c_0 + c_1 \left( \frac{1}{n} \right)^v , \quad (2.44)$$

where the exponent  $v$  is a fitting parameter which is determined directly from the LSUB $n$  data. We note that there are some cases (see e.g., Chap.8) where the simple two-term scheme of Eq. (2.44) is unstable in the critical regime. In order to solve this problem, we use the following extrapolation scheme [111]

$$M = c_0 + n^{-0.5} (c_1 + c_2 n^{-1}) . \quad (2.45)$$

Meanwhile, this extrapolation scheme (2.45) has been applied to investigate quantum critical phenomena for several frustrated spin models [111–115]. It has been found that the scheme (2.45) leads to accurate results for the position of quantum critical points.

We list below three fundamental rules, also based on our experience, as guidelines for the selection and extrapolation of the CCM raw data, using *any* approximation

scheme.

- Rule 1: As a fundamental rule of numerical fitting or numerical analysis, one should always have at least  $(n + 1)$  data points in order to have a robust and stable fit to any formula that contains  $n$  unknown parameters. This rule takes precedence over all other rules.
- Rule 2: Whenever possible one should avoid using the lowest (e.g., LSUB2, SUB2-2) data points since such points are rather far from the large- $n$  limit, unless it is necessary to do so to avoid breaking Rule 1.
- Rule 3: If Rule 2 has been broken then some other careful consistency checks should also be performed..

## 2.6. THE CCM FOR THE PURE HEISENBERG ANTIFERROMAGNET ON SQUARE AND CUBIC LATTICE

During the last few years the running time and memory requirements of the original CCM code have been considerably improved. [94, 116] Consequently, it is now possible to run higher levels of approximation by using an improved parallelization procedure. In this Section we present a collection of CCM results for the (unfrustrated) pure HAFM (see i.e., Eq. 2.20) on some basic lattices, and compare them with the most accurate results obtained by other methods. While some of the CCM results have already been published elsewhere, [89, 95] we also present here the new unpublished results from higher levels of approximation. The results are shown in Tables 2.1 and 2.2, in which the entries shown in boldface are the new ones.

**Table 2.1.:** Data for the spin-1/2 square-lattice pure HAFM.  $N_f$  is the number of fundamental configurations for the Néel reference state,  $E/N$  is the GS energy per spin and  $m$  is the sublattice magnetization. The LSUB $n$  results are extrapolated using Eq. (2.42) for  $E/N$  and Eq. (2.43) for  $m$ .

square lattice	$N_f$	$E/N$	$m$
LSUB2	1	-0.64833	0.42071
LSUB4	7	-0.66366	0.38240
LSUB6	75	-0.66700	0.36364
LSUB8	1287	-0.66817	0.35242
<b>LSUB10</b>	<b>29605</b>	<b>-0.66870</b>	<b>0.34483</b>
<b>Extrapolated CCM</b>	-	<b>-0.66936</b>	<b>0.31024</b>
3rd order SWT [105]	-	-0.66931	0.3069
QMC [117, 118]	-	-0.66944	0.3070

**Table 2.2.:** Data for the spin-1/2 simple-cubic lattice pure HAFM.  $N_f$  is the number of fundamental configurations for the Néel reference state,  $E/N$  is the GS energy per spin and  $m$  is the sublattice magnetization. The LSUB $n$  results are extrapolated using Eq. (2.42) for  $E/N$  and Eq. (2.43) for  $m$ .

<b>cubic lattice</b>	$N_f$	$E/N$	$m$
LSUB2	1	-0.89076	0.45024
LSUB4	9	-0.90043	0.43392
LSUB6	181	-0.90180	0.42860
LSUB8	<b>8809</b>	<b>-0.90214</b>	<b>0.42626</b>
<b>Extrapolated CCM</b>	-	<b>-0.90247</b>	<b>0.42054</b>
3rd order SWT [105]	-	-0.9025	0.4227

The Tables 2.1 and 2.2 indicate that the extrapolated CCM results for the ground-state energy and the sublattice magnetization of the spin-1/2 square-lattice and simple-cubic lattice are more accurate estimates than the results which are published in Ref. [89, 95]. We also see from Tables 2.1 and 2.2 that the new results are in excellent agreement with the results of third-order SWT [105] and QMC [117, 118].





## CHAPTER 3

# QUANTUM PHASE TRANSITIONS IN 2D UNFRUSTRATED HEISENBERG ANTIFERROMAGNET - $J$ - $J'$ MODEL

### 3.1. INTRODUCTION

The zero-temperature properties of low-dimensional quantum spin systems and the location and character of ground-state instabilities (critical points) as some parameter in the Hamiltonian is varied represent fundamental problems in condensed matter theory. The recent experimental results on spin-half Heisenberg antiferromagnets like  $\text{SrCu}_2(\text{BO}_3)_2$  [12, 13] and  $\text{CaV}_4\text{O}_9$  [14, 15] have stimulated the search for systems with disordered liquid-like magnetic ground states. In quantum systems a direct competition between bonds also exists which may lead to local singlet formation on certain antiferromagnet bonds (or plaquettes of four spins) if these bonds are increased in strength. By tuning the degree of competition zero-temperature order-disorder phase transitions can be realized.

A widely studied model describing competition without frustration and showing the 'melting' of semi-classical Néel order by local singlet formation is the HAFM on the square lattice with two non-equivalent nearest-neighbor bonds  $J$  and  $J'$  ( $J$ - $J'$  model) [18–20, 91, 119–123]. In these papers on the  $J$ - $J'$  model the extreme quantum case  $s = 1/2$  is considered and the competition can be tuned by variation of the exchange bond  $J'$ . One finds a second-order transition from the quasi-classically Néel ordered phase to a dimerized singlet phase at  $J'_c \approx 2.5 \dots 2.9J$ . It was argued in [120, 121] that the quantum phase transition is of the same universality class as the thermal phase transition of three-dimensional classical Heisenberg model. However, very recently by QMC [122] it has been found that the spin-half  $J$ - $J'$  model may belong to a new universality class. The strength of quantum fluctuations within this model can be varied either by anisotropy or by spin quantum number. Indeed it was found in [121] for the  $J$ - $J'$  model that the critical  $J'_c$  for the  $XY$  model is significantly larger than for the spin rotationally invariant Heisenberg model. The role of Ising exchange anisotropy  $\Delta_I$  and of the spin quantum number  $s$  was not systematically studied. Some results for spin models with  $s = 1$  can be found e.g., in [120, 124].

### 3.2. THE MODEL

We consider the  $J$ - $J'$  model on a square lattice, i.e. a HAFM with two kinds of antiferromagnet nearest-neighbor bonds  $J$  and  $J'$  (see Fig. 3.1) described by the Hamiltonian

$$H = J \sum_{\langle ij \rangle_1} (s_i^x s_j^x + s_i^y s_j^y + \Delta s_i^z s_j^z) + J' \sum_{\langle ij \rangle_2} (s_i^x s_j^x + s_i^y s_j^y + \Delta s_i^z s_j^z). \quad (3.1)$$

The sums over  $\langle ij \rangle_1$  and  $\langle ij \rangle_2$  run over the two kinds of nearest-neighbor bonds, respectively (cf. Fig. 3.1). We consider spin operators  $\mathbf{s}_i^2 = s(s+1)$  of spin quantum number  $s = 1/2, 1, 3/2$  and  $2$ . We also split the square lattice into the equivalent  $A$  and  $B$  sublattices shown in Fig. 3.1. Each square-lattice plaquette consists of three  $J$  bonds and one  $J'$  bond. In the case of ferromagnetic  $J'$  bonds (i.e.,  $J' < 0$ ), the plaquettes are frustrated. Conversely, for antiferromagnet  $J'$  bonds (i.e.,  $J' > 0$ ) there is no frustration in the system. This model for  $s = 1/2$  has been studied previously using perturbation theory [19], renormalized spin wave theory (RSWT) [119], and exact diagonalization (ED) [125]. Recently, for this model has been studied the influence of local singlet formation ( $J' > 1$ ) and frustration ( $J' < 1$ ) on the stability of the Néel order (see i.e., Ref. [18, 20]). We note that the case of antiferromagnet  $J'$  bonds with  $J' > J > 0$  resembles the situation in bilayer systems and in the depleted square lattice antiferromagnet  $\text{CaV}_4\text{O}_9$ , in which the competition between two different antiferromagnet bonds leads to a phase transition from antiferromagnet LRO to quantum disorder with a finite gap. There are some special cases of the model

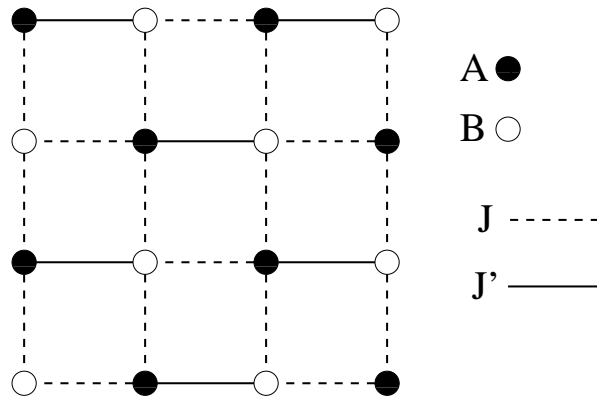


**Figure 3.1.:** Illustration of arrangement of bonds in the  $J$ - $J'$  model on the square lattice (Eq.(3.1)):  $J$  – dashed lines;  $J'$  – solid lines; A and B characterize the two sublattices of the classical Néel ground state. .

Hamiltonian of Eq.(3.1) with  $\Delta = 1$ :

- (i)  $J' = 1$ : square-lattice antiferromagnet, for which the ground state is long-range ordered;
- (ii)  $J' = 0$ : honeycomb-lattice antiferromagnet, for which the ground state is the long-range ordered;
- (iii)  $J' = -\infty$ : spin-1 triangle lattice, for which the ground state is long-range ordered;
- and (iv)  $J' = +\infty$ : valence-bond solid, for which the

ground state is a rotationally invariant quantum dimer state with an excitation gap.

### 3.3. INFLUENCE OF ISING-ANISOTROPY

We investigate the influence of the Ising anisotropy on the zero-temperature magnetic order-disorder transition for the  $J - J'$  spin-half XXZ antiferromagnet on the square lattice (Eq.(3.1)), using the coupled cluster method (CCM), a variational mean-field like approach (MFA) and exact diagonalization (ED). We consider antiferromagnet bonds  $J' \geq J > 0$ , i.e. there is no frustration in the model. In what follows we set  $J = 1$  and consider the Ising anisotropy  $\Delta \geq 1$  and  $J'$  as the parameters of the model. Since there is no frustration the classical ground state is the two-sublattice Néel state.

#### 3.3.1. Variational mean-field approach

For the square-lattice antiferromagnet ( $J = J'$ ) the ground state is Néel ordered. The corresponding uncorrelated mean-field state is the Néel state

$$|\phi_{MF_1}\rangle = |\uparrow\rangle|\downarrow\rangle|\uparrow\rangle|\downarrow\rangle \dots .$$

In the limit  $J' \rightarrow \infty$  and for finite  $\Delta$  the ground state approaches a rotationally invariant product state of local pair singlets (valence-bond state)

$$|\phi_{MF_2}\rangle = \prod_{i \in A} \{ |\uparrow_i\rangle|\downarrow_{i+\hat{x}}\rangle - |\downarrow_i\rangle|\uparrow_{i+\hat{x}}\rangle \} / \sqrt{2} ,$$

where  $i$  and  $i + \hat{x}$  correspond to those sites which cover the  $J'$  bonds. In order to describe the transition between both states, we consider an uncorrelated product state of the form [16, 18]

$$|\Psi_{var}\rangle = \prod_{i \in A} \frac{1}{\sqrt{1+t^2}} [ |\uparrow_i\downarrow_{i+\hat{x}}\rangle - t |\downarrow_i\uparrow_{i+\hat{x}}\rangle ]. \quad (3.2)$$

The trial function  $|\Psi_{var}\rangle$  depends on the variational parameter  $t$  and interpolates between the valence-bond state  $|\phi_{MF_2}\rangle$  realized for  $t = 1$  and the Néel state  $|\phi_{MF_1}\rangle$  realized for  $t = 0$ . By minimizing  $E_{var} = \langle \Psi_{var} | H | \Psi_{var} \rangle$  with respect to the variational parameter  $t$  we obtain

$$\frac{E_{var}}{N} = \begin{cases} -\frac{1}{24\Delta} (J'^2 + 3\Delta^2 J' + 9\Delta^2) & \text{for } J' \leq 3\Delta \\ -\frac{1}{8} J' (\Delta + 2) & \text{for } J' > 3\Delta . \end{cases} \quad (3.3)$$

The relevant order parameter describing the Néel order is the sublattice magnetization

$$M_s = \langle \Psi_{var} | s_{i \in A}^z | \Psi_{var} \rangle = \begin{cases} \frac{1}{2} \sqrt{1 - (J'/3\Delta)^2} & \text{for } J' \leq 3\Delta \\ 0 & \text{for } J' > 3\Delta. \end{cases} \quad (3.4)$$

$M_s$  vanishes at the critical value  $J'_c = 3\Delta J$ . The corresponding critical index is the mean-field index 1/2. Eq. (3.3) may be rewritten in terms of  $M_s$  as

$$E_{var}/N = -\frac{1}{8}J'\Delta - \frac{1}{4}J'\sqrt{1 - 4M_s^2} - \frac{3}{2}\Delta M_s^2. \quad (3.5)$$

We expand  $E_{var}$  up to the fourth order in  $M_s$  near the critical point and we find a Landau-type expression, given by

$$E_{var}/N = -\frac{1}{8}J'(\Delta + 2) + \frac{1}{2}(J' - 3\Delta)M_s^2 + \frac{1}{2}J'M_s^4. \quad (3.6)$$

### 3.3.2. Coupled cluster method

We apply a high-order CCM approach (for details see Chap.2) to the above model, and we choose the Néel state, in which the spins lie along the z-axis, to be the model state. Furthermore, we perform a rotation of the local axes of the up-pointing spins by 180° about the y axis, so that spins on both sublattices may be treated equivalent. After this transformation we have  $|\Phi\rangle = |\downarrow\rangle|\downarrow\rangle|\downarrow\rangle|\downarrow\rangle\cdots$ . Using the lattice symmetries, we have now to find all different possible configurations with respect to the point and space group symmetries of both the lattice and Hamiltonian with up to  $n$  spins spanning a range of no more than  $n$  adjacent lattice sites (LSUB $n$  approximation, Sec. (2.2.3)) and these are referred to as the fundamental configurations.

The Hamiltonian of Eq.(3.1) has four lattice point-group symmetries namely two rotational operations (0°, 180°) and two reflections (along the  $x$ - and  $y$ -axes), defined by:

$$\begin{aligned} x &\rightarrow x, y \rightarrow y; & x &\rightarrow -(x+1), y \rightarrow -y, \\ x &\rightarrow x, y \rightarrow -y; & x &\rightarrow -(x+1), y \rightarrow y. \end{aligned}$$

The rotation of 180° and the reflection along the  $y$ -axis are connected by a shift of ( $\hat{x} = (1, 0)$ ). To improve the results it is useful to extrapolate the 'raw' CCM-LSUB $n$  results to the limit  $n \rightarrow \infty$ . In order to determine the critical point  $J'_c$  where  $M_s(\infty)$  vanishes we use the extrapolation scheme of Eq. (2.43). The values for  $J'_c$  obtained by extrapolation of the LSUB $n$  results for  $M_s$  are, however, found to be slightly too large [18]. We may also consider the inflection points of the  $M_s(J')$  curve for the LSUB $n$  approximation, assuming that the true  $M_s(J')$  curve will have a negative curvature up to the critical point. We might expect that (for increasing  $n$ ) the inflection point  $J'_{inf}$  approaches the critical point  $J'_c$ . Thus determining the inflection points for the LSUB $n$  approximation again we can extrapolate to the limit

$n \rightarrow \infty$  using a scaling law of Eq. (2.43) and interpret  $J'_{inf}(\infty)$  as the critical value  $J'_c$ .

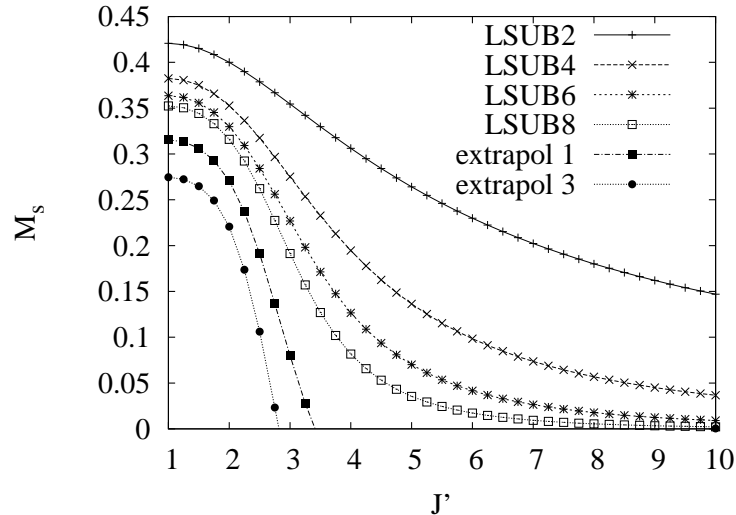


**Figure 3.2.:** Sublattice magnetization  $M_s$  versus  $J'$  obtained by CCM LSUB $n$  with  $n = 2, 4, 6, 8$  for  $\Delta = 1$  and its extrapolated values to  $n \rightarrow \infty$  using two different extrapolation schemes, namely according to Eq. (2.43)(extrapol 1) and to Eq. (2.45) (extrapol 3).

To illustrate the behaviour of the order parameter's dependence on  $J'$  we present  $M_s(J')$  calculated by CCM (Fig. 3.2, 3.3) and the resulting extrapolated values for a particular values of Ising anisotropy  $\Delta = 1, 2$ . For the isotropic Heisenberg case ( $\Delta = 1$ ) [18] the critical value  $J'_c = 3.4$  predicted by extrapolation of LSUB $n$  results according to Eq. (2.43) is found to be slightly large. But the results of inflection point  $J'_c = J'_{inf}(\infty) = 2.54$  are in good agreement with results of series expansions, exact diagonalization and quantum Monte Carlo(QMC) [18, 19, 122]. To get a better estimation for the critical value we use extrapolation scheme Eq. (2.45) for the order parameter and we find  $J'_c = 2.8$ (see Fig. 3.2) which is indeed in a better agreement with the results obtained by other approximations [18, 19, 122].

From the extrapolated order parameters one gets the critical values for  $\Delta = 2$ :  $J'_c = 6.46$  (CCM) and  $J'_c = 4.97$  (ED). The mean-field value is  $J'_c = 6$ . The inflection points of the  $M_s(J')$  curves in Fig. 3.3 are  $J'_{inf}(n) = 5.57$  (LSUB2), 5.42 (LSUB4), 5.26 (LSUB6), 5.11 (LSUB8) leading to an extrapolated value of  $J'_c = J'_{inf}(\infty) = 4.66$ . As mentioned above, the extrapolation of the CCM results of the order parameter tends to overestimate the critical value and yields the largest  $J'_c$ . This is connected with the change of the curvature in the  $M_s$ - $J'$  curve in the vicinity of the critical point, cf. Fig. 3.3. Therefore the critical value  $J'_c$  taken from the inflection points seems to be more realistic. Obviously, the difference in  $J'_{inf}$  between the LSUB $n$  approximations is small and the extrapolated value is quite close to the value for LSUB8. This statement holds for all values of  $\Delta$ . E.g. for  $\Delta = 4$  one finds  $J'_{inf} = 10.37$

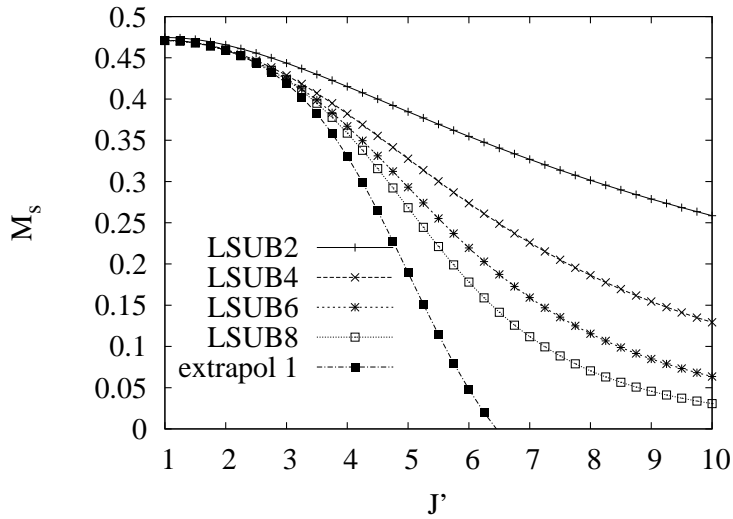


**Figure 3.3.:** Sublattice magnetization  $M_s$  versus  $J'$  for  $\Delta = 2$  using coupled cluster method (CCM), see Chap.2.

(LSUB2), 10.29 (LSUB4), 10.13 (LSUB6), 9.94 (LSUB8) leading to an extrapolated value of  $J'_c = J'_{inf}(\infty) = 9.41$ .

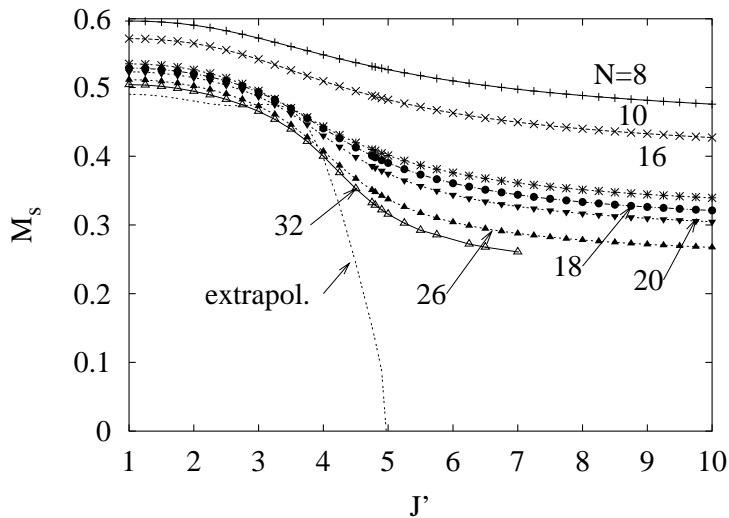


**Figure 3.4.:** Order parameter versus  $J'$  for  $\Delta = 2$  using exact diagonalization of finite lattices of different sizes  $N$ , see text.

### 3.3.3. Exact diagonalization

In addition to the variational mean-field approach and the CCM we use ED to calculate the order parameter, see Fig. 3.4. We consider finite square lattices of  $N =$

8, 10, 16, 18, 20, 26, 32 sites and employ periodic boundary conditions. The relevant order parameter for finite systems is the square of the sublattice magnetization  $M_s^2$ , here defined as  $M_s^2 = \langle [\frac{1}{N} \sum_{i=1}^N \tau_i \mathbf{s}_i]^2 \rangle$  with the staggered factor  $\tau_{i \in A} = +1$ ,  $\tau_{i \in B} = -1$ . For the finite-size scaling of  $M_s^2$  we use the standard three-parameter formula [126–129]  $M_s^2(N) = M_s^2(\infty) + c_1 N^{-1/2} + c_2 N^{-1}$ . The critical value  $J'_c$  is that point where  $M_s^2(\infty)$  vanishes.

### 3.3.4. Phase diagram

Our results for the critical point  $J'_c(\Delta)$  obtained by MFA, CCM and ED are collected in Fig. 3.5. We find that the CCM results obtained by the extrapolation of the order parameter are in good agreement with the MFA data. On the other hand, there is an excellent agreement between the CCM results obtained by the extrapolation of the inflection points and the ED results obtained by the extrapolation of the order parameter. Clearly we see indications for a linear increase in  $J'_c$  as predicted by mean-field theory. We mention that the curves shown in Fig. 3.5 cannot be extrapolated to  $\Delta < 1$ . Similar to the effect of the Ising anisotropy ( $\Delta > 1$ ) one rather expects an increase of  $J'_c$  due to XY anisotropy, i.e. for  $0 \leq \Delta < 1$ . Indeed for the pure XY  $J - J'$  model ( $\Delta = 0$ ) the critical value was estimated to  $J'_c = 4.56J$  [121]. In summary,

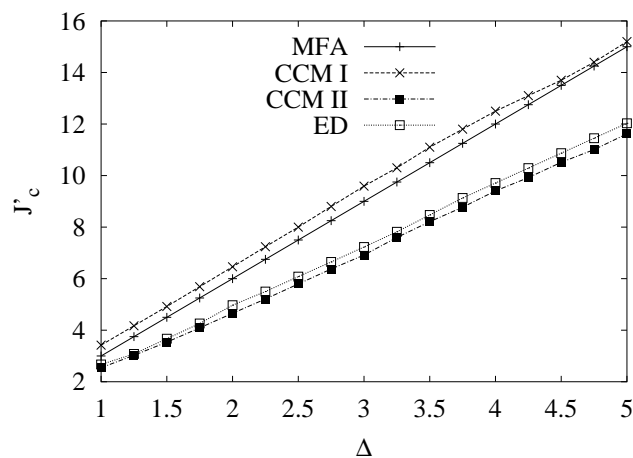


**Figure 3.5.:** The critical points  $J'_c$  versus anisotropy parameter  $\Delta$  using mean-field approach (MFA), CCM with extrapolation of the order parameter (CCM I), CCM with extrapolation of the inflection points (CCM II) and exact diagonalization (ED).

we have studied the zero-temperature magnetic ordering in a square-lattice spin-half anisotropic Heisenberg (XXZ) model with two kinds of nearest-neighbor exchange bonds  $J$  and  $J'$ , see Fig. 3.1. In particular we discuss the influence of the Ising anisotropy  $\Delta$  on the position of the quantum critical point  $J'_c$  separating the phase with semi-classical Néel order ( $J' < J'_c$ ) and the quantum paramagnetic phase without magnetic long-range order ( $J' > J'_c$ ). For this we calculate the order parameter within a

variational mean-field approach, the coupled cluster method and exact diagonalization of finite lattices up to  $N = 32$  sites. We find in good approximation a linear relation  $J'_c(\Delta) \propto \alpha\Delta$  ( $\Delta \geq 1$ ) with  $\alpha \sim 2.3 \dots 3.0$ . This result can be attributed to the reduction of quantum spin fluctuations with increasing Ising anisotropy. In the pure Ising limit ( $\Delta \rightarrow \infty$ ) the only remaining  $z-z$  terms in the Hamiltonian (3.1) commute with each other, i.e. no quantum spin fluctuations are present and, consequently, the critical point disappears in the pure Ising limit.

### 3.4. INFLUENCE OF THE SPIN QUANTUM NUMBER

In this section we study the ground state phase transition between a Néel ordered phase and a dimerized singlet phase of the model(3.1) with spin quantum number  $s = 1/2, 1, 3/2$  and  $2$  using a variational mean-field like approach (MFA), the coupled cluster method (CCM) and exact diagonalization (ED) of finite systems. We set  $J = 1$ ,  $\Delta = 1$  and consider  $J' \geq 1$  as the parameter of the model.

#### 3.4.1. Variational mean-field approach (MFA)

We set  $J = 1$ ,  $\Delta = 1$  and consider  $J' \geq 1$  as the parameter of the model. Using the MFA we calculate the ground-state magnetic order parameter of the  $J$ - $J'$  model (3.1). For the spin half HAFM this approach has been successfully applied to bilayer systems [16], to the isotropic [3, 18] and anisotropic [91]  $J$ - $J'$  model on the square lattice and on the  $1/5$  depleted square lattice for  $\text{CaV}_4\text{O}_9$  [1], but also on the strongly frustrated HAFM on the star lattice [130]. In this section we extend the basic ideas of this approach to higher spin quantum numbers  $s = 1, 3/2$  and  $2$ . We start with the two uncorrelated mean-field like states, namely the Néel state  $|\phi_{MF_1}\rangle = | +s\rangle | -s\rangle | +s\rangle | -s\rangle \dots$  and the dimerized rotationally invariant singlet product state (valence-bond state)  $|\phi_{MF_2}\rangle = \prod_{\langle ij \rangle} |\{i, j\}_s\rangle$ , where the product runs over all  $J'$  bonds, cf. (3.1).  $|\{i, j\}_s\rangle$  in  $|\phi_{MF_2}\rangle$  is a singlet state of two spins  $s$ , i.e. we have

$$|\{i, j\}_{s=1/2}\rangle = \frac{1}{\sqrt{2}} \left[ \left| +\frac{1}{2} \right\rangle \left| -\frac{1}{2} \right\rangle - \left| -\frac{1}{2} \right\rangle \left| +\frac{1}{2} \right\rangle \right] \quad (3.7)$$

$$|\{i, j\}_{s=1}\rangle = \frac{1}{\sqrt{3}} \left[ \left| +1 \right\rangle \left| -1 \right\rangle - \left| 0 \right\rangle \left| 0 \right\rangle + \left| -1 \right\rangle \left| +1 \right\rangle \right] \quad (3.8)$$

$$|\{i, j\}_{s=3/2}\rangle = \frac{1}{2} \left[ \left| +\frac{3}{2} \right\rangle \left| -\frac{3}{2} \right\rangle - \left| +\frac{1}{2} \right\rangle \left| -\frac{1}{2} \right\rangle + \left| -\frac{1}{2} \right\rangle \left| +\frac{1}{2} \right\rangle - \left| -\frac{3}{2} \right\rangle \left| +\frac{3}{2} \right\rangle \right] \quad (3.9)$$

$$|\{i, j\}_{s=2}\rangle = \frac{1}{\sqrt{5}} \left[ \left| +2 \right\rangle \left| -2 \right\rangle - \left| +1 \right\rangle \left| -1 \right\rangle + \left| 0 \right\rangle \left| 0 \right\rangle - \left| -1 \right\rangle \left| +1 \right\rangle + \left| -2 \right\rangle \left| +2 \right\rangle \right]. \quad (3.10)$$



In order to describe the transition between both states we consider for the different spin quantum numbers respective uncorrelated product trial states of the form

$$|\Psi_{var}^{s=1/2}\rangle = \prod_{\langle ij \rangle_2} \frac{1}{\sqrt{1+a^2}} \left[ \left| +\frac{1}{2} \right\rangle \left| -\frac{1}{2} \right\rangle - a \left| -\frac{1}{2} \right\rangle \left| +\frac{1}{2} \right\rangle \right] \quad (3.11)$$

$$|\Psi_{var}^{s=1}\rangle = \prod_{\langle ij \rangle_2} \frac{1}{\sqrt{1+b_1^2+b_2^2}} \left[ \left| +1 \right\rangle \left| -1 \right\rangle - b_1 \left| 0 \right\rangle \left| 0 \right\rangle + b_2 \left| -1 \right\rangle \left| +1 \right\rangle \right] \quad (3.12)$$

$$|\Psi_{var}^{s=3/2}\rangle = \prod_{\langle ij \rangle_2} \frac{1}{\sqrt{1+c_1^2+c_2^2+c_3^2}} \left[ \left| +\frac{3}{2} \right\rangle \left| -\frac{3}{2} \right\rangle - c_1 \left| +\frac{1}{2} \right\rangle \left| -\frac{1}{2} \right\rangle \right. \\ \left. + c_2 \left| -\frac{1}{2} \right\rangle \left| +\frac{1}{2} \right\rangle - c_3 \left| -\frac{3}{2} \right\rangle \left| +\frac{3}{2} \right\rangle \right] \quad (3.13)$$

$$|\Psi_{var}^{s=2}\rangle = \prod_{\langle ij \rangle_2} \frac{1}{\sqrt{1+d_1^2+d_2^2+d_3^2+d_4^2}} \left[ \left| +2 \right\rangle \left| -2 \right\rangle - d_1 \left| +1 \right\rangle \left| -1 \right\rangle \right. \\ \left. + d_2 \left| 0 \right\rangle \left| 0 \right\rangle - d_3 \left| -1 \right\rangle \left| +1 \right\rangle + d_4 \left| -2 \right\rangle \left| +2 \right\rangle \right], \quad (3.14)$$

where in the two-spin states  $|n\rangle|m\rangle$  the first bra vector belongs to site  $i$  and the second to site  $j$  of a  $J'$  bond. The trial wavefunctions depend on the variational parameters  $a$ ;  $b_1, b_2$ ;  $c_1, c_2, c_3$ ;  $d_1, d_2, d_3, d_4$  and interpolate between the valence-bond state  $|\phi_{MF_2}\rangle$  realized for  $a = 1$ ;  $b_1 = b_2 = 1$ ;  $c_1 = c_2 = c_3 = 1$ ;  $d_1 = d_2 = d_3 = d_4 = 1$  and the Néel state  $|\phi_{MF_1}\rangle$  for  $a = 0$ ;  $b_1 = b_2 = 0$ ;  $c_1 = c_2 = c_3 = 0$ ;  $d_1 = d_2 = d_3 = d_4 = 0$ , respectively. The ground-state energy per site  $e_{var}^s = \langle \Psi_{var}^s | H | \Psi_{var}^s \rangle / N$  is calculated as

$$e_{var}^{s=1/2}(a) = -\frac{J'}{2} \frac{a + \frac{1}{4}(1+a^2)}{1+a^2} - \frac{3}{2} \frac{(1-a^2)^2}{4(1+a^2)^2} \quad (3.15)$$

$$e_{var}^{s=1}(b_1, b_2) = -\frac{J'}{2} \frac{2b_1 + 2b_1b_2 + 1 + b_2^2}{1+b_1^2+b_2^2} - \frac{3}{2} \frac{(1-b_2^2)^2}{(1+b_1^2+b_2^2)^2} \quad (3.16)$$

$$e_{var}^{s=3/2}(c_1, c_2, c_3) = -\frac{J'}{2} \frac{3c_1 + 4c_1c_2 + 3c_2c_3 + \frac{1}{4}(9+c_1^2+c_2^2+9c_3^2)}{1+c_1^2+c_2^2+c_3^2} \\ - \frac{3}{2} \frac{(3+c_1^2-c_2^2-3c_3^2)^2}{4(1+c_1^2+c_2^2+c_3^2)^2} \quad (3.17)$$

$$e_{var}^{s=2}(d_1, d_2, d_3, d_4) = -\frac{J'}{2} \frac{4d_1 + 6d_1d_2 + 6d_2d_3 + 4d_3d_4 + d_1^2 + 4 + d_3^2 + 4d_4^2}{1+d_1^2+d_2^2+d_3^2+d_4^2} \\ - \frac{3}{2} \frac{(2+d_1^2-d_3^2-2d_4^2)^2}{(1+d_1^2+d_2^2+d_3^2+d_4^2)^2}. \quad (3.18)$$

The relevant order parameter describing the Néel order is the sublattice magnetization  $M = \langle \Psi_{var}^s | s_{i \in A}^z | \Psi_{var}^s \rangle$ . Using Eqs. (3.11), (3.12), (3.13), (3.14) we obtain

$$M_{s=1/2}(a) = \frac{1 - a^2}{2 + 2a^2} \quad (3.19)$$

$$M_{s=1}(b_1, b_2) = \frac{1 - b_2^2}{1 + b_1^2 + b_2^2} \quad (3.20)$$

$$M_{s=3/2}(c_1, c_2, c_3) = \frac{3 + c_1^2 - c_2^2 - 3c_3^2}{2(1 + c_1^2 + c_2^2 + c_3^2)} \quad (3.21)$$

$$M_{s=2}(d_1, d_2, d_3, d_4) = \frac{2 + d_1^2 - d_3^2 - 2d_4^2}{1 + d_1^2 + d_2^2 + d_3^2 + d_4^2}. \quad (3.22)$$

We minimize  $E = \langle \Psi_{var} | H | \Psi_{var} \rangle$  with respect to the variational parameters. As a result we obtain an analytic expression for  $a$  in the case of  $s = 1/2$ , but a set of two, three and four coupled nonlinear equations for  $s = 1, 3/2$  and  $2$  to determine the variational parameters. As reported in [3, 18] the sublattice magnetization for  $s = 1/2$  is  $M_{s=1/2}(J') = \frac{1}{2} \sqrt{1 - (J'/3)^2}$  for  $J' \leq 3$  but zero for  $J' > 3$ . Furthermore, one can express the ground-state energy as a Landau-type function of  $M$ ,  $e_{var}^{s=1/2} = -\frac{3}{8}J' + \frac{1}{2}(J' - 3)M^2 + \frac{1}{2}J'M^4$ , indicating the molecular field-like nature of the approach. For  $s = 1, 3/2$  and  $2$  we have to solve the corresponding set of nonlinear equations numerically. We show  $M(J')$  in Fig. 3.6.  $M(J')$  vanishes at a critical point  $J'_c = 3$  ( $s = 1/2$ ),  $J'_c = 8$  ( $s = 1$ ),  $J'_c = 15$  ( $s = 3/2$ ),  $J'_c = 24$  ( $s = 2$ ), respectively. The corresponding critical index is the mean-field index  $1/2$ .

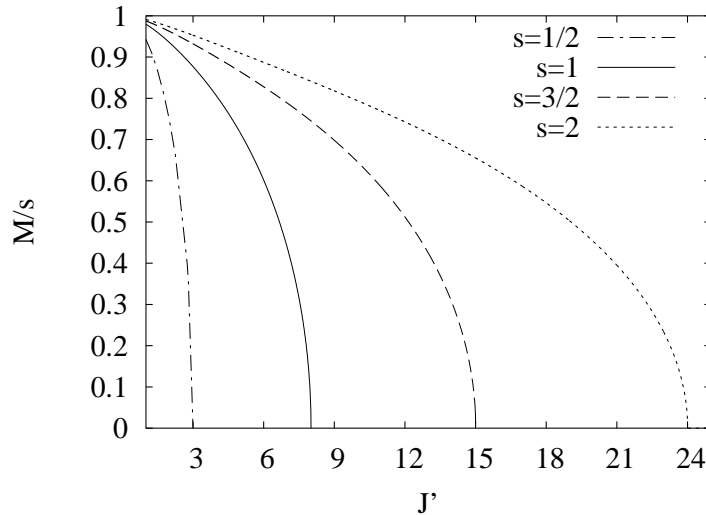


**Figure 3.6.:** Sublattice magnetization  $M/s$  versus  $J'$  calculated by the variational mean-field like approach (MFA), see text.

The sequence of critical points for  $s = 1/2, \dots, 2$  are precisely described by  $J_c(s) =$

$\frac{4}{3}s(s+1)(z-1)$ , where  $z = 4$  is the coordination number of the square lattice. Although we do not have results for  $s > 2$ , we argue that due to the systematic character of the MFA approach it seems to be likely that this expression is also valid for  $s > 2$ .

### 3.4.2. Coupled cluster method

In principle it is possible to apply the CCM for arbitrary spin quantum number  $s$ . However, within the used SUB $n$ - $n$  (Sec. 2.2.3) approximation scheme for higher  $s$  additional problems appear, namely

(i) the number of fundamental configurations (lattice animals)  $N_F$  increases with  $s$ , which makes the calculations on a certain level of approximation  $n$  more ambitious and

(ii) the total number of basis states grows drastically with  $s$  according to  $s^N$  and as a consequence the SUB $n$ - $n$  approximation may become less reliable.

While the latter point is irrelevant for systems where the quantum ground state is close to the reference state (i.e. in our model in the case of well-pronounced Néel order) it becomes relevant if the quantum ground state is far from the reference state (i.e., in our model when Néel order breaks down). Hence the results for higher spin quantum numbers must be taken with extra care. We have calculated CCM results within the SUB $n$ - $n$  approximation for  $n = 2, 4, 6$  for  $s = 1/2, 1, 3/2$  and  $2$ . For spin  $1/2$  results for  $n = 8$  are also available (see [18, 91]). First we report again the values for  $J'_c$  for spin  $s = 1/2$  (see also [18, 91] and Sec. 3.3.2). The extrapolation of the SUB $n$ - $n$  data for  $M$  with  $n = 2, 4, 6$  as described above leads to  $J'_c \approx 3.5$ . However, as discussed above the extrapolation of the order parameter tends to overestimate  $J'_c$  (note that  $J'_c$  obtained this way is even larger than the value found within MFA) and the extrapolation of the inflection point is favorable. We found as inflection points of the  $M_s(J')$  curves  $J'_{inf}(n) = 3.60$  (SUB2-2),  $3.33$  (SUB4-4),  $3.13$  (SUB6-6) leading to an extrapolated value of  $J'_c = J'_{inf}(\infty) = 2.56$ . We mention that the consideration of SUB8-8 data leads to a slight modification of  $J'_c$  to  $J'_c = J'_{inf}(\infty) = 2.54$ , only.

We now consider the case  $s = 1$ , where the results for the order parameter  $M$  are given in Fig. 3.7. Clearly we see the weakening of the magnetic order by increasing  $J'$ . The extrapolation of the SUB $n$ - $n$  data for  $M$  with  $n = 2, 4, 6$  leads to  $J'_c \approx 11.7$ , i.e. we get the same tendency as for the variational MFA, that  $J'_c$  increases with  $s$ . Again the extrapolation of the order parameter leads to an overestimation of  $J'_c$ . This overestimation is connected with the change in the sign of curvature of  $M(J')$  seen in Fig. 3.7. The favorable extrapolation of the inflection points leads to  $J'_c = J'_{inf}(\infty) \approx 6.4$ , where the inflection points for the different levels of SUB $n$ - $n$  approximations are  $J'_{inf}(n = 2) = 3.93$ ,  $J'_{inf}(n = 4) = 6.04$ ,  $J'_{inf}(n = 6) = 6.36$ .

Finally, we consider spin  $s = 3/2$  and  $s = 2$ . The results for the extrapolated sublattice magnetization for spin values  $s = 1/2, 1, 3/2$  and  $2$  using SUB $n$ - $n$  approximation for  $n = 2, 4, 6$  are shown in Fig. 3.8. Evidently the sublattice magnetization  $M/s$  increases with  $s$  demonstrating the decreasing influence of quantum fluctuations with

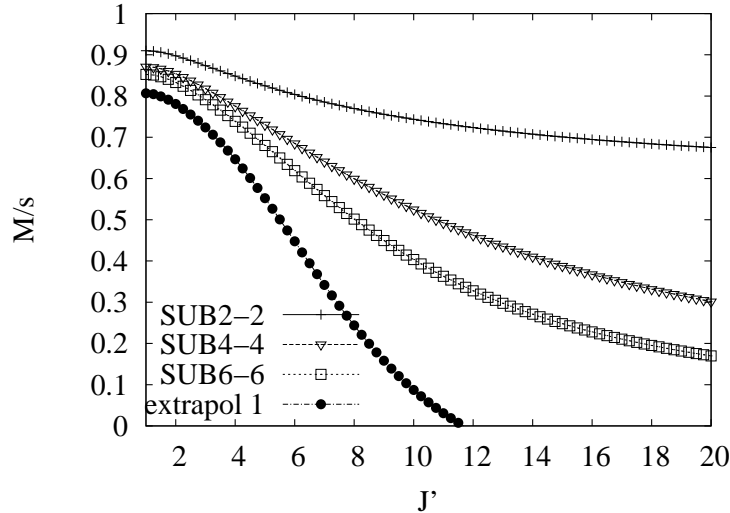


**Figure 3.7.:** Sublattice magnetization  $M/s$  versus  $J'$  for spin quantum number  $s = 1$  using coupled cluster method (CCM)

**Table 3.1.:** CCM results for the ground state of the Heisenberg antiferromagnet on the square lattice with spin quantum number  $s = 3/2$  and  $s = 2$  using the  $\text{SUB}n-n$  approximation with  $n = \{2, 4, 6\}$ . Note that  $N_F$  indicates the number of fundamental clusters at each level of approximation. For comparison we present the results of the second-order spin wave theory (SWT) [131].

	$S = 3/2$			$S = 2$		
	$N_F$	$E_g/N$	$M/S$	$N_F$	$E_g/N$	$M/S$
SUB2-2	1	-4.943927	0.936174	1	-8.593510	0.950368
SUB4-4	15	-4.976427	0.910266	15	-8.633108	0.93109
SUB6-6	461	-4.982685	0.89816	461	-8.640356	0.922284
SUB $\infty$	-	-4.9878	0.8687	-	-8.6461	0.9011
SWT	-	-4.9862	0.8692	-	-8.6442	0.9018

growing spin quantum number. The critical value for  $s = 3/2$  is obtained as  $J'_c \approx 18.5$  which is again too large in comparison to the MFA result. The extrapolation of the inflection points leads to  $J'_c \approx 10.9$ . Note that we have calculated  $M$  using the CCM up to  $J' = 100$  for  $s = 2$ . However, we were unable to find a vanishing  $M$  (i.e., the critical value  $J'_c$  obtained by extrapolation of the order parameter would be larger than 100.) Results for the point of inflection of  $M$  were similarly contradictory, and so the results for the position of the phase transition point predicted by the CCM for  $s = 2$  are not included here.

We conclude that the CCM  $\text{SUB}n-n$  approximation is inappropriate to describe the quantum phase transition correctly for higher spin values (namely,  $s > 3/2$ ) at the levels of approximation currently available for present-day computers. However,

we do observe that the tendency for critical value  $J'_c$  to increase with growing  $s$  is observed using the CCM for  $s \leq 3/2$ , as expected. This problem of reliability might be resolved by going to higher orders of truncation index  $n$ , although we note that the computational problem is very difficult (e.g., with  $N_F = 108033$  for SUB8-8 for  $s = 3/2$ ) and so this is not considered here. We note that LSUB $n$  calculations do not place a restriction on the total number of spin flips used in the CCM correlation operators, although the fundamental clusters are restricted to remain within a locale defined by  $n$ . However, this again leads to an extremely large number of fundamental clusters even for low values of  $n$  and for higher spin quantum numbers, and so LSUB $n$  is not considered here. Mean-field model states (e.g., based on the variational states in Sec. 3) might also provide enhanced results for the CCM.

As a byproduct we also present in Table 5.1 the results for the sublattice magnetization  $M/s$  for higher spin values for the pure square lattices ( $J' = 1$ ), which are so far not calculated within CCM. We point out that for the pure square lattice the results for  $M$  are expected to be quite reliable, since the true quantum ground state is close to the reference state used as starting point. This is indeed confirmed by comparison with high precision second-order spin wave results [131] also presented in Table 5.1. We mention that due the reduced symmetry the number of fundamental configurations  $N_F$  increases in case of  $J' \neq J$ . For SUB6-6 we find  $N_F = 267, 1420, 1744, 1744$  for  $s = 1/2, 1, 3/2$  and  $2$ , respectively. Note that  $N_F$  for  $s = 3/2$  and  $s = 2$  is equal only up to SUB6-6 but differs for higher levels of approximation. For completeness we also give the sublattice magnetization for  $s = 1/2$ :  $M/s = 0.63$  (note that this value can be improved by also considering SUB8-8 for the extrapolation, which yields  $M/s = 0.62$  [89]) and for  $s = 1$ :  $M = 0.81$  (see also [132]).

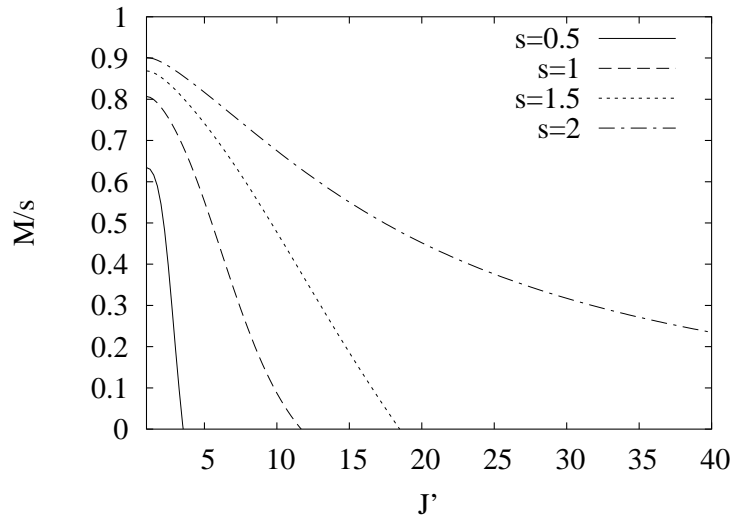


**Figure 3.8.:** Extrapolated sublattice magnetization  $M/s$  versus  $J'$  for various spin quantum numbers  $s$  using coupled cluster method (CCM)

### 3.4.3. Exact diagonalization

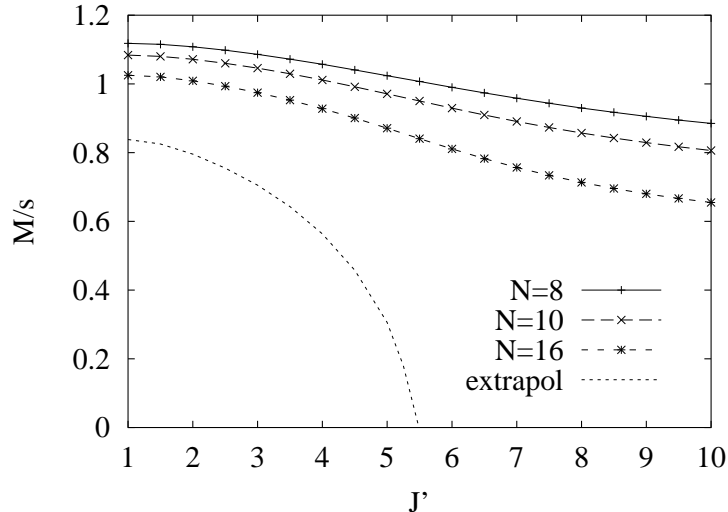


**Figure 3.9.:** Sublattice magnetization  $M/s$  versus  $J'$  for spin quantum number  $s = 1$  using exact diagonalization of finite lattices of  $N = 8, 10, 16$ , see text.

In order to compare with the MFA and the CCM results, we use the exact diagonalization Lanczos technique to calculate the order parameter for finite square lattices with periodical boundary conditions. We calculate the square of the sublattice magnetization  $M^2$  (see subsec. 3.3.3) For the finite-size scaling of  $M^2$  we use the standard three-parameter formula (see subsec. 3.3.3). The critical value  $J'_c$  is that point where  $M^2(\infty)$  vanishes. Again we are faced with the problem, that the method becomes less reliable for larger quantum numbers  $s$ . While for  $s = 1/2$  one can calculate the GS for the  $J$ - $J'$  model up to  $N = 32$  [18, 91, 121] sites one is restricted to lattices of up to  $N = 20$  for  $s = 1$ , up to  $N = 16$  for  $s = 3/2$  and up to  $N = 10$  for  $s = 3/2$ . Since for  $s = 2$  we have only two lattices ( $N = 10$  and  $N = 8$ ) with the full lattice symmetry, we do not consider  $s = 2$  within ED. To treat all three cases in a consistent way we consider only  $N = 8, 10, 16$  for  $s = 1/2, 1, 3/2$ . It is clear that the resulting finite-size extrapolation remains quite poor and allows only some qualitative conclusions. We present for illustration the results for the order parameter  $M$  for  $s = 1$  in Fig. 3.9. The critical values obtained by finite size extrapolation of  $M$  are:  $J'_c \approx 2.2$  for  $s = 1/2$ ,  $J'_c \approx 5.5$  for  $s = 1$  and  $J'_c \approx 10.1$  for  $s = 3/2$ . These data confirm the tendency found by MFA and CCM that the increase of  $J'_c$  with  $s$  is stronger than linear.

### 3.4.4. Phase diagram

To investigate the ground-state phase diagram of the 2D  $J$ - $J'$  model with general spin quantum number, we calculate the magnetic order parameter by means MFA, CCM, and ED. In particular, we have studied the influence of the spin quantum number  $s$

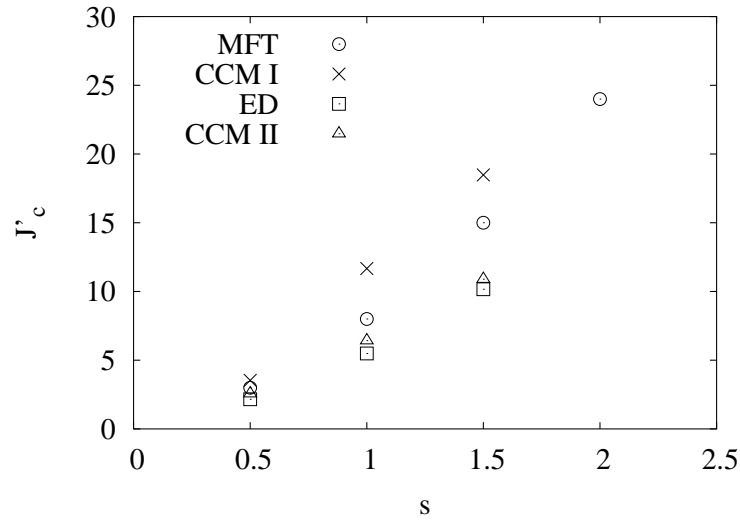


**Figure 3.10.:** The critical value  $J'_c$  versus spin quantum number  $s$  obtained by different methods. MFA: variational mean-field approach (see Sec. 3.4.1); CCM I: coupled cluster method (extrapolation of the order parameter, see Sec. 3.3.2); CCM II: coupled cluster method (extrapolation of the inflection point, see Sec. 3.3.2); ED: exact diagonalization (see Sec. 3.4.3).

on the quantum critical point  $J'_c$ . Our results for  $J'_c$  are presented in Fig. 3.10, and we note that a transition from a semi-classically Néel ordered phase to a magnetically disordered phase occurs at this point. Obviously, there is an increase of  $J'_c$  with  $s$  signaling the diminishing of quantum effects. We have presented evidence that the critical value  $J'_c$  increases with growing  $s$  according to  $J'_c \propto s(s+1)$ . We note that some of the results presented in this chapter are published in.<sup>1 2</sup>

<sup>1</sup>R. Darradi, J. Richter and S.E. Krüger, "The influence of Ising anisotropy on the zero-temperature phase transition in the square lattice spin-1/2 J-J' model" , J. Phys.: Condens. Matter **16**, 2681-2687 (2004)

<sup>2</sup>R. Darradi, J. Richter and J.J. Farnell, "Influence of the spin quantum number  $S$  on the zero-temperature phase transition in the square-lattice J-J' model" , J. Phys.: Condens. Matter **17**, 341-350 (2005)





## THE QUANTUM GROUND STATE PHASE DIAGRAM OF THE SHASTRY-SUTHERLAND MODEL

Quantum phase transitions between semiclassical magnetically ordered phases and magnetically disordered quantum phases which are driven by frustration attract much interest, see, e.g., Ref. [2]. In particular, frustration may lead to the breakdown of semiclassical Néel LRO in 2D quantum antiferromagnets. There are a variety of models which are known to exhibit the so-called frustration effects. A typical model is the Shastry-Sutherland antiferromagnet introduced in the eighties [74], which has special arrangement of frustrating next-nearest-neighbor  $J_2$  bonds on the square lattice, cf. Fig. 4.2. We note that for bonds of equal strength, i.e.,  $J_1 = J_2$ , the Shastry-Sutherland model is equivalent to a Heisenberg model on one of the eleven uniform Archimedean lattices [1]. Although the initial motivation to study this special frustrated square-lattice antiferromagnet is related to the existence of a simple singlet-product eigenstate (which becomes the ground state (GS) for strong frustration), the renewed interest in the last years was stimulated by the discovering of the new quantum phase in  $\text{SrCu}(\text{BO}_3)_2$  [14,75] which can be understood in terms of the Shastry-Sutherland model (see Fig. 4.1). Although the GS of this model in the limit of small frustration  $J_2$  and large  $J_2$  is well understood, the GS phase at moderate  $J_2$  is still a matter of discussion.

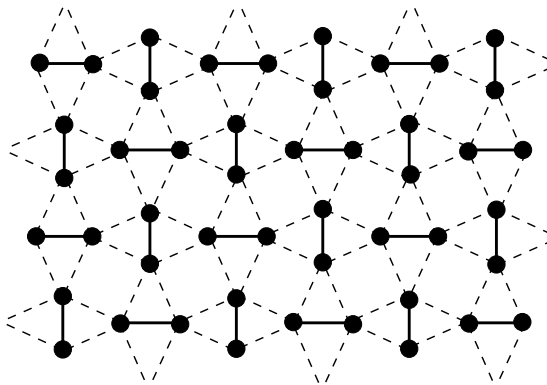


**Figure 4.1.:** Lattice structure of the  $\text{Cu}^{2+}$  spins closed circle of  $\text{SrCu}(\text{BO}_3)_2$ . The dashed and solid lines represent the nearest-neighbor bonds  $J_1$  and next-nearest-neighbor bonds  $J_2$  respectively.

## 4.1. MODEL

The Shastry-Sutherland model is a spin- $\frac{1}{2}$  Heisenberg model on a square lattice with antiferromagnetic nearest-neighbor bonds  $J_1$  and with one antiferromagnetic diagonal bond  $J_2$  in each second square (see Fig. 4.2). It is described by the Hamiltonian

$$H = J_1 \sum_{\langle i,j \rangle} s_i \cdot s_j + J_2 \sum_{\{i,k\}} s_i \cdot s_k, \quad (4.1)$$

where the operators  $s_i$  represent spin-half operators, i.e.,  $s_i = s(s+1)$  with  $s = 1/2$ . The sums over  $\langle i,j \rangle$  and  $\{i,k\}$  run over all nearest-neighbor bonds and over some of the next-nearest-neighbor bonds according to the pattern shown in Fig. 4.2. Due to the special arrangement of the  $J_2$  bonds the unit cell contains four sites. Therefore it is convenient to split the square lattice into four equivalent sublattices A, C, B and D as shown in Fig. 4.2. In what follows we set  $J_1 = 1$  and consider  $J_2 > 0$  as the parameter of the model.

## 4.2. THE CLASSICAL GROUND STATE

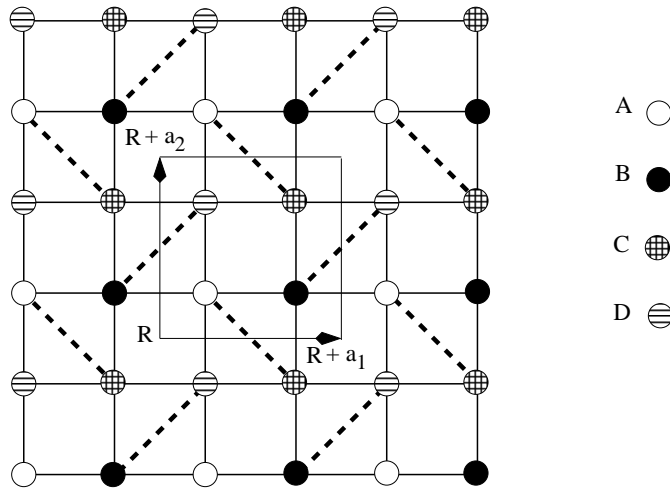


**Figure 4.2.:** Illustration of the Shastry-Sutherland model on the square lattice (Eq. (4.1)). The antiferromagnetic NN bonds  $J_1 = 1$  and NNN bonds  $J_2$  are represented by solid and dashed lines.

To discuss the influence the quantum fluctuations on the ground-state (GS) properties of the model we need to know the Classical GS of Eq. (4.1). The Classical spin (of length  $s$ ) sitting at cell  $R$  of the Bravais lattice on sublattice A, B, C, and D is given by:

$$\mathbf{S}_{R,n} = S \left[ \vec{e}_1 \cos(\vec{Q}\vec{R} + \varphi_n) + \vec{e}_2 \sin(\vec{Q}\vec{R} + \varphi_n) \right], \quad (4.2)$$

where  $\varphi_n$  is given by

$$\varphi_n = \begin{cases} \theta_{2,3,4} & \text{for } n = 2, 3, 4 \\ 0 & \text{for } n = 1, \end{cases} \quad (4.3)$$

and  $\vec{e}_1$  and  $\vec{e}_2$  are arbitrary orthogonal unit vectors, and  $\vec{Q}$  is spiral wave-vector. The spin orientations at A, B, C, and D lattice sites are defined by the angles  $0, \theta_2, \theta_3$  and  $\theta_4$  respectively. Using Eq. (4.2) the classical ground state energy is given by

$$\begin{aligned} E_{cl} = & J_1 N S^2 \left[ \cos(\theta_2) + \cos(\theta_4) + \cos(\vec{Q}\vec{a}_1 - \theta_2) + \cos(\vec{Q}\vec{a}_2 - \theta_4) + \cos(\theta_3 - \theta_2) \right] \\ & + J_1 N S^2 \left[ \cos(\vec{Q}\vec{a}_2 + \theta_2 - \theta_3) + \cos(\vec{Q}\vec{a}_1 + \theta_4 - \theta_3) + \cos(\theta_3 - \theta_4) \right] \\ & + J_2 N S^2 \left[ \cos(\vec{Q}\vec{a}_1 + \theta_4 - \theta_2) + \cos(\vec{Q}\vec{a}_2 - \theta_3) \right] \end{aligned} \quad (4.4)$$

where  $\vec{a}_1 = (1, 0)$  and  $\vec{a}_2 = (0, 1)$  are the Bravais lattice vectors. The numerical solution of  $\vec{Q}\vec{a}_1, \vec{Q}\vec{a}_2, \theta_2, \theta_3,$  and  $\theta_4$  correspond to the relations  $\theta_2 = \theta_4, \theta_3 = \vec{Q}\vec{a}_1,$  and  $\vec{Q}\vec{a}_2 = 0$ . We substitute the values of  $\theta_2 = \theta_4 = \pi + \phi, \vec{Q}\vec{a}_2 = 0,$  and  $\theta_3 = \vec{Q}\vec{a}_1 = 2\phi$  with  $\vec{Q} = (2\phi, 0)$  in Eq. (4.4) we get a simple form of classical energy which given by

$$E_{cl}/N S^2 = -8J_1 \cos(\phi) + 4J_2 \cos^2(\phi) - 2J_2. \quad (4.5)$$

By minimizing Eq. (4.5) with respect to the parameter  $\phi$  we find that the classical (i.e.,  $s \rightarrow \infty$ ) GS of the Shastry-Sutherland model is given by

$$\phi = \begin{cases} 0 & J_2/J_1 \leq 1 \\ \pi - \arccos(-J_1/J_2) & J_2/J_1 > 1 \end{cases}. \quad (4.6)$$

We note that for  $\phi = 0$  the spiral state becomes the collinear Néel state classically. The transition from the collinear Néel to noncollinear spiral state is of second order and takes place at  $J_2/J_1 = 1$ . We note further that there are only two different angles between interacting spins (see Fig. 4.3), namely,  $\phi + \pi$  for the  $J_1$  couplings and  $2\phi$  for the  $J_2$  couplings.

### 4.3. THE QUANTUM GROUND STATE

The quantum  $s = 1/2$  version of the model has been treated previously by various methods like Schwinger boson mean-field theory [133], exact diagonalization [75, 134], series expansions [15, 135–137], renormalization group [138] and also by a gauge-theoretical approach [139]. A recent review can be found in Ref. [140]. From these studies one knows that for small  $J_2 \leq J_1$  the physics of the quantum model is similar to that of the classical model, i.e., we have semi-classical Néel order. Furthermore, one knows already from the early work of Shastry and Sutherland [74] that for large  $J_2$  the quantum GS is a rotationally invariant product state of local pair singlets (so-

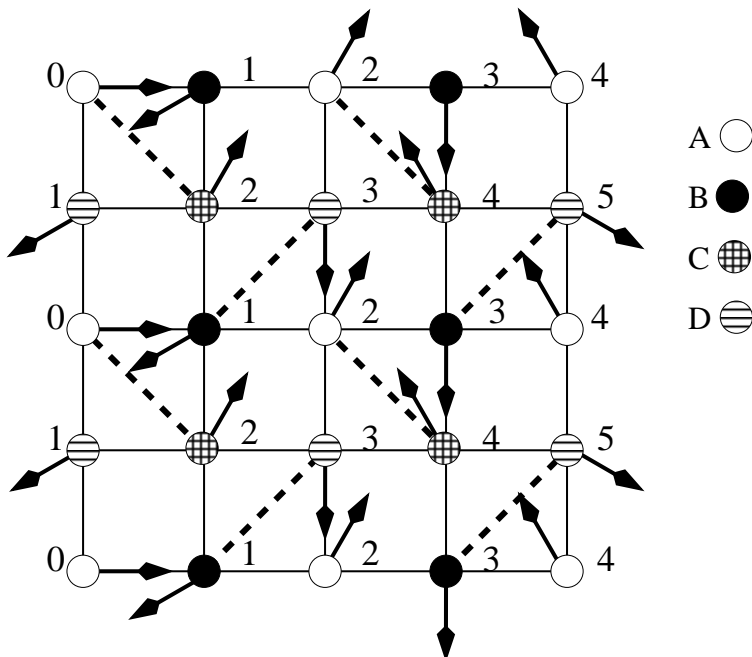


**Figure 4.3.:** Illustration of the Shastry-Sutherland model with antiferromagnetic NN bonds  $J_1 = 1$  (solid lines) and NNN bonds  $J_2$  (dashed lines), together with its classical spiral state. The spin orientations at lattice sites  $n$  are given by the angles  $\theta = n\phi_{\text{cl}}$ , where  $n = 0, 1, 2, \dots$ , and  $\phi_{\text{cl}}$  is the characteristic pitch angle of the classical spiral state. The state is shown for  $\phi_{\text{cl}} = 5\pi/6$  and  $n = 0, 1, \dots, 5$ .

called orthogonal-dimer state)  $|\Psi\rangle_{\text{dimer}} = \prod_{\{i,j\}_{J_2}} [|\uparrow_i\rangle|\downarrow_j\rangle - |\downarrow_i\rangle|\uparrow_j\rangle]/\sqrt{2}$ , where  $i$  and  $j$  correspond to those sites which cover the  $J_2$  bonds. The energy per site of this orthogonal-dimer state is  $E_{\text{dimer}}/N = -3J_2/8$ . It becomes the GS at around  $J_2^c \approx (1.44 \dots 1.49)J_1$  (see Table 2 in Ref. [140]). Note that such an orthogonal-dimer state can be observed also in corresponding one-dimensional and three-dimensional models [141–145]. The nature of the transition between the semi-classical Néel state and the orthogonal-dimer phase is still a matter of controversial discussion. In the region  $1.2J_1 \lesssim J_2 \lesssim 1.45J_1$  the main question is whether the system has an intermediate phase. A direct transition between the Néel phase and the orthogonal-dimer phase is favored in Refs. [75, 135, 136, 138], whereas in Refs. [133, 134, 137, 139] the existence of an intermediate phase is found. However, concerning the nature of this intermediate phase controversial results are reported, as candidates for the intermediate phase are quantum spiral phases [133, 139] or a plaquette or columnar singlet phases [134, 137] discussed.

To contribute to the solution of this open problem the CCM is an appropriate method, since it is one of the methods which can deal with spiral phases in quantum spin models. We apply a high-order CCM approach (for details see Chap. 2) to this model. We set the classical collinear Néel state ( $\phi = 0$ ) and noncollinear spiral state ( $\phi \neq 0$ ) to be the reference states  $|\Phi\rangle$ . We calculate the ground-state wave-

function,  $|\Psi\rangle = e^S|\Phi\rangle$ , within the LSUB $n$  approximation scheme. Using the canonical transformations of Eq. (2.10) the Hamiltonian(4.1) is then rewritten as

$$\begin{aligned}
H = & J_1 \sum_{\langle i,j \rangle}^N \left( \frac{1}{2} \sin \varphi_{i,j} [\hat{s}_i^+ \hat{s}_j^z - \hat{s}_i^z \hat{s}_j^+ + \hat{s}_i^- \hat{s}_j^z - \hat{s}_i^z \hat{s}_j^-] + \cos \varphi_{i,j} \hat{s}_i^z \hat{s}_j^z \right. \\
& + \frac{1}{4} (\cos \varphi_{i,j} + 1) [\hat{s}_i^+ \hat{s}_j^- + \hat{s}_i^- \hat{s}_j^+] + \frac{1}{4} (\cos \varphi_{i,j} - 1) [\hat{s}_i^+ \hat{s}_j^+ + \hat{s}_i^- \hat{s}_j^-] \left. \right) \\
& + J_2 \sum_{\{i,k\}}^N \left( \frac{1}{2} \sin \varphi_{i,k} [\hat{s}_i^+ \hat{s}_k^z - \hat{s}_i^z \hat{s}_k^+ + \hat{s}_i^- \hat{s}_k^z - \hat{s}_i^z \hat{s}_k^-] + \cos \varphi_{i,k} \hat{s}_i^z \hat{s}_k^z \right. \\
& \left. + \frac{1}{4} (\cos \varphi_{i,k} + 1) [\hat{s}_i^+ \hat{s}_k^- + \hat{s}_i^- \hat{s}_k^+] + \frac{1}{4} (\cos \varphi_{i,k} - 1) [\hat{s}_i^+ \hat{s}_k^+ + \hat{s}_i^- \hat{s}_k^-] \right), \quad (4.7)
\end{aligned}$$

where the angles  $\varphi_{i,j} \equiv \delta_j - \delta_i$ ,  $\varphi_{i,k} \equiv \delta_k - \delta_i$  between two nearest-neighbor and next-nearest-neighbor spins are  $\varphi_{i,j} = \pi + \phi$ ,  $\varphi_{i,k} = -2\phi$ , respectively, and  $s^\pm \equiv s^x \pm is^y$  are spin raising and spin lowering operators. We note that the reduction in the number of fundamental configurations can be made when the  $z$ -axis Néel model state is used in the CCM calculations. This comes about because, although the total uniform magnetisation  $s_T^z = \sum_i s_i^z$  (where  $s_i^z$  is defined with respect to a global quantisation axis and the sum on the index  $i$  runs over all lattice sites) is always a good quantum number independent of the model state used, only the  $z$ -axis Néel model state is an eigenstate of  $s_T^z$ . In contrast, the spiral state is not an eigenstate of  $s_T^z$ . Therefore, for the  $z$ -axis model state case one can explicitly conserve  $s_T^z$  by restricting the fundamental configurations to those which produce no change in  $s_T^z$  with respect to the  $z$ -axis Néel model state. This restriction, for example, reduces the number of the fundamental configurations retained in the LSUB4 approximation to LSUB8 if the  $z$ -axis Néel model state is employed in the CCM calculations.

We calculate the fundamental configurations numerically, and the results of the numbers of LSUB $n$  configurations for  $n \leq 8$  are given in Table. (5.1). By using parallel computing we are able to solve the 20892 equations of the CCM-LSUB8 approximation for the Néel reference state. However, for the spiral state the current limitations of computer power allow then solution of the CCM equations up to LSUB6, only.

To detect the existence of intermediate noncollinear spiral phase between collinear Néel -ordered and orthogonal-dimer phase, we calculate the GS energy as a function of  $J_2$  using as reference state a spiral state as sketched in Fig. 4.3. As quantum fluctuations may lead to a “quantum” pitch angle that is different from the classical case, we consider the pitch angle in the reference state as a free parameter. We then determine the “quantum” pitch angle  $\phi_{qu}$  by minimizing  $E_{\text{LSUB}m}(\phi)$  with respect to  $\phi$  in each order  $n$ . As for the classical model for small  $J_2$  the energy  $E_{\text{LSUB}m}(\phi)$  has its minimum at  $\phi_{qu} = 0$ , i.e., the quantum GS is the semi-classical collinear Néel state. Contrary to the classical case, this collinear quantum state can survive into the region  $J_2 > J_1$ , where classically it is already unstable. This effect is known as

**Table 4.1.:** Number of fundamental GS configurations of the LSUB $n$  approximation for the Shastry-Sutherland model using the Néel state ( $\phi = 0$ ) and the spiral state ( $\phi \neq 0$ ) as the CCM reference state.

LSUB $n$	Néel state: $\phi = 0$	spiral state: $\phi \neq 0$
2	1	12
4	35	248
6	794	6184
8	20892	166212

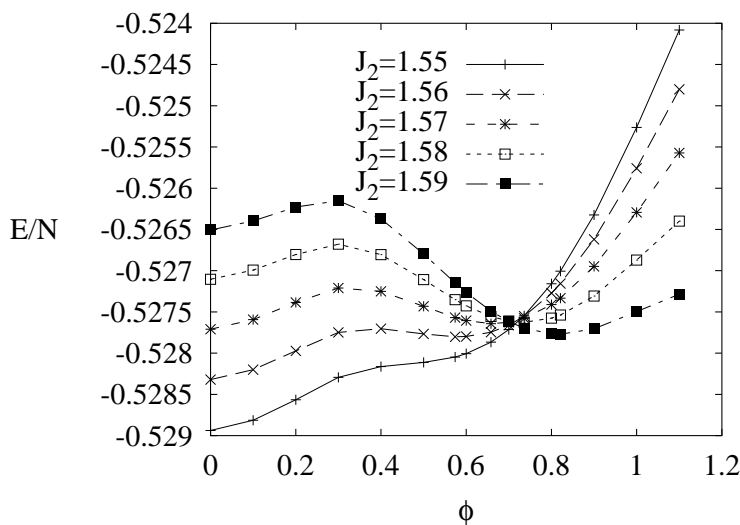


**Figure 4.4.:** Ground-state energy versus the pitch angle  $\phi$  within CCM-LSUB4 approximation for different values of  $J_2$  in the range  $1.55 \leq J_2 \leq 1.59$ .

*order from disorder* [146–148] and is widely observed in quantum spin systems, see, e.g., Refs. [18, 86]. For frustrating couplings  $J_2 \gtrsim 1.5J_1$  apart from the minimum at  $\phi = 0$  a second minimum at a finite  $\phi > 0$  emerges, which becomes the global minimum for strong enough  $J_2$ . This scenario illustrated in Fig. 4.4 is typical for a first-order transition, i.e., we find indications that quantum fluctuations may change the nature of the phase transition between the collinear Néel phase to the noncollinear spiral phase from a second-order classical transition to a first-order quantum transition. Note that a similar situation can be found in other frustrated spin systems [18, 20]. The “quantum” pitch angle  $\phi_{qu}$ , where  $E_{LSUBm}(\phi)$  has its global minimum, is shown in Fig. 4.5.  $\phi_{qu}$  shows a typical jump from  $\phi_{qu} = 0$  to a finite value. Our data clearly indicate that the quantum noncollinear spiral phase has lower energy than the collinear phase only for strong frustration  $J_2 \gtrsim 1.5J_1$ . Next we compare the energy of the orthogonal-dimer state  $|\Psi\rangle_{dimer}$  and the energy of the collinear quantum ground

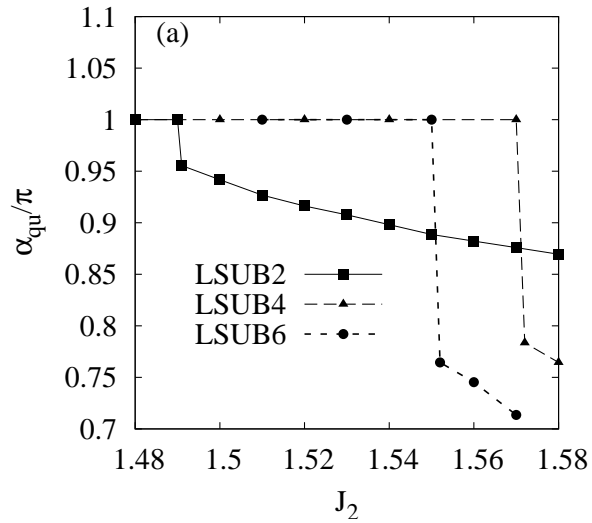


**Figure 4.5.:** The “quantum” pitch angle  $\phi_{qu}$  as a function of  $J_2$  calculated within CCM-LSUB $n$  approximation with  $n = 2, 4, 6$ .

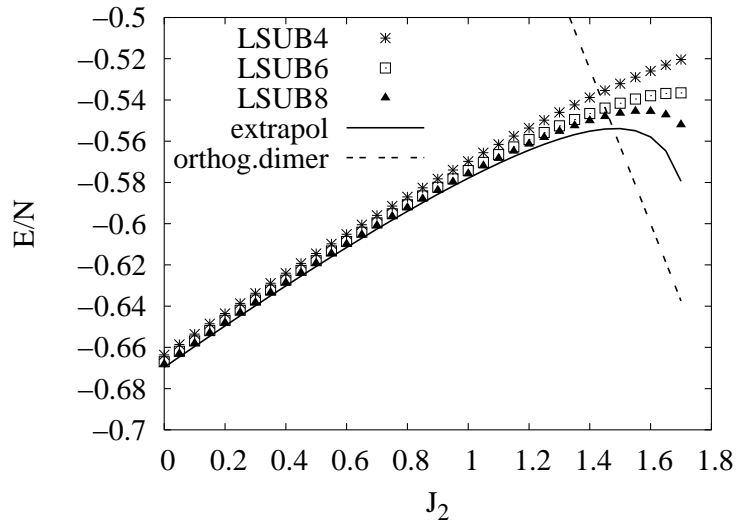


**Figure 4.6.:** The energy of (i) the collinear quantum ground state as function of  $J_2$  obtained by CCM-LSUB $n$  with  $n = 4, 6, 8$  and its extrapolated value to  $n \rightarrow \infty$ , see Eq. (2.42), and (ii) of the orthogonal-dimer state.

state (i.e. the reference state  $|\Phi_0\rangle$  is the Néel state), see Fig. 4.6. We can postpone the discussion of the question whether that quantum ground state possesses Néel LRO or not, since it is possible (starting from the Néel reference state) to calculate the energy up to high accuracy even in a parameter regime where the Néel order breaks

down due to quantum fluctuations, i.e. for a magnetically disordered state, see e.g. Refs. [18, 20, 87, 88, 91, 92]. Our results demonstrate, that the orthogonal-dimer state has lower energy than the collinear state for  $J_2 \gtrsim 1.477J_1$ .  $|\Psi\rangle_{dimer}$  remains the state of lowest energy also in the region where the noncollinear spiral state has lower energy than the collinear phase. We conclude that there is no intermediate spiral phase in the quantum model. Our estimate of the critical value  $J_2^d = 1.477J_1$  where the transition to the orthogonal-dimer phase takes place is in good agreement with other results, cf. Table 2 in Ref. [140]. So far we have discussed mainly the energy of competing GS phases. The last question we would like to discuss is the question of the stability of the Néel LRO in the frustrated regime. For that we calculate the order parameter (sublattice magnetization)  $M$  within the LSUB $n$  approximation scheme up to  $n = 8$  and extrapolate to  $n \rightarrow \infty$  using three variants of extrapolation as described in Sect. 3.3.2. The results are shown in Fig. 4.7. The extrapolated data clearly demonstrate that the LRO vanishes before the orthogonal-dimer state becomes the GS. The transition from Néel LRO to magnetic disorder is of second order. Hence we come to the second important statement that there exists an intermediate magnetically disordered phase. Within the used CCM scheme starting from the Néel reference state we are able to discuss the nature of the magnetically disordered state preceding the orthogonal-dimer state (see. Sec. 4.4). Though there are some first attempts to develop a CCM formalism for magnetically disordered valence bond phases [149], a high level of approximation is reached currently only starting with Néel or spiral reference states.

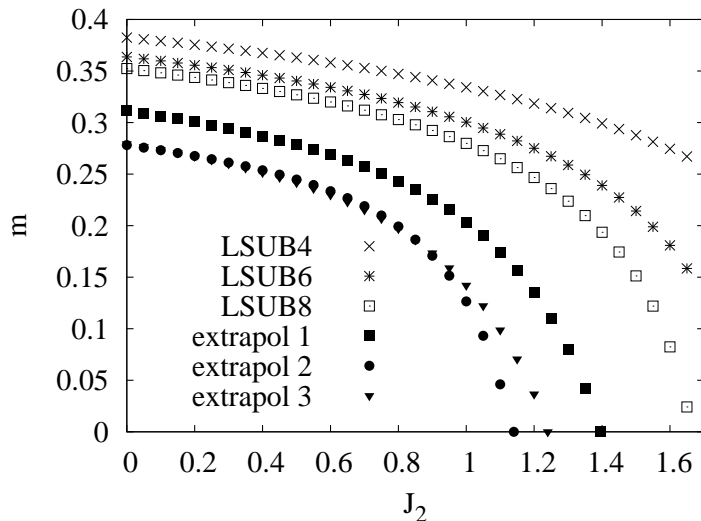


**Figure 4.7.:** Sublattice magnetization  $M$  versus  $J_2$  obtained by CCM-LSUB $n$  with  $n = 4, 6, 8$  and its extrapolated values to  $n \rightarrow \infty$  using two different extrapolation schemes, namely according to Eq. (2.43) (extrapol 1), Eq. (2.44) (extrapol 2) and Eq. (2.45) (extrapol 3)



Obviously, the critical value where  $J_2^c$  the Néel LRO breaks down depends on the used extrapolation formula. The extrapolation according to Eq. (2.43) leads accurate results for  $M$  in the unfrustrated ( $J_2 = 0$ ) square-lattice limit and yields  $J_2^c \sim 1.39J_1$ . As discussed in Sect. 3.3.2 this extrapolation scheme tends to overestimate the region of magnetic LRO and indeed the value  $J_2^c/J_1 = 1.39$  is significantly larger than the corresponding value calculated by series expansion, see Table 2 in Ref. [140]. The extrapolation according to Eq. (2.44) with a variable exponent  $c_2$  is less accurate in the unfrustrated limit but it seems to be more appropriate to find the position of the critical point  $J_2^c$ , since the scaling behavior might be changed at the critical point. We get  $J_2^c \sim 1.14J_1$  which fits well to the corresponding value calculated by series expansion. In addition to the extrapolation of Eq. (2.44) we use the three-term scheme of eq. (2.45) and we get  $J_2^c \sim 1.24J_1$ .

#### 4.4. THE PLAQUETTE VALENCE BOND ORDER IN THE NONMAGNETIC PHASE

The nature of the nonmagnetic GS in the region  $1.14J_2 \lesssim J_2 \lesssim 1.477J_2$  is a matter of some controversy in the literature. A favored candidate is a plaquette singlet phase. [134,137] To address this question we follow similar reasoning to that used in Ref. [47] and consider the response of the spin system to a field  $F_p$  given by

$$F_p = \delta \sum_{x,y} [(-1)^x \mathbf{s}_{x,y} \cdot \mathbf{s}_{x+1,y} + (-1)^y \mathbf{s}_{x,y} \cdot \mathbf{s}_{x,y+1}], \quad (4.8)$$

where  $x, y$  are components (integer numbers) of the lattice vectors of the square lattice. This field corresponds to a plaquette valence bond order (as illustrated in the inset of Fig. 4.8), which breaks the lattice symmetry. Thus, we use the CCM with the Néel state as reference state to calculate the energy per site  $e(J_1, J_2, \delta)$  for  $H + F_p$ , namely the Hamiltonian of Eq. (2.1) perturbed by the additional term of Eq. (4.8). The susceptibility  $\chi_p$  is then defined by Eq. (2.41) [47].

In Fig. 4.6 we present the results for the inverse susceptibility,  $1/\chi_p$ , as a function of  $J_2$ . The extrapolation to  $n \rightarrow \infty$  is performed using an extrapolation scheme with leading power  $1/n$  as in Eq. (2.43). Clearly, in the magnetically ordered Néel phase  $\chi_p$  is finite as it should be. However, close to the transition to the magnetically disordered phase at  $J_2^c \approx 1.14J_1$  the susceptibility becomes very large and diverges at  $J_2 \approx 1.26J_1$ , which is close to  $J_2^c$ .

#### 4.5. CONCLUSIONS

In conclusion, we have studied the GS phase diagram of the spin half Shastry-Sutherland antiferromagnet making use of high-order coupled cluster calculations. Comparing the energies of competing Néel, spiral and orthogonal-dimer phases we can rule out the existence of a noncollinear spiral phase. Considering the Néel order parameter we

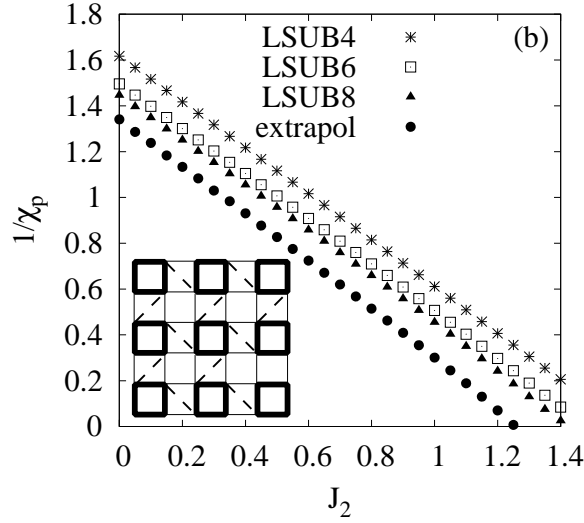


**Figure 4.8.:** the inverse susceptibility  $1/\chi_p$  versus  $J_2$  obtained within the CCM LSUB $n$  approximation with  $n = 4, 6, 8$  and extrapolated to  $n \rightarrow \infty$  using Eq. (2.43). Inset: Pattern of plaquette valence bond order.

find that the semi-classical Néel long-range order disappears before the orthogonal-dimer phase sets in. Hence we conclude that the Néel phase and the dimer phase are separated by a magnetically disordered intermediate phase. We also investigate the nature of nonmagnetic phase and we conclude from our CCM data that there exists a valence-bond phase between the Néel -ordered phase and the orthogonal-dimer phase. We note that some of the results presented in this chapter are published in.<sup>1 2</sup>

<sup>1</sup>R. Darradi, J. Richter and D.J.J. Farnell, "Coupled cluster treatment of the Shastry-Sutherland antiferromagnet", Phys. Rev. B **72**, 104425 (2005)

<sup>2</sup>J. Richter, R. Darradi, R. Zinke and R. F. Bishop, "Frustrated quantum antiferromagnets: application of high-order coupled cluster method", International Journal of Modern Physics B **21**, 2273-2288 (2007)

## SPIN STIFFNESS OF QUANTUM HEISENBERG ANTIFERROMAGNETS

To understand the low-energy behavior and quantum phase transitions of the system, an important issue is the determination of the microscopic parameters. For quantum Heisenberg antiferromagnet on square, cubic, and triangular lattice, these parameters are magnetic order and spin stiffness. The spin stiffness  $\rho_s$  constitutes, together with the spin-wave velocity, a fundamental parameter that determines the low-energy dynamics of magnetic systems. [101, 103, 104] In particular, in two-dimensional quantum antiferromagnets, where magnetically ordered as well as quantum disordered ground-state phases are observed, the ground-state stiffness measures the distance of the ground state from criticality [103] and can be used, in addition to the sublattice magnetization  $M$ , to test the existence or absence of magnetic long-range order (LRO).

Over the last 15 years in a series of papers several methods like series expansion, [105, 110] spin-wave theory, [102, 105–109] quantum Monte Carlo, [150] exact diagonalization, [31, 100, 108] Schwinger-boson approach, [30, 151] and renormalization group theory [152] have been used to calculate the spin stiffness of the spin-half Heisenberg antiferromagnet (HAFM) on the square, the triangular and the cubic lattices.

The spin stiffness  $\rho_s$  measures the increase in the amount of energy when we rotate the order parameter of a magnetically long-range ordered system along a given direction by a small angle  $\theta$  per unit length, see Eq. (2.39). In the thermodynamic limit, a positive value of  $\rho_s$  means that there is LRO in the system, while a value of zero reveals that there is no LRO.

In this chapter we use the method presented in Sec. 2 to calculate the spin stiffness for the quantum-spin HAFM using the coupled cluster method, see Chap. 2. In the field of magnetism an important advantage of this approach is its applicability to strongly frustrated quantum spin systems in any dimension. To demonstrate the potential of the presented method we calculate the spin stiffness for the spin- $\frac{1}{2}$  HAFM with nearest-neighbor interaction on the cubic, the square, and on the triangular lattices and compare our results with available data in the literature. While for the square and the cubic lattices accurate high order spin-wave results are available which can be used to estimate the accuracy of the CCM results, the known results for the frustrated HAFM on the triangular lattice with a non-collinear ground state seem to be less reliable, since the used methods are less accurate. Therefore, results for the triangular lattice seem to be less precise than those for the square lattice due to strong frustration. Published values show significant variability. We argue that our result for

the stiffness of the HAFM on the triangular lattice obtained by CCM in high order of approximation is better than the so far available results. The model we consider is the spin-Half HAFM of Eq. (5.1) which reads in new rotated coordinate system

$$H = J \sum_{\langle i,j \rangle} \left\{ \frac{1}{2} \sin \varphi [s_i^+ s_j^z - s_i^z s_j^+ + s_i^- s_j^z - s_i^z s_j^-] + \cos \varphi s_i^z s_j^z \right. \\ \left. + \frac{1}{4} (\cos \varphi + 1) [s_i^+ s_j^- + s_i^- s_j^+] + \frac{1}{4} (\cos \varphi - 1) [s_i^+ s_j^+ + s_i^- s_j^-] \right\}, \quad (5.1)$$

with  $\varphi$  being the angle between the two spins, and  $s^\pm \equiv s^x \pm is^y$  are the spin-raising and spin-lowering operators. According to Fig. 5.1 we have e.g. for the twisted Néel state on the square lattice  $\varphi = \pi$  for nearest-neighbors along the  $y$  direction but  $\varphi = \pi + \theta$  along the  $x$  direction and for the twisted  $120^\circ$  Néel state on the triangular lattice we have  $\varphi = 2\pi/3 + \theta/2$  for nearest neighbors along the  $\frac{1}{2}\vec{e}_x + \vec{e}_y$  direction but  $\varphi = 4\pi/3 + \theta$  along the  $x$  direction.

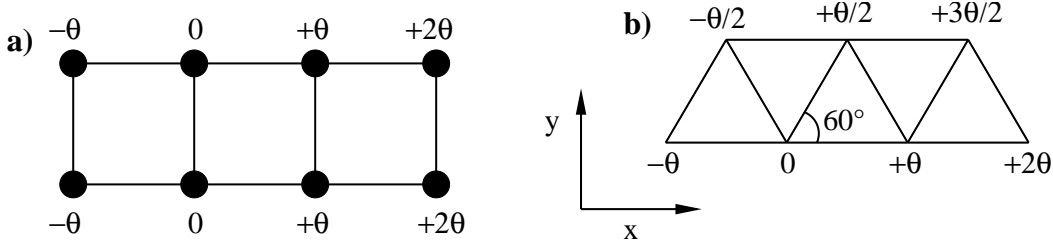


**Figure 5.1.:** Illustration of the twisted Néel state (a: square lattice; b: triangular lattice). The twist is introduced along rows in  $x$  direction. The angles at the lattice sites indicated the twist of the spins with respect to the corresponding Néel state.

The spin stiffness considered in this chapter is the stiffness of the Néel order parameter (sublattice magnetization). Hence the corresponding model state  $|\Phi\rangle$  is the Néel state. This is the ordinary collinear two-sublattice Néel state for the square and the cubic lattices. The model state is a noncollinear  $120^\circ$  three-sublattice Néel state for the triangular lattice. Note that for the collinear Néel state only LSUB $n$  approximations with even  $n$  are relevant [18, 89]. In order to calculate the spin stiffness directly using Eq. (2.39) we must modify the model (Néel) state by introducing an appropriate twist  $\theta$ , see Fig. 5.1. Thus the ket-state correlation coefficients  $\mathcal{S}_I$  (after solving the CCM equations (2.7)) depend on  $\theta$  and hence the ground-state energy  $E$  is also dependent on  $\theta$ . Note that our numerical code for the CCM-LSUB $n$  approximation allows us to calculate  $E(\theta)$  with very high precision of about 14 digits. First we have checked numerically that the ground-state energy calculated in LSUB $n$  approximation does indeed fulfill the relation (2.39) with high precision for  $\theta \lesssim 0.01$ . The stiffness now can easily be calculated using numerical differentiation of  $E(\theta)$  which was done using a three-point formula 2.40 with  $\theta = -10^{-4}, 0, +10^{-4}$ .

Since the LSUB $n$  approximation becomes exact for  $n \rightarrow \infty$ , it is useful to extrapolate the 'raw' LSUB $n$  results to the limit  $n \rightarrow \infty$ . Although we do not know the exact scaling of the LSUB $n$  results, there is some empirical experience [88, 89] how the ground-state energy and the order parameter for antiferromagnetic spin models scale with  $n$  (see Sec. 2.5). Based on this experience we have tested several fitting functions for the stiffness and we have found the best extrapolation is obtained by the fitting function of Eq. (2.43) (extrapol 1). We show this extrapolation in Fig. 5.2.

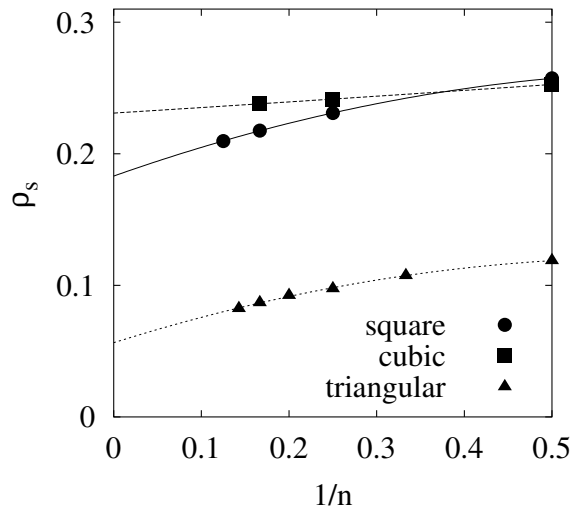


**Figure 5.2.:** Extrapolation of the CCM-LSUB $n$  results for the stiffness. The points represent the CCM-LUB $n$  results and the lines correspond to the function (2.43) fitted to this data points.

### 5.1. THE SQUARE LATTICE

We start with the results for the square lattice. By using the lattice symmetries we are able to perform calculations up to LSUB8, where for the twisted state 21124 ket equations (2.7) have to be solved. The results for the stiffness are given in Tab. (5.1). The results for the stiffness are given in Tab. (5.1). Using LSUB $n$  with  $n = 2, 4, 6, 8$  the extrapolated result is  $\rho_s = 0.1831$ . As known from the sublattice magnetization even better results can be obtained by excluding the LSUB2 data. Indeed the extrapolation using the LSUB4, LSUB6, LSUB8 data yields  $\rho_s = 0.1812$ . Note that the corresponding extrapolated value for the sublattice magnetization (see Tab.2.1)  $M = 0.31024$  is in good agreement with other results [105, 117, 118]. A certain estimate of the accuracy can be obtained by an extrapolation using LSUB2, LSUB4, LSUB6, only, which yields  $\rho_s = 0.1839$ . We compare our results for  $\rho_s$  with some data obtained by other methods in Tab. (5.2). In particular, we find that the value of spin stiffness obtained by quantum Monte Carlo in Ref. [21] is in a good agreement with the results of the CCM. We also think, that the high-order spin-wave theory [105] is

**Table 5.1.:** Spin stiffness  $\rho_s$  for the spin-1/2 HAFM on the square lattice calculated by various CCM-LSUB $n$  approximations and the result of the  $n \rightarrow \infty$  extrapolation using LSUB $n$  with  $n = 4, 6, 8$ .

LSUB $n$	Number of equations	$\rho_s$
2	3	0.2574
4	40	0.2310
6	828	0.2176
8	21124	0.2097
extrapol 1	–	0.1812

the most systematic approach, since one can see how the stiffness changes with increasing order of approximation. Assuming the third-order order spin-wave results as a benchmark we find that our CCM result deviates by about 3%.

**Table 5.2.:** Collection of data for the spin stiffness  $\rho_s$  for the spin-1/2 HAFM on the square lattice calculated by different methods.

method	$\rho_s$
first-order spin-wave theory [105, 107]	0.191
second-order spin-wave theory [105, 107]	0.181
third-order spin-wave theory [105]	0.175
series expansion [105]	0.182
exact diagonalization [31]	0.183
quantum Monte Carlo [21]	0.185
Schwinger-boson approach I [153]	0.176
Schwinger-boson approach II [151]	0.153
CCM	0.181

## 5.2. THE TRIANGULAR LATTICE

For the triangular lattice the twist we consider (see Fig. 5.1) corresponds to the in-plane spin stiffness. Due to the noncollinear structure of the three-sublattice Néel state also LSUB $n$  approximations with odd  $n$  appear. Furthermore the number of ket equations in a certain level of approximation becomes larger than for the square lattice and as a results the highest level of approximation we are able to consider is LSUB7. The results for different LSUB $n$  approximations are given in Tab. (5.3). The extrapolation of the LSUB $n$  data according to Eq. (2.43) with  $n = 2, 4, 6$  leads to  $\rho_s = 0.0604$  and with  $n = 2, 3, 4, 5, 6, 7$  to  $\rho_s = 0.0564$ . Again the difference in the two values can be

considered as a certain estimate of the accuracy. As a byproduct of our high-order calculation we can give here improved values for the sublattice magnetization  $M$ . So far results for  $M$  up to LSUB6 [88, 132] are published. We can add  $M = 0.3152$  (LSUB7) and  $M = 0.3018$  (LSUB8). The corresponding extrapolated value using Eq. (2.43) and LSUB $n$  with  $n = 2, 3, 4, 5, 6, 7, 8$  is  $M = 0.2134$ , which is close to spin-wave [102, 154] and Green's function Monte Carlo [155] results. The small values of the stiffness and the order parameter in comparison with the square lattice are attributed to the frustration leading to a noncollinear ground state and in combination with quantum fluctuations to a drastic weakening of magnetic order in the spin-half HAFM. We compare our results for  $\rho_s$  with available results from literature, see Tab. (5.4).

**Table 5.3.:** In-plane spin stiffness  $\rho_s$  for the spin-1/2 HAFM on the triangular lattice calculated by various CCM-LSUB $n$  approximations and the result of the  $n \rightarrow \infty$  extrapolation using LSUB $n$  with  $n = 2, 3, 4, 5, 6, 7$ .

LSUB $n$	Number of equations	$\rho_s$
2	3	0.1188
3	14	0.1075
4	67	0.0975
5	370	0.0924
6	2133	0.0869
7	12878	0.0824
extrapol 1	–	0.0564

Comparing the methods used to calculate  $\rho_s$  for the square lattice (Tab. 5.2) and for the triangular lattice (Tab. 5.4) we see that the results for the triangular lattice are much less reliable, since here the accuracy of the methods used in Refs. [102, 108, 151] is limited. Assuming the same tendency as for the square lattice we can expect that the first-order spin-wave value for  $\rho_s$  [102, 108] becomes smaller (and therefore closer to our CCM result) going to second- and third-order spin-wave theories. We believe that our result is indeed of higher accuracy than data for  $\rho_s$  so far available.

**Table 5.4.:** Collection of data for the spin stiffness  $\rho_s$  for the spin-1/2 HAFM on the triangular lattice calculated by different methods.

method	$\rho_s$
exact diagonalization [108]	0.05
first-order spin-wave theory [102, 108]	0.080
Schwinger-boson approach [151]	0.088
CCM	0.056

## 5.3. THE CUBIC LATTICE

**Table 5.5.:** Spin stiffness  $\rho_s$  for the spin-1/2 HAFM on the cubic lattice calculated by various CCM-LSUB $n$  approximations and the result of the  $n \rightarrow \infty$  extrapolation using LSUB $n$  with  $n = 2, 4, 6$ .

LSUB $n$	Number of equations	$\rho_s$
2	4	0.2527
4	106	0.2416
6	5706	0.2380
extrapol 1	–	0.2312

We present now our results for  $\rho_s$  for the simple cubic lattice, see Tab. (5.5). Here the highest level of approximation we can consider is LSUB6. From Fig. 5.2 it becomes obvious, that there is only a weak dependence on the level of CCM approximation  $n$ . Therefore we expect that the extrapolation according to Eq. (2.43) yielding  $\rho_s = 0.2312$  is particularly accurate. Indeed we find that our result is in very good agreement with the result obtained by second-order spin-wave theory [105]  $\rho_s = 0.2343$ . Note that the  $1/s$  spin-wave expansion seems to converge very rapidly [105] and therefore the second-order spin-wave theory is expected to yield a very precise result for  $\rho_s$ . For the sublattice magnetization a corresponding extrapolation leads to  $M = 0.42054$  (see Tab.2.2) is in excellent agreement with the high precision third-order spin-wave result. [105]

In summary, we have presented a method for the direct calculation of the spin stiffness within the framework of the coupled cluster method. We obtain accurate values for the stiffness by applying this algorithm to high orders of LSUB $n$  approximations for the spin-half isotropic Heisenberg antiferromagnet on various lattices with and without frustration. We note that some of the results presented in this chapter are published in.<sup>1 2</sup>

<sup>1</sup>S.E. Krüger, R. Darradi, J. Richter and D.J.J. Farnell, "Direct calculation of the spin stiffness of the spin-1/2 Heisenberg antiferromagnet on square, triangular and cubic lattices using the coupled cluster method", Phys. Rev. B **73**, 094404 (2006)

<sup>2</sup>J. Richter, R. Darradi, R. Zinke and R. F. Bishop, "Frustrated quantum antiferromagnets: application of high-order coupled cluster method", Int. J. Mod. Phys B **21**, 2273 (2007)



# GROUND-STATE PHASES OF THE SPIN-1/2 $J_1$ - $J_2$ HEISENBERG ANTIFERROMAGNET ON THE SQUARE LATTICE

## 6.1. INTRODUCTION

In this chapter we investigate the zero-temperature phase diagram of spin-1/2 Heisenberg antiferromagnet with nearest-neighbor  $J_1$  and frustrating next-nearest-neighbor  $J_2$  coupling ( $J_1$ - $J_2$  model) on the square lattice. This model has attracted a great deal of interest during the last twenty years (see, e.g., Refs. [22–52] and references therein). Recent interest in this model comes also from the synthesis of layered magnetic materials  $\text{Li}_2\text{VO}_2\text{SiO}_4$ ,  $\text{Li}_2\text{VOGeO}_4$ ,  $\text{VO}_2\text{MoO}_4$ , and  $\text{BaCdVO}(\text{PO}_4)_2$  [54, 56, 156–159] that might be described by the  $J_1$ - $J_2$  model. A new promising perspective is also opened by the recently discovered layered Fe-based superconducting materials [69] which may have a magnetic phase that can be described by a  $J_1$ - $J_2$  model with spin quantum number  $s > 1/2$ . [70, 160]

For the square-lattice spin-1/2  $J_1$ - $J_2$  model it is well-accepted that there are two magnetically long-range ordered ground-state (GS) phases at small and at large  $J_2$  separated by an intermediate quantum paramagnetic phase without magnetic long-range order (LRO) in the parameter region  $J_2^{c1} \leq J_2 \leq J_2^{c2}$ , where  $J_2^{c1} \approx 0.4J_1$  and  $J_2^{c2} \approx 0.6J_1$ . The magnetic phase at low  $J_2 < J_2^{c1}$  exhibits semiclassical Néel LRO with a magnetic wave vector  $\mathbf{Q}_0 = (\pi, \pi)$ . The magnetic phase at large  $J_2 > J_2^{c2}$  shows so-called collinear LRO. It is twofold degenerate and the corresponding magnetic wave vectors are  $\mathbf{Q}_1 = (\pi, 0)$  or  $\mathbf{Q}_2 = (0, \pi)$ , respectively. These two collinear states are characterized by a parallel spin orientation of nearest neighbors in vertical (horizontal) direction and an antiparallel spin orientation of nearest neighbors in horizontal (vertical) direction.

The nature of the transition between the Néel and the quantum paramagnetic phase as well as the properties of the quantum paramagnetic phase and the precise values of the transition points are still under debate [22–52]. In particular, stimulated by the recent discussion of deconfined quantum criticality in two-dimensional spin systems, [72, 73] a renewed interest in the nature of the phase transition between the semiclassical Néel phase and the quantum paramagnetic phase has been emerged [37, 47, 161, 162]. However, in spite of numerous intensive efforts focused on the transition between the Néel and the quantum paramagnetic phase in the  $J_1$ - $J_2$

square-lattice antiferromagnet and some other candidate models, [122, 123, 163–166] this field remains still highly controversial.

For completeness we mention that the classical square-lattice  $J_1$ - $J_2$  model ( $s \rightarrow \infty$ ) exhibits a direct first-order transition between Néel state and collinear state at  $J_2/J_1 = 1/2$ .

Recently, several extensions of  $J_1$ - $J_2$  model have been studied. Interestingly, with increasing of the space dimension from  $D = 2$  to  $D = 3$  the intermediate quantum paramagnetic phase disappears. [42, 167, 168] Also spatial [111, 169–172] and spin anisotropies [41, 112, 173] as well as the spin quantum number  $s$  [27, 37, 113, 114] have a great influence on the GS phase diagram.

The goal of this work is to study the GS phase diagram for spin-half  $J_1$ - $J_2$  model on the square lattice using a high-order CCM (for further details see Chap.2). We complement the CCM treatment by ED for finite lattices for a qualitative check of our CCM data. By calculating GS quantities such as the energy, the magnetic order parameter, the spin stiffness and generalized susceptibilities we will investigate the quantum phase transitions present in the model as well as the properties of the quantum paramagnetic phase. We will compare our results with the ones obtained recently using series expansions. [47]

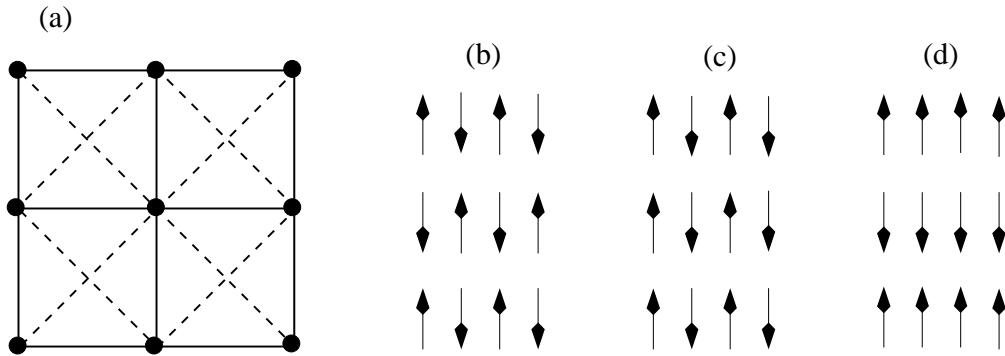


**Figure 6.1.:** (a)  $J_1$ - $J_2$  model; —  $J_1$ ; - -  $J_2$ ; (b) Néel state, (c) stripe state - columnar and (d) stripe state - row. Arrows in (b), (c) and (d) represent spins situated on the sites of the square lattice (indicated by • in (a)).

The Hamiltonian of the considered  $J_1$ - $J_2$  model reads

$$H = J_1 \sum_{\langle ij \rangle} \mathbf{s}_i \mathbf{s}_j + J_2 \sum_{[ij]} \mathbf{s}_i \mathbf{s}_j, \quad (6.1)$$

where  $J_1$  is the nearest-neighbor and  $J_2$  is the next-nearest-neighbor exchange coupling (see Fig.7.1). Both couplings are antiferromagnetic,  $J_1 > 0$ ,  $J_2 > 0$ . In our CCM and ED calculations we set  $J_1 = 1$ . We consider spin quantum number  $s = 1/2$ , i.e.  $\mathbf{s}_i^2 = 3/4$ .

We begin our CCM calculation with a reference state corresponding to semiclassical order, one can compute the GS energy also in parameter regions where semiclassical

magnetic LRO is destroyed, and it is known [18, 22, 42, 93, 94, 111, 112] that the CCM yields precise results for the GS energy beyond the transition from the semiclassical magnetic phase to the quantum paramagnetic phase. The necessary condition for the convergence of the CCM equations is a sufficient overlap between the reference state and the true ground state.

It has been already demonstrated (Chap.5) that the CCM can also be used to calculate the spin stiffness  $\rho_s$  with high accuracy. In the thermodynamic limit, a positive value of  $\rho_s$  means that there is magnetic LRO in the system, while a value of zero reveals that there is no magnetic LRO. To calculate the spin stiffness within the CCM using Eq. (2.39) we must modify the corresponding reference states (Néel or collinear) by introducing an appropriate twist  $\theta$ , see Fig. 7.2.

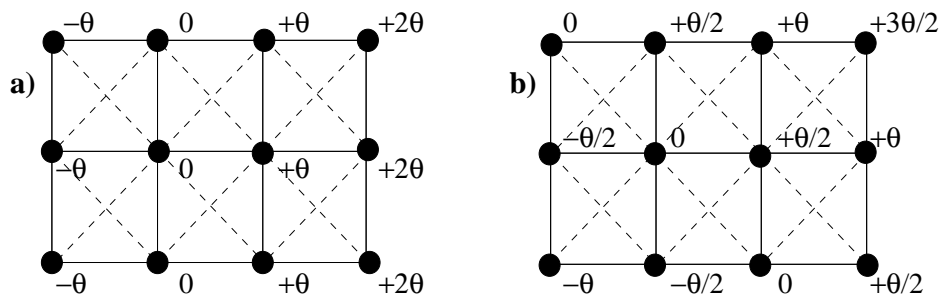


**Figure 6.2.:** Illustration of the twisted reference states used for the calculation of the spin stiffness  $\rho_s$ . The angles at the lattice sites indicate the twist of the spins with respect to the Néel or the collinear state. (a): Twisted Néel state, the twist is introduced along rows in  $x$  direction. (b): Twisted collinear state, the twist is introduced along rows in  $\vec{e}_x + \vec{e}_y$  direction.

Thus the ket-state correlation coefficients  $\mathcal{S}_I$  (after solving the CCM equations (2.7)) depend on  $\theta$  and, hence, the GS energy  $E$  is also dependent on  $\theta$ .

To study the properties of the quantum paramagnetic phase existing in the vicinity of  $J_2 = J_1/2$  as well as the phase transitions to that phase we will consider generalized susceptibilities  $\chi_F$  that describe the response of the system to certain ‘field’ operator  $F$  [23, 25, 26, 47, 49, 50] (see Sec.2.4.3). To calculate such a susceptibility  $\chi_F$  we add to the Hamiltonian (7.1) a ‘field’ term  $F = \delta \hat{O}$ , where  $\hat{O}$  is an operator that breaks some symmetry of  $H$  and the coefficient  $\delta$  determines the strength of the field. Using the CCM with either the Néel or the collinear reference state we calculate the energy per site  $E(\delta)/N = e(\delta)$  for  $H + F$ , i.e. for the Hamiltonian of Eq. (7.1) perturbed by the additional term  $\delta \hat{O}$ . The susceptibility  $\chi_F$  is then defined by Eq. (2.41). For the considered quantum spin model we have to use approximations in order to truncate the expansion of  $S$  and  $\tilde{S}$ .

We use the well elaborated LSUB $n$  scheme [83, 84, 88, 89, 92, 93] in which in the correlation operators  $S$  and  $\tilde{S}$  one takes into account all multispin correlations over all distinct locales on the lattice defined by  $n$  or fewer contiguous sites. In the CCM-LSUB10 approximation we have finally 29 605 (45 825) fundamental configurations for the Néel (collinear) reference state. Note, however, that for the calculation of the

stiffness (the susceptibilities) the twisted reference state (the modified Hamiltonian  $H + F$ ) is less symmetric which leads to more fundamental configurations. As a result we are then limited to LSUB8 approximation.

## 6.2. GROUND-STATE PHASE DIAGRAM

### 6.2.1. Ground-state energy

As already mentioned in section 6.1, the considered  $J_1$ - $J_2$  model has two semiclassical magnetic GS phases (small and large  $J_2$ ) separated by nonmagnetic quantum phase (intermediate  $J_2$ ). To detect the quantum critical points by the above described CCM we discuss the magnetic order parameter  $M$ , see Eq. (2.36), and the spin stiffness  $\rho_s$ , see Eq. (2.39). Both,  $M$  and  $\rho_s$ , are finite in the magnetically ordered phases but vanish in the intermediate quantum paramagnetic phase.

For completeness, we show first the CCM and the ED GS energies per spin  $e = E/N$  in Fig. 7.3. The CCM curve consists of two parts corresponding to the Néel and

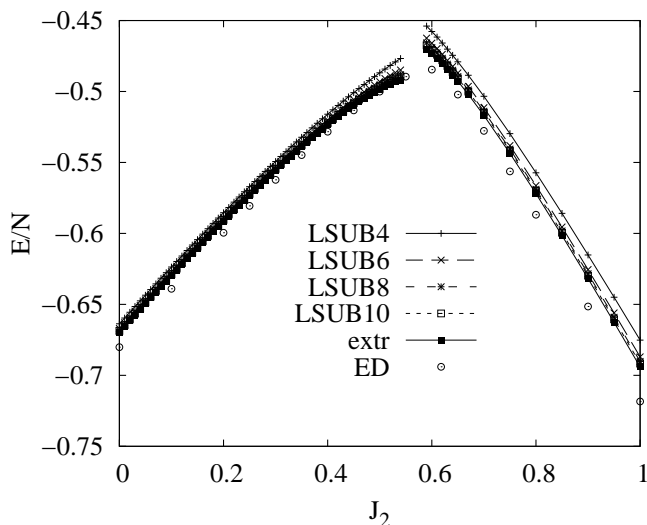


**Figure 6.3.:** The GS energy per spin as function of  $J_2$  obtained by CCM-LSUB $n$  with  $n = 4, 6, 8, 10$  and its extrapolated values to  $n \rightarrow \infty$  using the extrapolation scheme of Eq. (2.42). ED results for  $N = 32$  are shown by circles.

collinear reference state, respectively. The dependence  $e(J_2)$  for ED and CCM is qualitatively the same, however, due to finite-size effects, the ED curve is below the CCM curves. Let us mention again that CCM GS energy corresponding to the Néel (collinear) reference state is expected to be precise also in the intermediate quantum paramagnetic phase if  $J_2$  is not too far beyond the transition points.

### 6.2.2. Magnetic order parameter

The magnetic order parameter for both Néel state and collinear state dependence on  $J_2$  is illustrated by Fig. 6.4. Note again that only for the magnetic order parameter  $M$  and

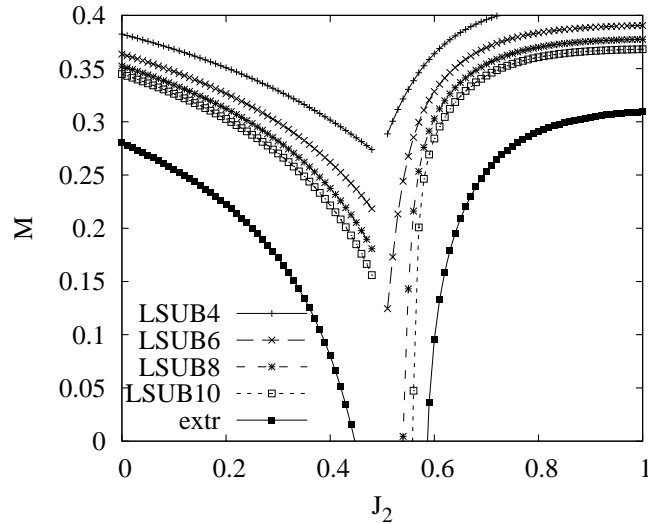


**Figure 6.4.:** Magnetic order parameter  $M$  versus  $J_2$  obtained by CCM-LSUB $n$  with  $n = 4, 6, 8, 10$  and its extrapolated values to  $n \rightarrow \infty$  using the extrapolation scheme of Eq. (2.45).

the GS energy we are able to solve the CCM-LSUB $n$  equations up to  $n = 10$ , while for the stiffness and the susceptibilities we are restricted to  $n \leq 8$ . Hence the extrapolation to the limit  $n \rightarrow \infty$  is most reliable for  $M$  and the estimation of the phase transition points by using the data for  $M$  is most accurate. The extrapolation to  $n \rightarrow \infty$  shown in Fig. 6.4 is based the extrapolation scheme  $M(n) = b_0 + b_1(1/n)^{1/2} + b_2(1/n)^{3/2}$  and uses CCM-LSUB $n$  data with  $n = 4, 6, 8, 10$ . We find for the phase transition points between the semiclassical phases and the quantum paramagnetic phase  $J_2^{c1} = 0.447J_1$  and  $J_2^{c2} = 0.586J_1$ .

To check the robustness of this extrapolation we have also extrapolated  $M$  using the data of  $n = 2, 4, 6, 8, 10$  which leads to  $J_2^{c1} = 0.443J_1$  and  $J_2^{c2} = 0.586J_1$ . Those values  $J_2^{c1} \approx 0.44 \dots 0.45J_1$  and  $J_2^{c2} \approx 0.58 \dots 0.59J_1$  are in agreement with CCM predictions of Refs. [111, 112].

Although the behavior of the extrapolated values of the magnetic order parameter around  $J_2^{c1}$  and  $J_2^{c2}$  presented in Fig. 6.4 show a continuous behavior near  $J_2^{c1}$  and near  $J_2^{c2}$ , it is obvious that the decay of the collinear order parameter to zero at  $J_2^{c2}$  is much steeper than the decay of the Néel order parameter at  $J_2^{c1}$ . That might give some hint for a first-order phase transition from the collinear to the paramagnetic phase, by contrast to a continuous transition from the Néel to the paramagnetic phase [43–45, 49].

### 6.2.3. Spin stiffness

As mentioned above, another way to find the phase transition points is to consider the spin stiffness  $\rho_s$  which is nonzero in a magnetically long-range ordered phase but vanishes in the magnetically disordered quantum phase. The spin stiffness measures the distance of the ground state from criticality [103], and constitutes together with the spin-wave velocity the fundamental parameters that determines the low-energy dynamics of magnetic systems [101,104,174]. In order to calculate the stiffness directly using Eq. (2.39) we have to modify the both reference (Néel, collinear) states by introducing an appropriate twist  $\theta$ , see Fig. 6.5. The CCM LSUB $n$  results for spin stiffness as well as the extrapolated values for both reference states as a function of  $J_2$  are given in Fig. 6.5. The results show that approaching the magnetically disordered

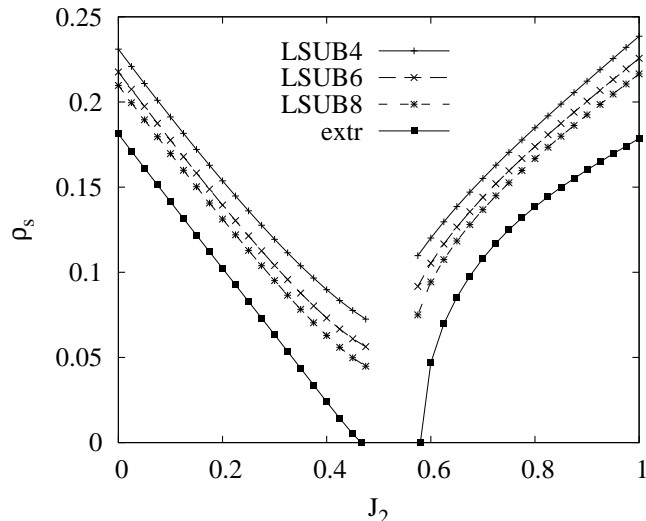


**Figure 6.5.:** The spin stiffness  $\rho_s$  versus  $J_2$  obtained by CCM-LSUB $n$  with  $n = 4, 6, 8$  and its extrapolated values to  $n \rightarrow \infty$  using the extrapolation scheme  $\rho_s(n) = c_0 + c_1(1/n) + c_2(1/n)^2$ .

phase the stiffness is decreased until it vanishes at  $J_2 = 0.466J_1$  coming from the Néel phase and at  $J_2 = 0.578J_1$  coming from the collinear phase. These values obtained by extrapolation including up to LSUB8 data are in reasonable agreement with the critical points determined by extrapolating  $M$ . Note that our data for  $\rho_s$  are also in good agreement with corresponding results of the other methods (see Refs. [30,31,34,175]). Note further that similar as for  $M$  we observe also for  $\rho_s$  that the curvature near the critical points is different at  $J_2^{c1}$  and at  $J_2^{c2}$  that might be again a hint on the different nature of both transitions.

To summarize, the CCM results for the GS energy, the magnetic order parameter, and the spin stiffness support a general physical picture known from earlier numerical studies (including ED, [28,32,39,40,43,44] variational quantum Monte Carlo, [24,26] series expansions [47,50]): For intermediate values of  $J_2$ ,  $J_2^{c1} \leq J_2 \leq J_2^{c2}$  with  $J_2^{c1} \approx 0.44 \dots 0.45J_1$  and  $J_2^{c2} \approx 0.58 \dots 0.59J_1$  there is no magnetic order.

## 6.3. ORDER OF THE PHASE TRANSITION. GENERALIZED SUSCEPTIBILITIES

While the phase transition from the collinear to the paramagnetic phase is most likely of first order, [43–45, 49] concerning the nature of phase transition from the Néel to the paramagnetic phase so far no conclusive answers are known. However, the question about the order of the phase transition from the Néel to the paramagnetic phase is of great interest in particular in connection with the validity of the Landau-Ginzburg paradigm [72, 73]. Very recently by Sirker et al. [47] a number of arguments based on series expansions and spin-wave theory have been given that this transition is of first order. We reconsider this issue below using CCM and complementary ED results.

The first type of arguments in favor of the first-order phase transition from the Néel to the paramagnetic phase presented in Ref. [47] was based on the combination of field theory with series-expansion data. In what follows we use the same approach as Sirker et al., [47] however, instead of series-expansion data we use CCM and ED data. Interestingly, we will arrive at a different conclusion concerning the nature of the phase transition.

The second type of arguments supporting the first-order phase transition from the Néel to the paramagnetic phase were based on series-expansion data for several susceptibilities that test a possible valence-bond solid (VBS) order in the paramagnetic phase. In what follows we use the CCM and ED to compute four different susceptibilities  $\chi_j$  defined in Eq. (2.41) for the  $J_1$ – $J_2$  model. The corresponding perturbations (fields)  $F_j = \delta \hat{O}_j$ ,  $j = 1, \dots, 4$  are given by

$$F_1 = \delta \sum_{i,j} (-1)^i \mathbf{s}_{i,j} \mathbf{s}_{i+1,j}, \quad (6.2)$$

$$F_2 = \delta \sum_{i,j} (\mathbf{s}_{i,j} \mathbf{s}_{i+1,j} - \mathbf{s}_{i,j} \mathbf{s}_{i,j+1}), \quad (6.3)$$

$$F_3 = \delta \sum_{i,j} (-1)^{i+j} (s_{i,j}^x s_{i+1,j+1}^x + s_{i,j}^y s_{i+1,j+1}^y), \quad (6.4)$$

$$F_4 = \delta \sum_{i,j} [(-1)^i \mathbf{s}_{i,j} \mathbf{s}_{i+1,j} + (-1)^j \mathbf{s}_{i,j} \mathbf{s}_{i,j+1}], \quad (6.5)$$

where  $i, j$  are components (integer numbers) of the lattice vectors of the square lattice, see Fig. 6.6. where we visualize the perturbation terms (6.2) – (6.5). The above definitions, Eqs. (6.2) – (6.5), are in accordance with previous discussions [25, 26, 47, 49, 50] of possible valence-bond states or broken symmetries in the magnetically disordered quantum phase. Previous results for  $\chi_1$  can be found in Refs. [25, 26, 47, 49, 50], for  $\chi_2$  in Refs. [26, 47], and for  $\chi_3$  in Refs. [47, 50]. Note that in Refs. [47, 50] the results for the perpendicular  $\chi_3$  (i.e. the field  $F_3 = \delta \hat{O}_3$  contains only  $x$  and  $y$  components, see Eq. (6.4)) were reported only.

For reasons of comparison with the available series-expansion data we consider in

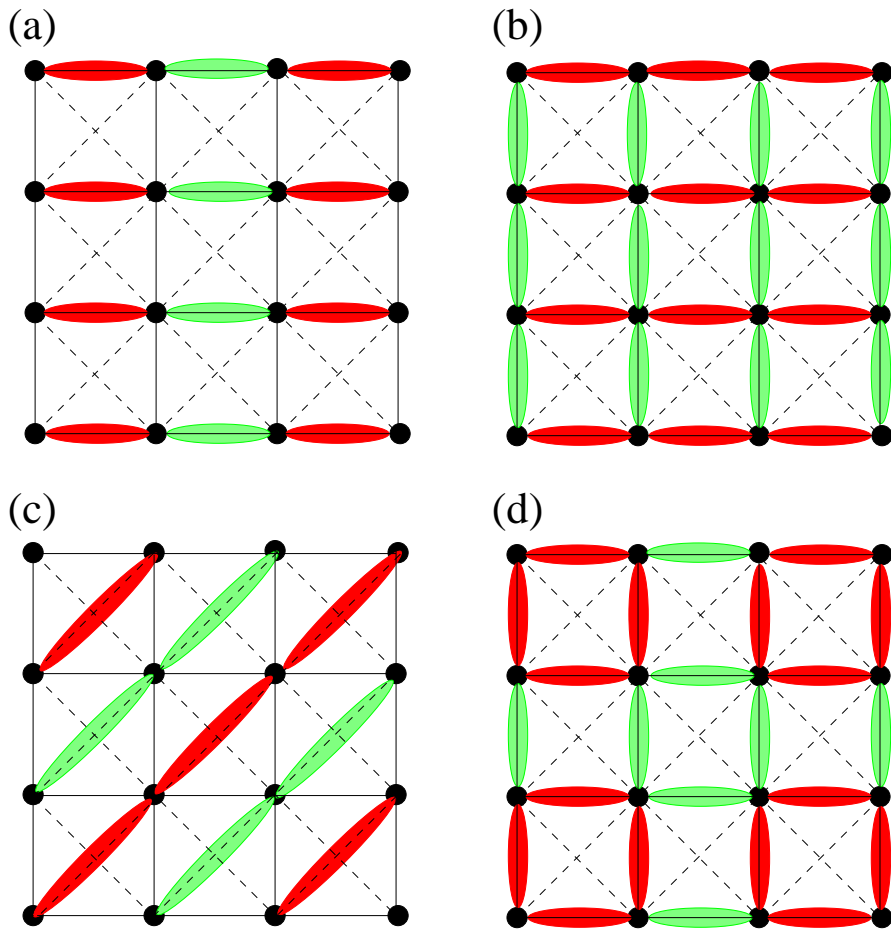


**Figure 6.6.:** (Color online) Illustration of perturbations (fields)  $F_j$  related to generalized susceptibilities  $\chi_j$ : (a) perturbation  $F_1$  (6.2), (b) perturbation  $F_2$  (6.3), (c) perturbation  $F_3$  (6.4), (d) perturbation  $F_4$  (6.5). Dark (red) [light (green)] shadows correspond to enforced [weakened] exchange couplings.

the present study also the perpendicular  $\chi_3$ . To our best knowledge so far no data for the susceptibility  $\chi_4$  are published.

Note that all susceptibilities defined by Eqs. (6.2) – (6.5) break the symmetry of the initial square lattice, for details, see Refs. [25, 26, 47, 49, 50]. The susceptibilities  $\chi_1$  and  $\chi_4$  are most interesting, since they belong to order-parameter operators  $\hat{O}_1$  and  $\hat{O}_4$  probing directly columnar and plaquette valence-bond ordering. As discussed in Ref. [73] they can also be interpreted as a single complex order parameter with a different phase for the two patterns. Note that for the field  $F_1$  we have chosen the  $x$ -axis for the alignment of modified nearest-neighbor bonds, see Fig. 6.6a. Alternatively, the  $y$ -axis can be chosen. It is worth mentioning that the field  $F_4$  (6.5) is a sum of fields  $F_1$  aligned along  $x$  and  $y$  axes, i.e.  $F_4 = F_1^{(x)} + F_1^{(y)}$ , and hence  $\chi_4 = \chi_1^{(x)} + \chi_1^{(y)}$ . If, in addition, a symmetry with respect to a  $\pi/2$ -rotation in the square-lattice plane holds (that is, however, not the case, e.g., for the CCM calculations for large  $J_2$ ), one



has  $\chi_1^{(x)} = \chi_1^{(y)}$  and  $\chi_4 = 2\chi_1$ .

Analyzing the behavior of these susceptibilities as  $J_2$  approaches the critical value  $J_2^{c1}$  we will again arrive at a different conclusion in comparison to Ref. [47].

We begin with the examination of the order of the phase transition from the Néel to the VBS state. By contrast to the transition from the VBS to the collinear state where an energy level crossing indicates a first-order transition [45, 47, 111] the energy behaves smoothly as  $J_2$  varies around  $J_2^{c1}$  and a more sensitive method to distinguish between first- and second-order transitions has to be applied. [47] For that we consider the GS energy  $e(\delta)$  for the Hamiltonian (7.1) perturbed by the field  $F_1 = \delta\hat{O}_1$  (6.2). We have performed CCM calculations for  $e(\delta)$  choosing the Néel state as the reference state and extrapolating LSUB $n$  data with  $n = 4, 6, 8$  according to the scaling law  $e(n) = a_0 + a_1(1/n)^2 + a_2(1/n)^4$  (see Fig. 6.7a). We have also performed complementary ED for a finite square lattice of  $N = 32$  sites (see Fig. 6.7b) for a qualitative check of the CCM results. The obtained dependence  $e(\delta)$  may be fitted for a fixed  $J_2$  to the following polynomial form

$$e(\delta) - e(0) = \frac{a}{2}\delta^2 + \frac{b}{4}\delta^4 + \frac{c}{6}\delta^6. \quad (6.6)$$

To determine the order of the phase transition we use the method described in Ref. [47]. For a two-dimensional antiferromagnet, the system could be described by the following  $O(3)$ -model

$$H_v = \frac{1}{2} \left[ (\partial_t \vec{v})^2 + c_v^2 (\vec{\nabla} \vec{v})^2 + m_v^2 \vec{v}^2 \right] + \frac{u_v}{4} (\vec{v}^2)^2. \quad (6.7)$$

Consider now the case that we are in the magnetically ordered phase and add the field  $F_1$  (6.2) with  $|\delta| \ll 1$ . The Néel order will then coexist with a small dimerization described by a scalar field

$$H_\phi = \frac{1}{2} \left[ (\partial_t \phi)^2 + c_\phi^2 (\vec{\nabla} \phi)^2 + m_\phi^2 \phi^2 \right] + \frac{u_\phi}{4} \phi^4 + \frac{r_\phi}{6} \phi^6 - \delta \phi. \quad (6.8)$$

The fields  $\vec{v}$  and  $\phi$  are not independent, and the interaction between them reads

$$H_{\text{int}} = \frac{u_{v\phi}}{2} \vec{v}^2 \phi^2. \quad (6.9)$$

The effective field theory in the ordered phase for  $\delta \neq 0$  is then given by  $H = H_v + H_\phi + H_{\text{int}}$ . Combining Eqs. (6.7), (6.8), (6.9) we will have a nonzero GS expectation value

$$\langle \phi \rangle = \frac{\delta}{A} - \frac{u_\phi}{A^4} \delta^3 + \frac{3u_\phi^2 - Ar_\phi}{A^7} \delta^5 + \mathcal{O}(\delta^7) \quad (6.10)$$

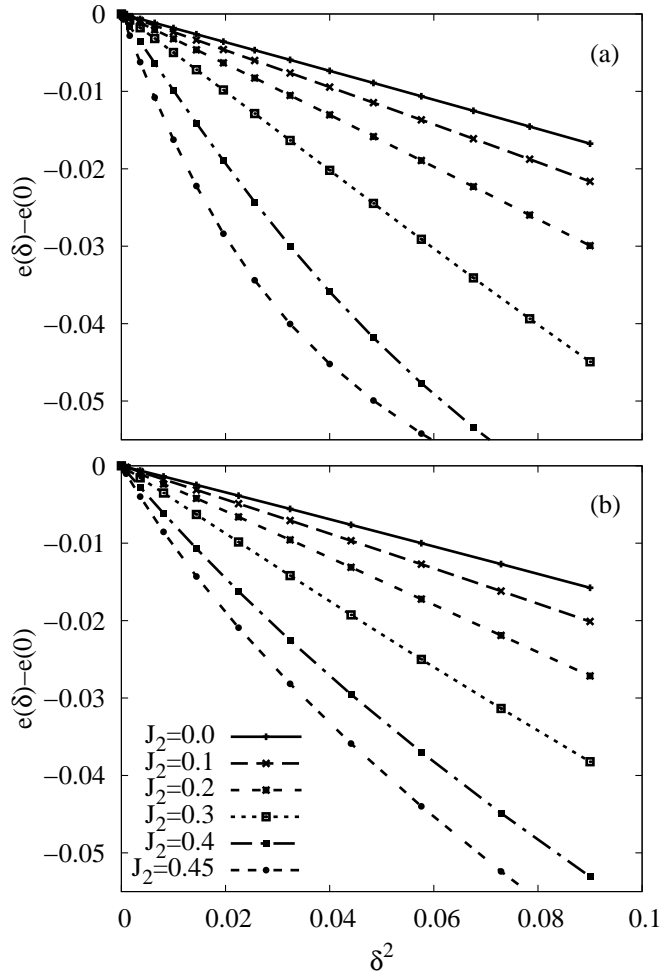


**Figure 6.7.:** The GS energy  $e(\delta) - e(0)$  versus square of field strength  $\delta$  for  $H + \delta \hat{O}_1$ , see Eq. (6.2), for  $J_2 = 0.0, 0.1, 0.2, 0.3, 0.4, 0.45$  (from top to bottom). (a): CCM results extrapolated to  $n \rightarrow \infty$  using the extrapolation scheme  $e(n) = a_0 + a_1(1/n)^2 + a_2(1/n)^4$ . (b): ED results for  $N = 32$ . The displayed curves might be compared to the ones in Fig. 1 of Ref. [47] where corresponding series-expansion data for  $e(\delta)$  are reported (however, only up to  $J_2 = 0.3$ ).

with  $A = m_\phi^2 + u_\phi \langle \vec{v} \rangle^2$ . Eq. (6.10) leads to a GS energy given by

$$e(\delta) - e(\delta = 0) = -\frac{1}{2A}\delta^2 + \frac{u_\phi}{4A^4}\delta^4 + \frac{Ar_\phi - 3u_\phi^2}{6A^7}\delta^6 + \mathcal{O}(\delta^8). \quad (6.11)$$

The coefficient of the  $\delta^4$ -term in Eq. (6.11) may be positive or negative depending on the sign of the parameter  $u_\phi$ . In the case of  $u_\phi > 0$  we have a second-order transition with respect to  $\phi$  at a critical point, and a first-order transition if  $u_\phi < 0$ .

Using the polynomial in Eq. (6.6) we have fitted the data of  $e(\delta)$ ,  $\delta^2 = 0 \dots 0.09$  for various  $J_2$  including values near the critical point  $J_2^{c1}$  (see Fig. 6.7a). We find that the

coefficient of the  $\delta^4$ -term  $b$  is negative for small values of  $J_2$  but becomes positive if  $J_2$  approaches  $J_2^{c1}$ , see Fig. 6.8. This behavior is found for the CCM data as well as for

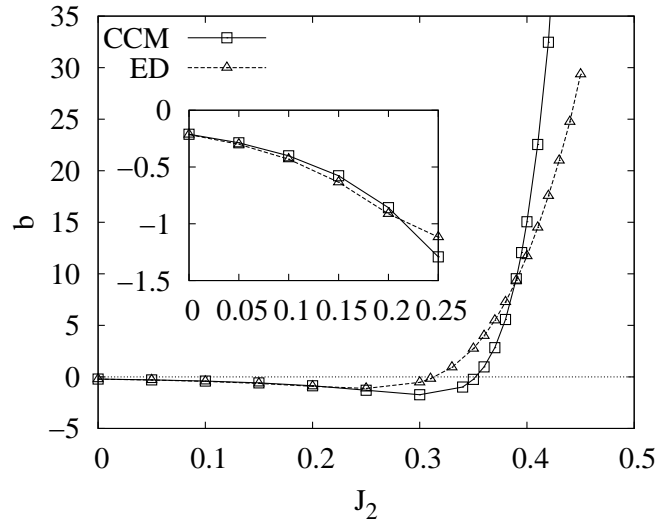


**Figure 6.8.:** The coefficient  $b$  of the quartic term in Eq. (6.6) obtained from a fit of the CCM data in Fig. 6.7a and the ED data in Fig. 6.7b in dependence on  $J_2$ . This figure might be compared to Fig. 3 of Ref. [47]. Inset: The coefficient  $b$  versus  $J_2$  shown for small  $J_2$  with an enlarged scale.

the ED data. In particular,  $b$  calculated by the CCM (calculated by the ED) changes its sign at  $J_2 \approx 0.35$  (at  $J_2 \approx 0.31$ ).

Comparing Fig. 6.8 with the results reported in Fig. 3 of Ref. [47] we note that CCM data for  $J_2$  below 0.2 are in reasonable agreement with series expansions, linear spin-wave theory or mean field spin-wave theory [in particular, CCM yields  $b(J_2 = 0.1) \approx -0.40$ ,  $b(J_2 = 0.2) \approx -0.86$ ,  $b(J_2 = 0.25) \approx -1.29$ ,  $b(J_2 = 0.3) \approx -1.73$  that is in between the series-expansion data and the spin-wave theory results]. A drastical difference between the series-expansion data and the CCM results emerges if  $J_2$  approaches the critical value  $J_2^{c1}$ : The series expansion gives  $b < 0$  whereas the CCM and the ED yield  $b > 0$  for  $J_2 \rightarrow J_2^{c1}$ . We recall that any predictions from spin-wave theory for the considered  $J_1$ - $J_2$  model are likely to be unreliable if  $J_2$  exceeds 0.35. [33] Combining Eqs. (6.6) and (6.11) we get  $b = u_\phi a^4$  and determining  $a$  and  $b$  using CCM data (Fig. 6.7a) for  $J_2 = 0.36 \dots 0.42$  we find  $u_\phi \approx 0.75 > 0$ . In summary, the presented CCM and ED data, by contrast to series-expansion data of Ref. [47], do not support a weak first-order phase transition from the Néel to the VBS state [47] but give evidence that this transition is continuous.

Next we examine the susceptibilities associated with the probing fields (6.2) – (6.5) directly. The CCM results are shown in Fig. 6.9. We also present in this figure the ED data for  $N = 16, 24, 32$  lattice in the insets (we do not show  $N = 24$  results for  $\chi_1$  and  $\chi_2$  since the system of rectangular shape perturbed by  $F_1$  or  $F_2$  does not possess symmetry with respect to a  $\pi/2$ -rotation in the square-lattice plane). Note that a sophisticated finite-size analysis has to be performed in order to derive the correct

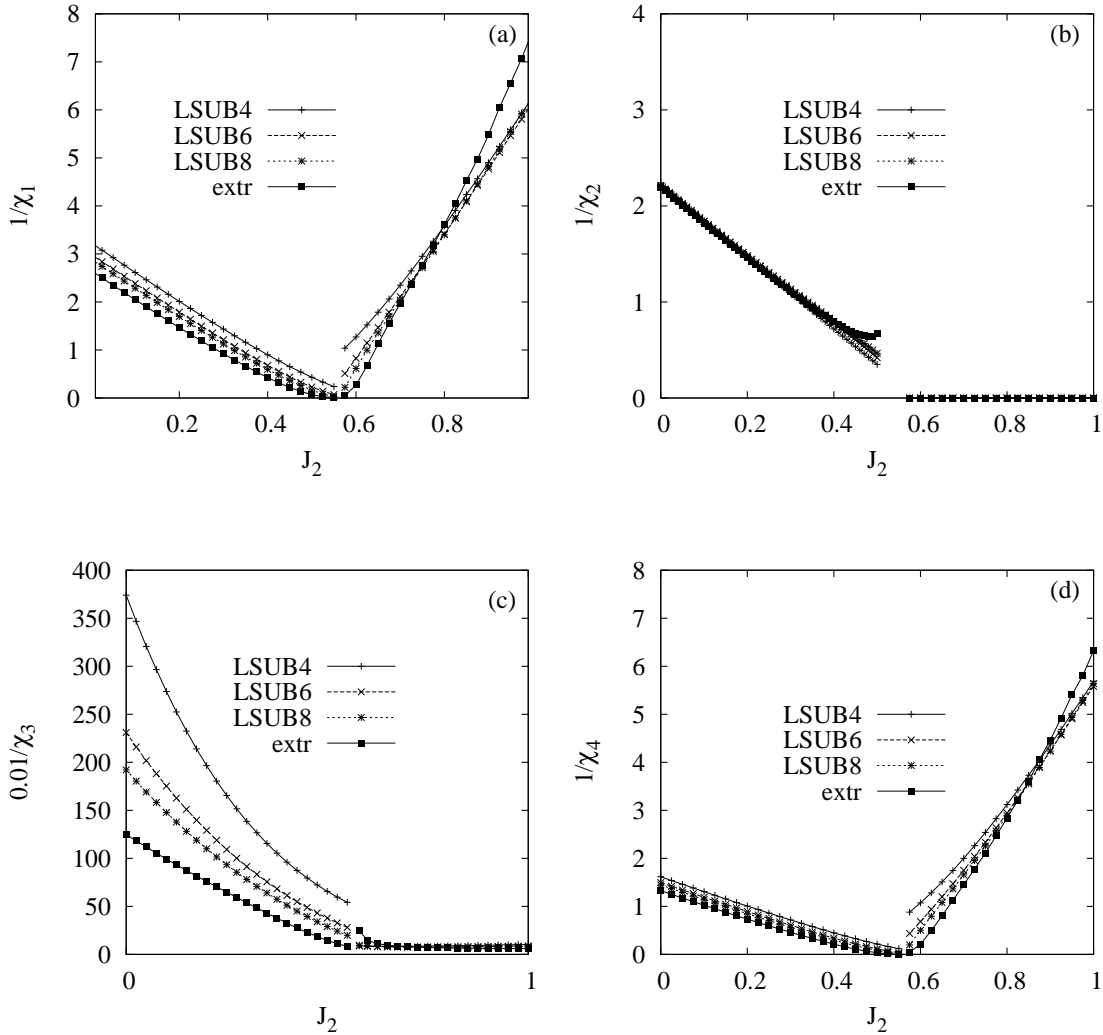


**Figure 6.9.:** The inverse susceptibilities (a)  $1/\chi_1$ , (b)  $1/\chi_2$ , (c)  $1/\chi_3$  (please note the scaling factor 0.01 at the  $y$ -axis), and (d)  $1/\chi_4$  versus  $J_2$  obtained within the CCM LSUB $n$  approximation with  $n = 4, 6, 8$  and extrapolated to  $n \rightarrow \infty$  using  $\chi(n) = c_0 + c_1(1/n) + c_2(1/n)^2$ .

behavior of susceptibilities in the thermodynamic limit [26]. Such an analysis goes beyond the scope of the present study, since we use the ED data as a qualitative check of our CCM results, only. We notice here that although  $\chi_1$  and  $\chi_4$  are related to each other (see above), they are calculated completely independently. We have confirmed the expected relation between these susceptibilities thus providing an additional double check for our numerics.

As it has been already mentioned above, the susceptibilities  $\chi_1$ ,  $\chi_2$  and  $\chi_3$  were calculated in earlier studies using different methods. Our CCM results for  $\chi_1$  and  $\chi_2$  are in a good quantitative agreement with series-expansion results reported for  $J_2 = 0 \dots 0.5$  in Refs. [47, 49] [for instance, one can compare our CCM data,  $1/\chi_1(J_2 = 0.3) \approx 0.92$ ,  $1/\chi_1(J_2 = 0.35) \approx 0.66$  and  $\chi_2(J_2 = 0.3) \approx 0.90$ ,  $\chi_2(J_2 = 0.35) \approx 1.06$ ,

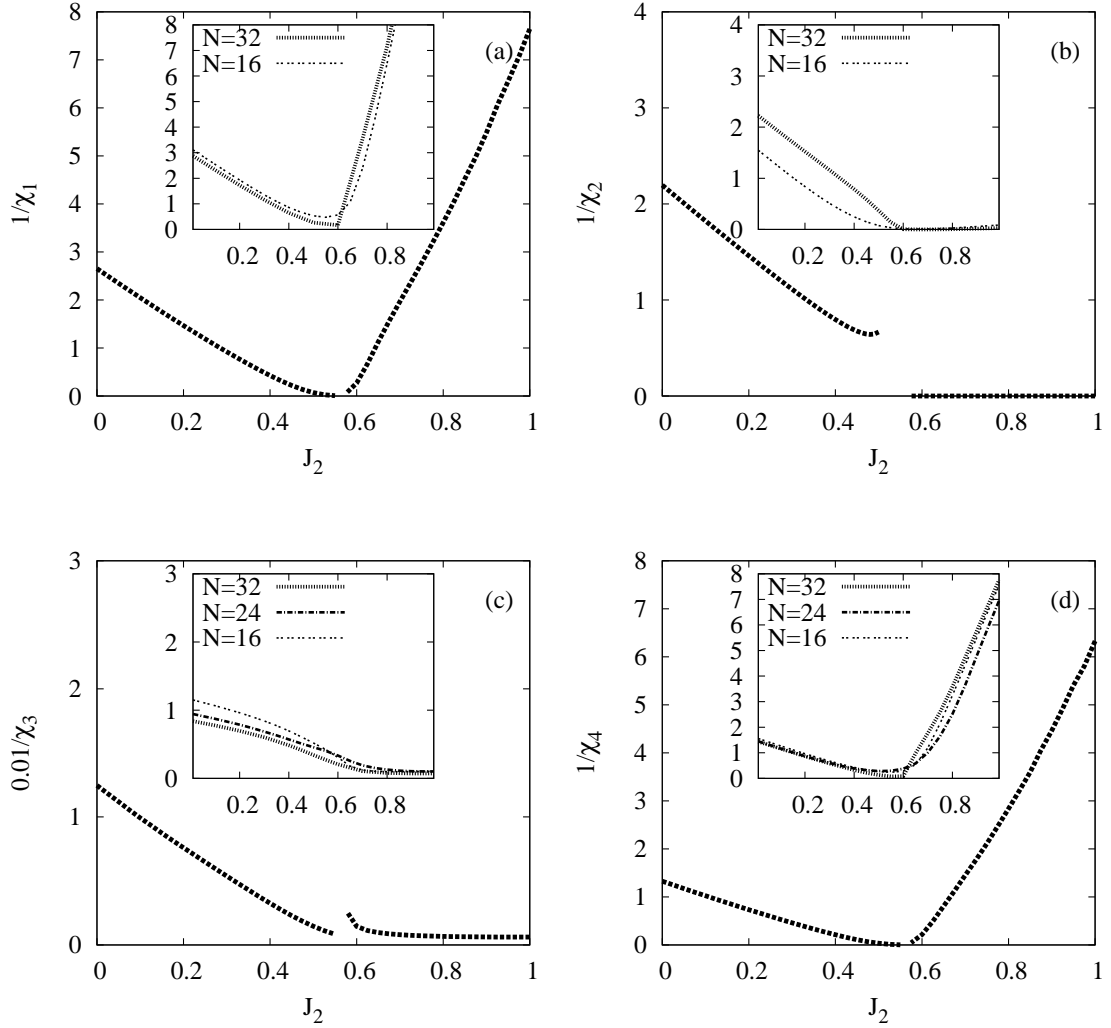


**Figure 6.10.:** The inverse susceptibilities (a)  $1/\chi_1$ , (b)  $1/\chi_2$ , (c)  $1/\chi_3$  (please note the scaling factor 0.01 at the  $y$ -axis), and (d)  $1/\chi_4$  versus  $J_2$  obtained within the CCM LSUB $n$  approximation with  $n = 4, 6, 8$  and extrapolated to  $n \rightarrow \infty$  using  $\chi(n) = c_0 + c_1(1/n) + c_2(1/n)^2$ . Insets: The same as in the main panels but using ED for finite lattice of  $N = 16, 24, 32$ . Panel (a) might be compared to Fig. 2 of Ref. [47] and Fig. 3 of Ref. [49], panel (b) might be compared to Fig. 5 of Ref. [47], panel (c) might be compared to Fig. 6 of Ref. [47] and Fig. 3 of Ref. [50].

with the data shown in Fig. 2 and Fig. 5 in Ref. [47].] The CCM results for  $\chi_1$  and  $\chi_2$  also qualitatively agree with variational quantum Monte Carlo method and ED results reported (for some  $J_2$  only) in Ref. [26]. The CCM results for  $\chi_3$ , however, exhibit a different qualitative dependence on  $J_2$  as  $J_2$  approaches  $J_2^{c1}$  in comparison with series-expansion data, [47, 50] compare, e.g., Fig. 6 in Ref. [47] and Fig. 6.10c in the present paper. According to series-expansion data  $\chi_3$  decreases by about 20% as  $J_2$  increases from 0 to 0.4. In contrast, according to CCM data shown in Fig. 6.10c  $\chi_3$  increases by a factor about 4 as  $J_2$  increases from 0 to 0.4.

Let us now discuss some general features of the generalized susceptibilities shown

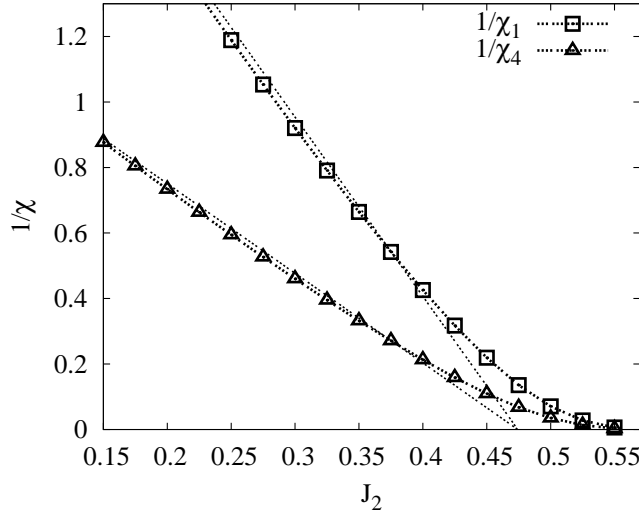


**Figure 6.11.:** Susceptibilities  $1/\chi_1$  (red) and  $1/\chi_4$  (gray) around the critical point  $J_2^{c1}$ . Bold curves correspond to the CCM curves shown in Fig. 6.10a and Fig. 6.10d. Thin lines obtained from a linear fit of the CCM data for  $0 \leq J_2 \leq J_2^{c1}$ . Extrapolated (thin) lines for both inverse susceptibilities become zero at  $J_2 \approx 0.47$ .

in Fig. 6.10. Obviously, a divergence of a certain susceptibility (or  $1/\chi \rightarrow 0$ ) at a particular value of  $J_2$  indicates an instability of a GS phase regarding to a possible new GS order. It can be seen from Fig. 6.10, that all susceptibilities increase with growing  $J_2$  in the Néel phase. Near the critical point  $J_2^{c1}$  both  $1/\chi_1$  and  $1/\chi_4$  (CCM data imply  $\chi_4 = 2\chi_1$ ) are significantly smaller than  $1/\chi_2$  and  $1/\chi_3$  indicating that the valence-bond states belonging to the columnar dimerized and plaquette patterns are favorable in the magnetically disordered quantum phase.

A similar behavior of  $\chi_1$  and  $\chi_4$  (CCM data imply  $\chi_4 = \chi_1^{(x)} + \chi_1^{(y)}$ ) is observed if  $J_2$  approaches  $J_2^{c2}$  from the collinear phase, i.e. from  $J_2 > J_2^{c2}$ . On this side the behavior of  $\chi_2$  and  $\chi_3$  is not conclusive, since both are already large in the collinear phase.

The behavior of the susceptibilities  $\chi_1$  and  $\chi_4 (= 2\chi_1)$  near the critical point  $J_2^{c1}$  is shown in more detail in Fig. 6.11. Obviously, approaching  $J_2^{c1}$  from the Néel phase,  $\chi_1$  ( $\chi_4$ ) becomes very large, however, remains finite in the region around  $J_2^{c1}$  up to  $J_2 = 0.55$ . That might be attributed to limited accuracy of CCM results, since we have (i) data only up to LSUB8 for extrapolation and (ii) and LSUB $n$  data based on the Néel reference state may become less accurate for values of  $J_2$  exceeding  $J_2^{c1}$ . However, if the phase transition with respect to the corresponding VBS order parameter characterizing the quantum paramagnetic phase would be of second order we may expect an almost linear decreasing of the inverse susceptibility if  $J_2$  approaches  $J_2^{c1}$ , i.e.  $1/\chi_1 \propto (J_2^{c1} - J_2)^{\gamma_\phi}$  with  $\gamma_\phi \approx 1$ . [47] Hence a linear fit of the CCM data of  $1/\chi_1$  ( $1/\chi_4$ ) versus  $J_2$  using data points only within the Néel ordered region  $0 \leq J_2 \leq J_2^{c1}$  might give reasonable results. We find that the linear fit for both,  $1/\chi_1$  ( $1/\chi_4$ ) vanishes at the same point  $J_2 \approx 0.47J_1$ , see Fig. 6.11. This is in agreement with the scenario of

deconfined criticality, that predicts such divergence if the deconfined critical point is approached from the Néel phase [47, 73].

To conclude this part, the CCM and ED data for all examined susceptibilities,  $\chi_1$ ,  $\chi_2$ ,  $\chi_3$ , and  $\chi_4$ , exhibit an enhancement while the system runs out of the Néel phase. This enhancement is most pronounced for  $\chi_1$  ( $\chi_4$ ). Moreover,  $\chi_1$  ( $\chi_4$ ) most likely show the same critical behavior diverging at a value of  $J_2$  close to the quantum critical point  $J_2^{c1} \approx 0.44 \dots 0.45 J_1$  determined by the most accurate data for the Néel order parameter  $M$ . This finding is consistent with the predictions for a deconfined quantum critical point. [73] Furthermore we find that our CCM data for  $\chi_1$  and  $\chi_2$  agree with the series-expansion data [47]. By contrast, for  $\chi_3$  we observe a qualitatively different behavior. Finally, the enhancement/divergence of the considered susceptibilities if  $J_2$  approaches  $J_2^{c1}$  indicates that the translational symmetry is broken in the quantum paramagnetic phase, i.e. most likely a spatially homogeneous spin-liquid phase for  $J_2^{c1} < J_2 < J_2^{c2}$  can be excluded.

#### 6.4. CONCLUSIONS

To summarize, in this paper we have applied the CCM in high orders of approximation to the spin-1/2  $J_1$ - $J_2$  Heisenberg antiferromagnet on the square lattice and present a comprehensive analysis of the GS phase diagram of the model. For this purpose we have calculated the GS energy, the magnetic order parameter, the spin stiffness and several generalized susceptibilities.

Our results enrich the list of available data and are complementary to other existing results obtained using different approximate methods like series expansions or variational quantum Monte Carlo for the spin-1/2  $J_1$ - $J_2$  square-lattice Heisenberg antiferromagnet. In addition to the CCM results we present also ED results that are found to be in good agreement with the CCM data.

Our findings confirm the basic picture discussed earlier: For intermediate values of  $J_2^{c1} \leq J_2 \leq J_2^{c2}$  the ground state is a paramagnetic quantum state. The CCM prediction for the boundaries of the paramagnetic region is  $J_2^{c1} \approx 0.44 \dots 0.45 J_1$  and  $J_2^{c2} \approx 0.58 \dots 0.59 J_1$ . To discuss the nature of the quantum phase transition from the semiclassical Néel phase to the quantum paramagnetic state at  $J_2^{c1}$  we use the CCM (and ED) data as an input for the method developed in Ref. [47] to distinguish between a first- and a second-order transition. Our analysis leads to the conclusion that the phase transition from the Néel to the paramagnetic state at  $J_2^{c1}$  is second order. This outcome contradicts the conclusion of Ref. [47] based on series-expansion data, but agrees with the deconfined critical point scenario proposed in Refs. [72, 73].

Another way to check the predictions of the theory of deconfined quantum criticality is to examine the susceptibilities related to order parameters of a possible VBS ordering emerging, if the deconfined critical point is approached from the magnetically ordered Néel phase. The obtained data shown in Fig. 6.10 and Fig. 6.11 give another hint that  $\chi_1$  ( $\chi_4$ ) diverges at  $J_2^{c1}$  which does not contradict the deconfined critical point

scenario [72, 73].

Finally, the divergence/enhancement of the generalized susceptibilities obtained by CCM and ED approaching  $J_2^{cl}$  from the Néel phase gives evidence in favor of ground states breaking translational symmetry and, therefore, our data yield further arguments against a structureless (i.e. a spatially homogeneous) spin-liquid state without any LRO. We note that some of the results presented in this chapter are published in.<sup>1</sup>

---

<sup>1</sup>R. Darradi, O. Derzhko, R. Zinke, J. Schulenburg, S.E. Krüger, and J. Richter, " Ground-state phases of the spin-1/2  $J_1$ - $J_2$  Heisenberg antiferromagnet on the square lattice: A high-order coupled cluster treatment", Phys. Rev. B **78**, 214415-1-10 (2008)



# THE QUANTUM $J_1$ – $J_2$ ANTIFERROMAGNET ON THE STACKED SQUARE LATTICE

## 7.1. INTRODUCTION

The properties of quantum magnets strongly depend on the dimensionality. [176] Though the tendency to order is more pronounced in three-dimensional (3d) systems than in low-dimensional ones, a magnetically disordered phase can also be observed in frustrated 3d systems such as the HAFM on the pyrochlore lattice [177] or on the stacked kagomé lattice. [178] On the other hand, recently it has been found that the 3d  $J_1$ – $J_2$  model on the body-centered cubic lattice does not have an intermediate quantum paramagnetic phase. [167, 168]

As already mentioned in Chap. 6 the  $J_1$ – $J_2$  model on the square lattice is a canonical model to study quantum phase transitions in  $d = 2$ . [22–24, 26–28, 39, 43–49] However, in experimental realizations of the  $J_1$ – $J_2$  model the magnetic couplings are expected to be not strictly 2d, since a nonzero interlayer coupling  $J_\perp$  is always present. For example, recently Rosner *et al.* [159] have found  $J_\perp \approx 0.07J_1$  for  $\text{Li}_2\text{VO}_2\text{SiO}_4$ , a material which can be described by a square lattice  $J_1$ – $J_2$  model with large  $J_2$ . [54, 159]

This motivates us to consider an extension of the  $J_1$ – $J_2$  model, namely the  $J_1$ – $J_2$  spin-1/2 HAFM on the stacked square lattice (see Fig.7.1) described by the Hamiltonian

$$H = \sum_n \left( J_1 \sum_{\langle ij \rangle} \mathbf{s}_{i,n} \cdot \mathbf{s}_{j,n} + J_2 \sum_{[ij]} \mathbf{s}_{i,n} \cdot \mathbf{s}_{j,n} \right) + J_\perp \sum_{i,n} \mathbf{s}_{i,n} \cdot \mathbf{s}_{i,n+1}, \quad (7.1)$$

where  $n$  labels the layers and  $J_\perp \geq 0$  is the interlayer coupling. The expression in parentheses represents the  $J_1$ – $J_2$  model of the layer  $n$  with intralayer NN bonds  $J_1 = 1$  and NNN bonds  $J_2 \geq 0$ . The classical GS's of the model are the Néel state for  $J_2 < 0.5J_1$  and another particular collinear state for  $J_2 > 0.5J_1$ . The latter state (which we henceforth refer to as the collinear-columnar or, simply the collinear state) is a columnar  $(\pi, 0)$  state characterized by a parallel spin orientation of nearest neighbors along the direction of one axis (say, the vertical or columnar direction) in each layer, and an antiparallel spin orientation of nearest neighbors along the perpendicular (say, horizontal or row) direction. It is well known [22–24, 26–28, 39, 43–49] that for  $J_\perp = 0$  the quantum model has two corresponding GS phases with semi-classical magnetic LRO, one (Néel -like) for small  $J_2 \lesssim 0.4J_1$  and one (collinear-columnar-like) for large  $J_2 \gtrsim 0.6J_1$ , which are separated by a magnetically disordered (quantum paramagnetic)

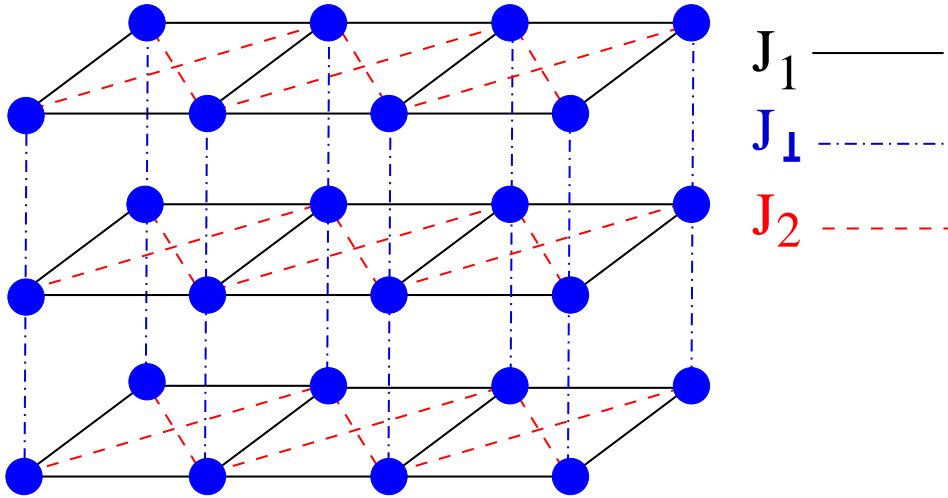


**Figure 7.1.:** Illustration of arrangement of bonds in the  $J_1$ - $J_2$  model on the Stacked Square Lattice (Eq.(7.1)).

GS phase.

For the treatment of the model of Eq. (7.1) with arbitrary  $J_{\perp}$  we apply the CCM for more details (see Chap.2) and use classical GS Néel (collinear-columnar) as reference states for small  $J_2$  (for large  $J_2$ ). We note once more that the number of fundamental configurations  $N_f$  can be reduced exploiting lattice symmetry and conservation laws. However, this number  $N_f$  increases with increasing the number of dimension. In the CCM-LSUB8 approximation we have finally 25953 (43070) fundamental configurations for the Néel (collinear) reference state. To solve the set of the corresponding ket equations we use parallel computing. [116]

Since the LSUB $n$  approximation becomes exact for  $n \rightarrow \infty$ , it is useful to extrapolate the 'raw' LSUB $n$  data to  $n \rightarrow \infty$ . An appropriate extrapolation rule for the order parameter of systems showing a GS order-disorder transition is the 'leading power-law' extrapolation of Eq. (2.44) [93] where the results of the LSUB4,6,8 approximations are used for the extrapolation. For the GS energy per spin we use Eq. (2.42) which is a reasonable extrapolation ansatz. [18]

## 7.2. RESULTS AND DISCUSSIONS

As in the 2d case the GS of the stacked model is characterized by two magnetically long-range ordered phases, namely a Néel phase for small  $J_2$  and a collinear phase for large  $J_2$ . For not too large  $J_{\perp}$  both magnetic phases are separated by a magnetically disordered quantum paramagnetic phase, where the phase transition points are functions of  $J_{\perp}$ . In order to determine the GS phase transition points we calculate the order parameters for various values of  $J_{\perp}$  and determine those values  $J_2 = \alpha_{\text{Néel}}(J_{\perp})$  and  $J_2 = \alpha_{\text{col}}(J_{\perp})$  where the order parameters vanish.

In Fig.7.2 we present some typical curves showing the extrapolated order parameters

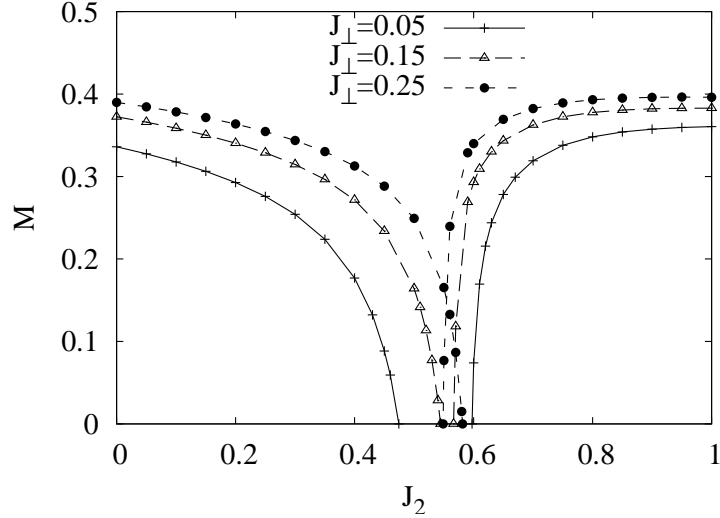


**Figure 7.2.:** The magnetic order parameter  $m$  versus  $J_2$  for various strengths of the interlayer coupling  $J_\perp$  (with  $J_1 = 1$ ).

(according to Eq. (2.44)) versus  $J_2$  for some values of  $J_\perp$ . The magnetic order parameters of both magnetically long-range ordered phases vanish continuously as is typical for second-order transitions. We note, however, that there are arguments [43, 44, 49] that the transition from the collinear-columnar phase to the quantum paramagnetic phase should be of first order. The order parameters for both phases are monotonically increasing functions of  $J_\perp$ , and the transition points  $\alpha_{\text{Néel}}$  and  $\alpha_{\text{col}}$  also move together as  $J_\perp$  increases.

In Fig. 7.3 we present the dependence on  $J_\perp$  of these transition points. Close to the strictly 2d case (i.e., for small  $J_\perp \ll J_1$ ) the influence of the interlayer coupling is largest. For a characteristic value of  $J_\perp^* \approx 0.19J_1$  the two transition points  $\alpha_{\text{Néel}}$  and  $\alpha_{\text{col}}$  meet each other. For larger  $J_\perp$  exceeding  $J_\perp^*$ , we have a direct first-order transition between both types of magnetic LRO as is also observed in the classical model and in the 3D quantum  $J_1$ - $J_2$  model on the body-centered cubic lattice [167, 168]. We can add to the above discussion of the order parameters a comparison of the energies. Provided that the CCM equations converge for the Néel and the collinear reference state far enough beyond those points where the order parameters vanish we can determine the point where both energies become equal. For the considered LSUBn approximation, this happens for  $J_\perp \gtrsim 0.1$ . In the inset of Fig. 7.4 we show the energies versus  $J_2$  for  $J_\perp = 0.2$  calculated by extrapolation. The corresponding points  $J_2 = \alpha'_{\text{coll}}(J_\perp)$  where both energies meet are shown in Fig. 7.3 as dashed line.

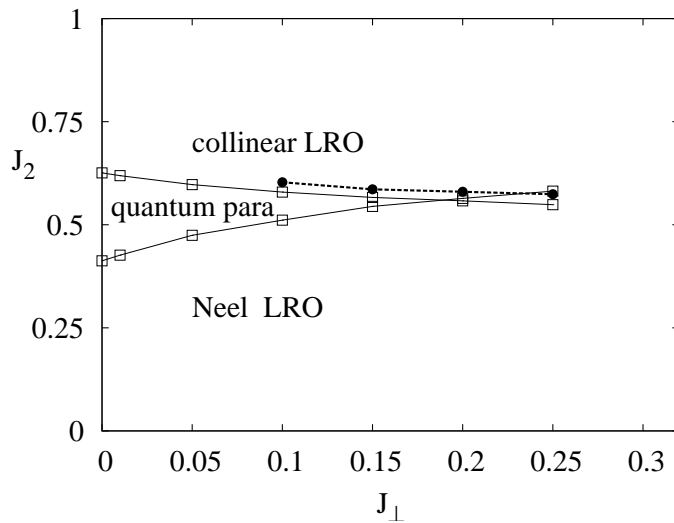


**Figure 7.3.:** The ground-state phase diagram (where the solid lines show those values of  $J_2$  for which the order parameters vanish and the dashed line represents those values of  $J_2$  where the two energies calculated for the Néel and collinear reference states). Note that  $J_1 = 1$ .

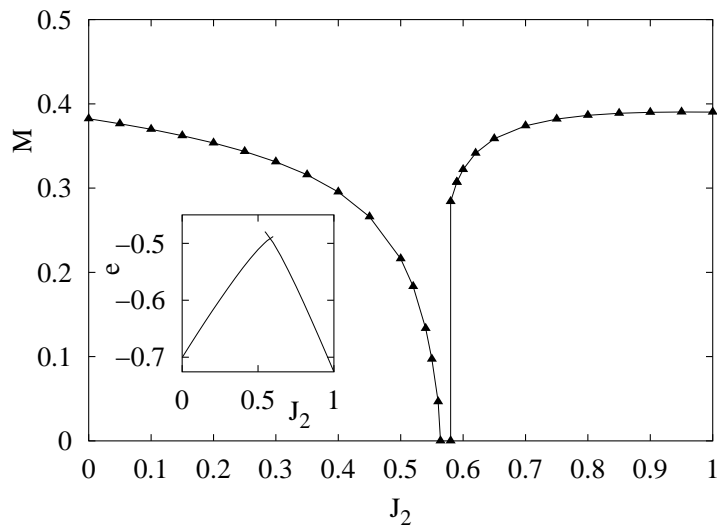


**Figure 7.4.:** CCM results for the energy per spin  $e$  for both reference states (inset) and the order parameter  $M$  for  $J_\perp = 0.2$ . Both quantities are obtained by extrapolation of the 'raw' LSUB $n$  results to the limit  $n \rightarrow \infty$  as explained in the text. The energies calculated with the Néel and collinear reference states become equal at  $J_2 \approx 0.58$  indicating a first-order transition. For the order parameter  $M$ , we take that value calculated with the reference state of lower CCM energy.

### 7.3. CONCLUSIONS

We obtain that both transition points  $\alpha_{coll}$  and  $\alpha'_{coll}$  are close to each other and show a similar dependence on  $J_\perp$ . Secondly, we find that, at least for  $J_\perp \gtrsim 0.1$ , the energy

obtained with the Néel reference state is lower than that obtained with the collinear reference state even for  $J_2$  values where the Néel order parameter is already zero but the collinear order parameter is still finite. Thus, this energetic consideration leads to the following sequence of zero-temperature transitions: Second-order transition from Néel LRO to a quantum paramagnetic phase at  $J_2 = \alpha_{Neel}$  and then a first-order transition from the quantum paramagnetic phase to collinear LRO at  $J_2 = \alpha'_{coll} > \alpha_{coll} > \alpha_{Neel}$ . This behavior is illustrated in Fig. 7.4, where the order parameter  $M$  is shown versus  $J_2$  for fixed  $J_\perp = 0.2$ . For a certain value of  $J_\perp \approx 0.23$  both transition points  $\alpha_{Neel}$  and  $\alpha'_{coll}$  become equal, and one has a direct first-order transition between the two semiclassically long-range ordered phases. We note that some of the results presented in this chapter are published in.<sup>12</sup>

---

<sup>1</sup>D. Schmalfuß, R. Darradi, J. Richter, J. Schulenburg and D. Ihle, "Quantum J1-J2 Antiferromagnet on a Stacked Square Lattice: Influence of the Interlayer Coupling on the Ground-State Magnetic Ordering", Phys. Rev. Lett **97**, 157201 (2006)

<sup>2</sup>J. Richter, R. Darradi, R. Zinke and R. F. Bishop, "Frustrated quantum antiferromagnets: application of high-order coupled cluster method", International Journal of Modern Physics B **21**, 2273-2288 (2007)



## THE SPIN-1/2 AND SPIN-1 QUANTUM $J_1$ - $J'_1$ - $J_2$ HEISENBERG MODELS ON THE SQUARE LATTICE

### 8.1. INTRODUCTION

In the previous two chapters (6) and (7) the ground-state properties of the spin-1/2  $J_1$ - $J_2$  frustrated Heisenberg antiferromagnet on the square lattice, the nature of the magnetically disordered quantum phase and the influence of the interlayer coupling on the ground-state magnetic ordering have been discussed. However, an interesting generalization of this model has also introduced recently by Nersesyan and Tsvelik [169]. They consider a 2D spatially anisotropic spin-1/2  $J_1$ - $J'_1$ - $J_2$  model on the square lattice, where the nearest-neighbour bonds have different strengths  $J_1$  and  $J'_1$  in, say, the  $x$  (intrachain) and  $y$  (interchain) directions respectively. This model has been further studied by other groups using the exact diagonalization (ED) of small lattice samples of  $N \leq 36$  sites [170], and the continuum limit of the model [171]. Both groups support the prediction by Nersesyan and Tsvelik [169] of a resonating valence bond state for  $J_2 = 0.5J'_1 \ll J_1$ , and the limit of small interchain coupling extends along a curve nearly coincident with the line where the energy per spin is maximum. The model has also been studied by Moukouri [172] using a two-step density-matrix renormalization group approach.

Although spin problems are conceptually simple, they often exhibit rich and interesting phase diagrams due to the strong influence of quantum fluctuations in these strongly correlated systems. The strength of the quantum fluctuations can be tuned by varying either the anisotropy terms in the Hamiltonian or the spin quantum number  $s$  (see e.g., in Chapter. 3: Sec. 3.3, 3.4). Thus, lattice quantum spin problems maintain an important role in the study of quantum phase transitions. Very few calculations have been performed for the  $J_1$ - $J'_1$ - $J_2$  model for the case of  $s = 1$  up till now. It has, however, been studied using the two-step density-matrix renormalization group method, but only for the specific value of  $J'_1/J_1 = 0.2$ , and a second-order transition from a Néel phase to a disordered phase is observed with a spin gap [179]. It has also been observed that quantum fluctuations can destabilize the ordered classical ground state, even for large values of  $s$ , for large enough values of the frustration [27, 37].

Furthermore, it has been argued recently that the quantum phase transition between the semiclassical Néel phase and the quantum paramagnetic phase present in the 2D  $J_1$ - $J_2$  model is not described by a Ginzburg-Landau type critical theory, but rather may exhibit a deconfined quantum critical point [47, 72, 73, 115].

Our main goal in this chapter is to further the study of the  $J_1$ - $J'_1$ - $J_2$  model by using the CCM (see e.g., Chap.2). A particularly important result from our calculations is the indicated existence of a quantum triple point (QTP) at nonzero (positive) values of  $J_1$ ,  $J'_1$  and  $J_2$ .

## 8.2. THE MODEL

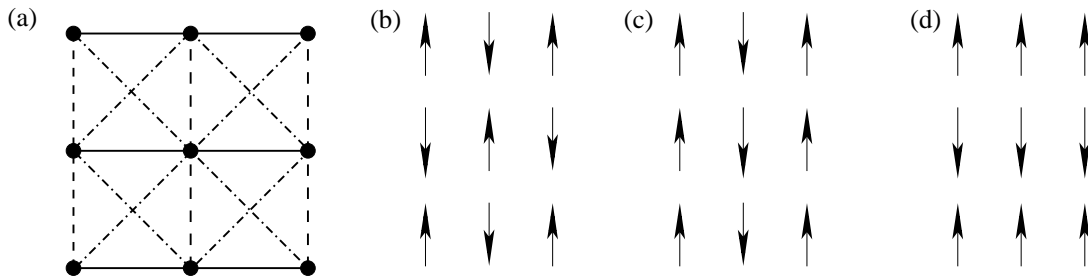


**Figure 8.1.:** (a)  $J_1$ - $J'_1$ - $J_2$  model; —  $J_1$ ; - -  $J'_1$ ; · · ·  $J_2$ ; (b) Néel state, (c) stripe state - columnar and (d) stripe state - row. Arrows in (b), (c) and (d) represent spins situated on the sites of the square lattice (indicated by • in (a)).

The  $J_1$ - $J'_1$ - $J_2$  model is a general spin- $s$  Heisenberg model on a square lattice with three kinds of exchange bonds, with strength  $J_1$  along the row direction,  $J'_1$  along the column direction, and  $J_2$  along the diagonals, as shown in Fig. 8.1. All exchanges are assumed positive here, and we set  $J_1 = 1$ . The Hamiltonian of the model is described by

$$\begin{aligned}
 H = & J_1 \sum_{i,l} \mathbf{s}_{i,l} \cdot \mathbf{s}_{i+1,l} + J'_1 \sum_{i,l} \mathbf{s}_{i,l} \cdot \mathbf{s}_{i,l+1} \\
 & + J_2 \sum_{i,l} (\mathbf{s}_{i,l} \cdot \mathbf{s}_{i+1,l+1} + \mathbf{s}_{i+1,l} \cdot \mathbf{s}_{i,l+1}). \quad (8.1)
 \end{aligned}$$

This model has two types of classical ground state, namely, the Néel  $(\pi, \pi)$  state and stripe states (columnar stripe  $(\pi, 0)$  and row stripe  $(0, \pi)$ ), the spin orientations of which are shown in Figs. 8.1(b,c,d) respectively. There is clearly a symmetry under the interchange of rows and columns,  $J_1 \rightleftharpoons J'_1$ , which implies that we need only consider the range of parameters with  $J'_1 < J_1$ . The ground-state (gs) energies of the



various classical states are given by

$$\begin{aligned}\frac{E_{\text{Néel}}^{\text{cl}}}{N} &= (-J_1 - J'_1 + 2J_2)|s|^2, \\ \frac{E_{\text{columnar}}^{\text{cl}}}{N} &= (-J_1 + J'_1 - 2J_2)|s|^2, \\ \frac{E_{\text{row}}^{\text{cl}}}{N} &= (J_1 - J'_1 - 2J_2)|s|^2.\end{aligned}\tag{8.2}$$

We take  $J_1 = 1$  and  $J'_1 < 1$ . Clearly, from Eq. (8.2), the classical GS is then either the Néel state (if  $J'_1 > 2J_2$ ) or the stripe state (if  $J'_1 < 2J_2$ ). Hence, the (first-order) classical phase transition between the Néel and stripe (columnar) states occurs at  $J_2^c = \frac{1}{2}J'_1$ ,  $\forall J_1 > J'_1$ .

We now apply the CCM formalism to the spin-1/2 and spin-1 quantum  $J_1$ - $J'_1$ - $J_2$  Heisenberg models on the square lattice, and we choose the Néel and stripe states as the model state. For the case of  $s = 1/2$  we employ here, as in our previous work [22,42,88,92,93], the localized LSUB $n$  scheme. The numbers of such fundamental configurations (viz., those that are distinct under the symmetries of the Hamiltonian and of the model state  $|\Phi\rangle$ ) that are retained for the Néel and stripe states of the current model in various LSUB $n$  approximations are shown in Table 8.1.

We note next that the number of fundamental LSUB $n$  configurations for  $s = 1$  becomes appreciably higher than for  $s = 1/2$ , since each spin on each site  $i$  can now be flipped twice by the spin-raising operator  $s_i^+$ . Thus, for the  $s = 1$  model it is more practical to use the alternative SUB $n$ - $m$  scheme 2.2.3, where  $m$  is the size of the locale on the lattice and  $n$  is the maximum number of spin-flips. In our case we set  $m = n$ , and hence employ the SUB $n$ - $n$  scheme. More generally, the LSUB $m$  scheme is thus equivalent to the SUB $n$ - $m$  scheme for  $n = 2sm$ . Hence, LSUB $m \equiv \text{SUB}2sm$ - $m$ . For  $s=1/2$ , LSUB $n \equiv \text{SUB}n$ - $n$ ; whereas for  $s = 1$ , LSUB $n \equiv \text{SUB}2n$ - $n$ . The numbers of fundamental configurations retained at various SUB $n$ - $n$  levels for the  $s = 1$  model are shown in Table 8.1.

In order to solve the corresponding coupled sets of CCM ket- and bra-state (see Eq. 2.7, 2.8) equations we use parallel computing [116].

In our results below the LSUB $n$  results for  $n = \{4, 6, 8, 10\}$  are extrapolated for  $s = 1/2$ , in order to preserve the three rules (see e.g., Sec. 2.5), whereas the SUB $n$ - $n$  results for  $n = \{2, 4, 6, 8\}$  are extrapolated for  $s = 1$ , in each case using the schemes indicated above. For both the  $s = 1/2$  and the  $s = 1$  models we perform two separate sets of CCM calculations for given parameters ( $J_1 \equiv 1, J'_1, J_2$ ) based respectively on the Néel state and the stripe state as the model state  $|\Phi\rangle$ .

**Table 8.1.:** Numbers of fundamental configurations ( $N_f$ ) for  $s = 1/2$  and  $s = 1$  in various CCM approximations.

$s = 1/2$			$s = 1$		
Scheme	$N_f$		Scheme	$N_f$	
	Néel	stripe		Néel	stripe
LSUB2	2	1	SUB2-2	2	1
LSUB4	13	9	SUB4-4	28	21
LSUB6	146	106	SUB6-6	744	585
LSUB8	2555	1922	SUB8-8	35629	29411
LSUB10	59124	45825	-	-	-

### 8.3. RESULTS AND DISCUSSION

#### 8.3.1. Ground-state energy

Figures 8.2, 8.3 shows the gs energy per spin as a function of  $J_2$  for various values of  $J'_1$  (all with  $J_1 \equiv 1$ ), extrapolated from both the  $s = 1/2$  and  $s = 1$  models from the raw CCM data as discussed above. Both the raw LSUB $n$  data for the  $s = 1/2$  model and the raw SUB $n$ - $n$  data for the  $s = 1$  model terminate at some particular values. This occurs for the CCM curves based on both the Néel state and the stripe state as the model state  $|\Phi\rangle$ . In all cases such a termination point arises due to the solutions of the CCM equations becoming complex at this point, beyond which there exist two branches of complex-conjugate solutions. In the region where the solution reflecting the true physical situation is real, there actually also exists another real solution. However, only the (shown) upper branch of these two solutions reflects the true physical situation, whereas the lower branch does not. The branch reflecting the true physical situation of the solutions is the one which becomes exact in some appropriate (e.g., perturbative) limit. This physical branch then meets the corresponding unphysical branch at some termination point beyond which no real solutions exist. The termination points shown in Figures 8.2, 8.3 are the extrapolated  $n \rightarrow \infty$  termination points and are evaluated using data only up to the highest level of the CCM approximation schemes used here, namely LSUB10 for the  $s = 1/2$  model and SUB8-8 for the  $s = 1$  model. The SUB $n$ - $n$  and LSUB $n$  termination points are also reflections of phase transitions in the real system, as we discuss more fully below.

We observe from Fig. 8.2 that for the case of the  $s = 1/2$  model the two curves, based on the Néel and stripe model states, for a given value of  $J'_1$ , cross (or, in the

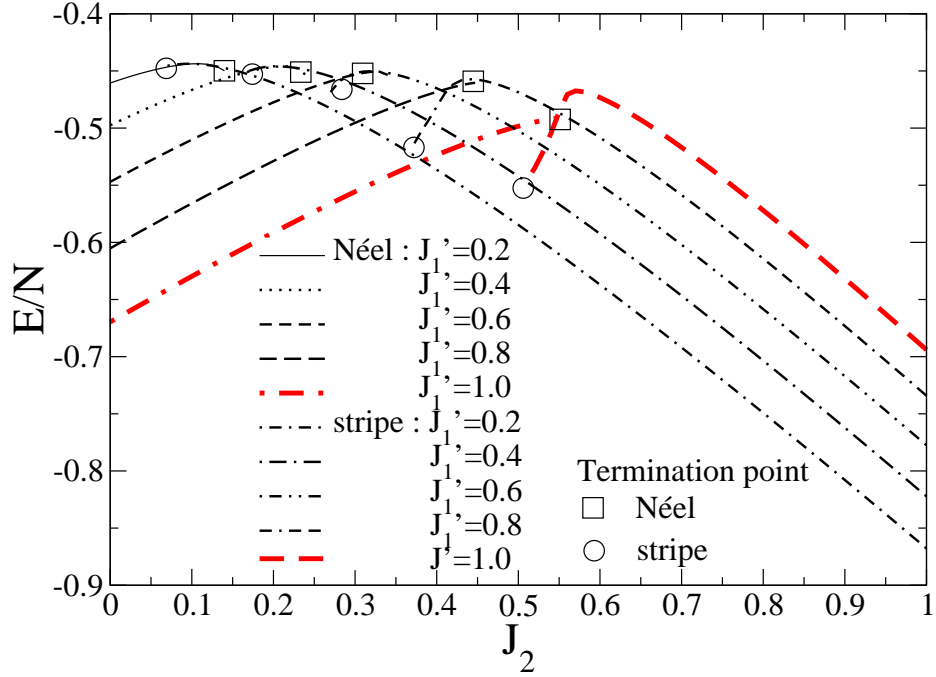


**Figure 8.2.:** Extrapolated CCM LSUB $n$  results for the gs energy per spin,  $E/N$ , for  $J_1' = 0.2, 0.4, 0.6, 0.8, 1.0$ , using the Néel and stripe states of the  $s = 1/2$   $J_1 - J_1' - J_2$  model. The LSUB $n$  results are extrapolated (according to Eq. (2.43)) in the limit  $n \rightarrow \infty$  using the set  $n = \{4, 6, 8, 10\}$ . The NN exchange coupling  $J_1 = 1$ .

limit, meet) very smoothly near their maxima for all values of  $J_1' \lesssim 0.6$ , at a value of  $J_2$  slightly larger than the classical transition point of  $0.5J_1'$ . This behaviour is indicative of a second-order quantum phase transition between these two phases, by contrast with the first-order classical transition from Eq. (8.2). Conversely, for values  $J_1' \gtrsim 0.6$  the curves no longer cross at a physical value (viz., where the calculated staggered magnetization is positive), indicating the opening up of an intermediate quantum phase between the Néel and stripe phases. For the case of  $s = 1$  (see Fig. 8.3), the extrapolated gs energy curves of the Néel and stripe states again meet smoothly with the same slope for  $J_1' \lesssim 0.66 \pm 0.03$ . This behaviour is again indicative of a second-order phase transition. By contrast, for  $J_1' \gtrsim 0.66 \pm 0.03$  the behaviour is typical of a first-order phase transition where the curves now cross with a discontinuity in the slope. Figures 8.2, 8.3 clearly show the distinct differences in the gs energy curves for the two models with  $s = 1/2$  and  $s = 1$ . This different behaviour observed in the gs energy for the two models is reinforced by the gs staggered magnetization results discussed below.

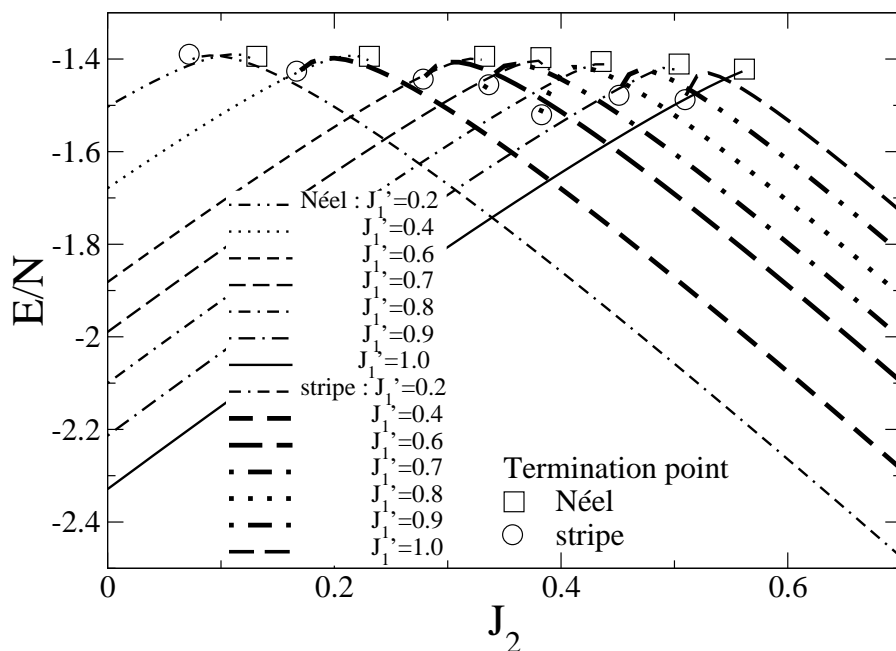


**Figure 8.3.:** Extrapolated CCM SUB $n$ - $n$  results for the gs energy per spin,  $E/N$ , of the  $s = 1$   $J_1$ - $J_1'$ - $J_2$  model, for  $J_1' = 0.2, 0.4, 0.6, 0.7, 0.8, 0.9, 1.0$ . The SUB $n$ - $n$  results are extrapolated (according to Eq. (2.43)) in the limit  $n \rightarrow \infty$  using the set  $n = \{2, 4, 6, 8\}$ .

### 8.3.2. Magnetic order parameter

For the gs staggered magnetization for the  $s = 1/2$  model we find that the extrapolation of Eq. (2.44) produces smooth and physically reasonable results, except for a very narrow anomalous “shoulder” region near the points where  $M$  vanishes for  $0.6 \lesssim J_1' \lesssim 0.75$  for the Néel state (see Fig. 8.4(a)). This critical regime is undoubtedly difficult to fit with the simple two-term scheme of Eq. (2.44). Our method for curing this problem and for stabilizing the curves is to make efficient use of the information we obtain in Eq. (2.44) to extract the exponent  $\nu$ , and then to use that value to infer the next term in the series. We find, very gratifyingly, that the value for  $\nu$  fitted to Eq. (2.44) turns out to be very close to 0.5 for all values of  $J_1'$  and  $J_2$  except very close to the critical point. Therefore, we use the form of Eq. (2.45). The use of Eq. (2.45) removes the anomalous shoulder, as shown in Fig. 8.4(b). Henceforth, in all of the results we discuss, we use Eq. (2.45) for the staggered magnetization.

We have also checked that for the  $s = 1/2$  model the extrapolated results using the data sets with  $n = \{2, 4, 6, 8, 10\}$  and  $n = \{4, 6, 8, 10\}$  are very similar, thereby adding credence to the validity and stability of our results. Conversely, the results using the data set with  $n = \{6, 8, 10\}$  again display a minor spurious “shoulder” which is almost certainly due to violating our Rule 1 (see e.g., Chap. 2: Sec. 2.5).

For the  $s = 1$  model, no narrow anomalous “shoulder” region is observed in the raw SUB $n$ - $n$  results. We have also performed some vigorous tests in the extrapola-

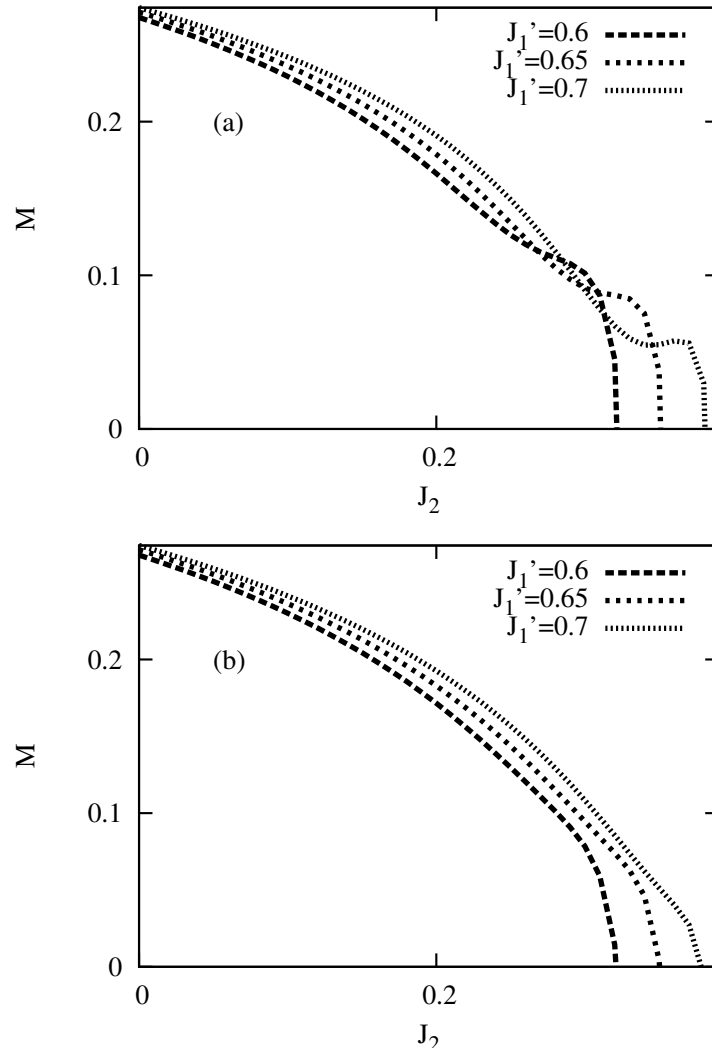


**Figure 8.4.:** Extrapolated CCM LSUB $n$  results for the gs staggered magnetization,  $M$ , for  $J_1' = 0.6, 0.65, 0.7$  for the Néel state of the  $s = 1/2$   $J_1 - J_1' - J_2$  model. (a) Results using Eq. (2.44), (b) Results using Eq. (2.45). The LSUB $n$  results are extrapolated in the limit  $n \rightarrow \infty$  using the set  $n = \{4, 6, 8, 10\}$ . The NN exchange coupling  $J_1 = 1$ .

tion schemes for the staggered magnetization in this case. Our main finding is that Eq. (2.45) using the data set with  $n = \{2, 4, 6, 8\}$  is the most consistent in terms of both the gs energy meeting point and the staggered magnetization critical point, as discussed below. Figures 8.5, 8.6 shows our extrapolated results for the the gs staggered magnetization  $M$  for both models. The quantum phase transition or critical point marking the end of either the quantum Néel state or the quantum stripe state is determined by calculating the order parameter  $M$  for various values of  $J_1'$  to obtain those values of  $J_2$  where  $M$  vanishes. However, as seen in Figs. 8.5, 8.6, there also occur cases where the order parameters of the two states meet before the order

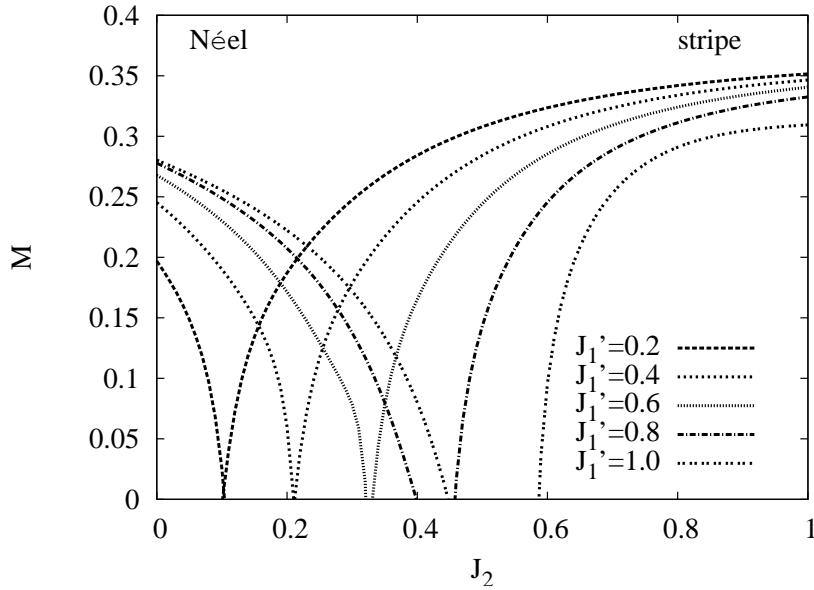


**Figure 8.5.:** The extrapolated CCM LSUB $n$  results for the staggered magnetization,  $M$ , for  $J_1' = 0.2, 0.4, 0.6, 0.8, 1.0$  of the  $s = 1/2$   $J_1$ - $J_1'$ - $J_2$  model. The LSUB $n$  results are extrapolated (according to Eq. (2.45)) in the limit  $n \rightarrow \infty$  using the set  $n = \{4, 6, 8, 10\}$ . The NN exchange coupling  $J_1 = 1$ .

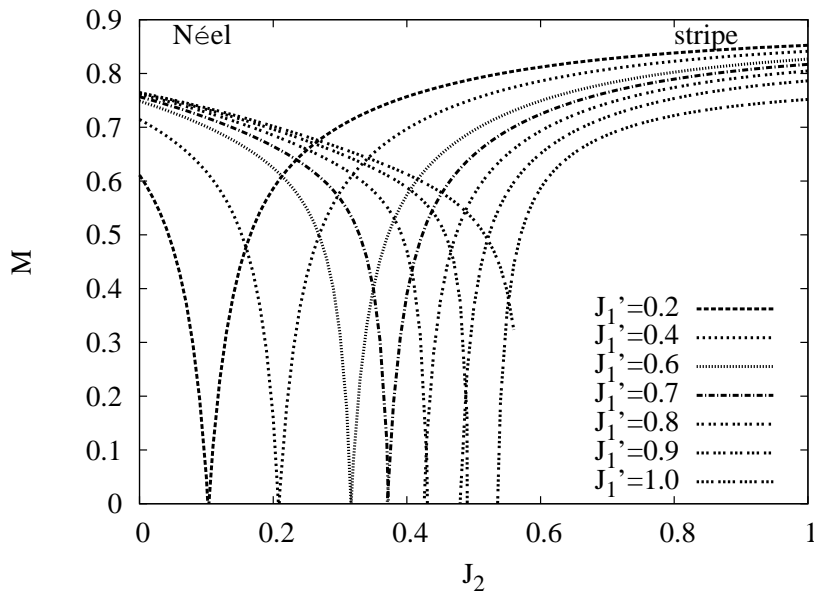


**Figure 8.6.:** Extrapolated CCM SUB $n$ - $n$  results for the gs staggered magnetisation,  $M$ , of the  $s = 1$   $J_1$ - $J_1'$ - $J_2$  model, for  $J_1' = 0.2, 0.4, 0.6, 0.7, 0.8, 0.9, 1.0$ . The SUB $n$ - $n$  results are extrapolated (according to Eq. (2.45)) in the limit  $n \rightarrow \infty$  using the set  $n = \{2, 4, 6, 8\}$ .

parameter vanishing point. In these cases we take the meeting point to define the phase boundary between the quantum Néel and quantum stripe states. Thus, our

definition of the quantum critical point is the point where there is an occurrence of a phase transition between the two states considered or where the order parameter vanishes, whichever occurs first.

For the  $s = 1/2$  model we note that  $M$  vanishes for both the quantum Néel and stripe phases at almost exactly the same critical value of  $J_2$ , for a given  $J'_1$ , so long as  $J'_1 \lesssim 0.6$ . Conversely, for  $J'_1 \gtrsim 0.6$  there exists an intermediate region between the critical points at which  $M \rightarrow 0$  for these two phases. The order parameters  $M$  of both the Néel and the stripe phases vanish continuously both below and above the point  $J'_1 \approx 0.60$ , as is again typical of second-order transitions.

By contrast, we note the surprising result for the  $s = 1$  model that the order parameter  $M$  goes to zero smoothly at the same point for both the quantum Néel and stripe phases with the same value of  $J'_1$ , for all values of  $J'_1 \lesssim 0.66 \pm 0.03$ , whereas the corresponding curves for the two phases meet at a nonzero value for higher values of  $J'_1$ . Thus, in this regime we have behaviour typical of a second-order phase transition between the quantum Néel and stripe phases. Furthermore, the transition occurs at a value of  $J_2$  very close to the classical transition point at  $J_2 = 0.5J'_1$ . Conversely, for values of  $J'_1 \gtrsim 0.66 \pm 0.03$ , the order parameters  $M$  of the two states meet at a finite value, as is typical of a first-order transition.

### 8.3.3. Ground-state phase diagrams

We show in Figs. 8.7, 8.8 the zero-temperature phase diagrams of both the spin-1/2 and spin-1  $J_1$ - $J'_1$ - $J_2$  models on the square lattice, as obtained from our extrapolated results for both the gs energy and the gs order parameter  $M$ . In the case of the spin-1/2 model our results provide clear and consistent evidence for a *quantum triple point* (QTP) at  $(J'_1 \approx 0.60 \pm 0.03, J_2 \approx 0.33 \pm 0.02)$  for  $J_1 = 1$ . For  $J'_1 \lesssim 0.60$  there exist only the Néel and stripe phases, with a second-order transition between them, whereas for  $J'_1 \gtrsim 0.60$  there also exists an intermediate (disordered, paramagnetic) quantum phase, which requires further investigation. Although the nature of the intermediate phase is still under discussion, a valence-bond crystal phase seems to be the most favoured from other investigations [40, 47]. On the other hand, another possibility for this intermediate phase is the resonating valence bond (RVB) phase [170]. Other calculations on this spin-1/2 model [170, 171] differ predominantly by giving a QTP at  $(J'_1 = 0, J_2 = 0)$  for  $J_1 = 1$ . We believe that the difference arises essentially from the nature of the alternative methods used. For example, due to the small size of the lattices used, the ED calculations of Sindzingre [170] might easily miss the longer-range correlations that become increasingly important the nearer one approaches the QTP.

Unlike the  $s = 1/2$  case there is no sign at all of any intermediate disordered phase for any value of the parameters  $J'_1$  or  $J_2$  (for  $J_1 = 1$ ) for the case of  $s = 1$ . Hence, in this respect the quantum spin-1 model is much closer to the classical case, viz., the  $s \rightarrow \infty$  limit. However, unlike the classical case, there now appears to be a *quantum tricritical point* (QTCP) at  $(J'_1 \approx 0.66 \pm 0.03, J_2 \approx 0.35 \pm 0.02)$  for  $J_1 = 1$ , where

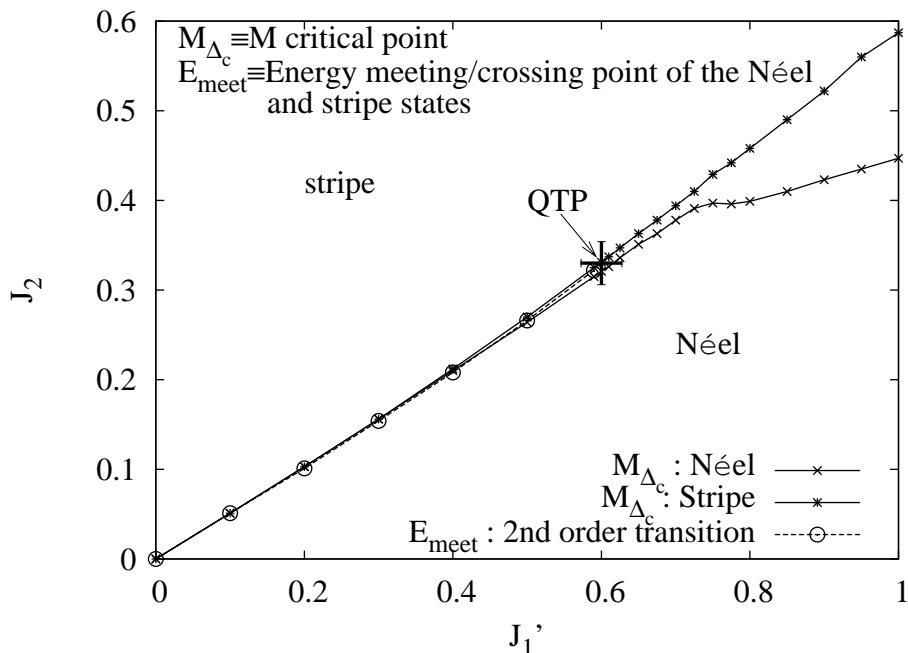


**Figure 8.7.:** The extrapolated CCM LSUB $n$  results for the gs phase diagram of the  $s = 1/2$   $J_1$ - $J_1'$ - $J_2$  model. The LSUB $n$  results are extrapolated in the limit  $n \rightarrow \infty$  using the set  $n = \{4, 6, 8, 10\}$ . The NN exchange coupling  $J_1 = 1$ . QTP  $\equiv$  quantum triple point.

a tricritical point is defined here to be a point at which a line of second-order phase transitions meets a line of first-order phase transitions. We note that the behaviour of both the order parameter (which goes to zero smoothly at the same point for both Néel and stripe phases below the QTCP, but which goes to a nonzero value above it) and the gs energy curves for the two phases (which meet smoothly with the same slope below the QTCP, but which cross with a discontinuity in slope above it) tell exactly the same story. We note that some of the results presented in this chapter are published in.<sup>1 2</sup>

<sup>1</sup>R. F. Bishop, P. H. Y. Li, R. Darradi and J. Richter "The quantum  $J_1$ - $J_1'$ - $J_2$  spin-1/2 Heisenberg model: influence of the interchain coupling on the ground-state magnetic ordering in two dimensions", J. Phys.: Condens. Matter **20**, 255251 (2008)

<sup>2</sup>R. F. Bishop, P. H. Y. Li, R. Darradi and J. Richter, "The quantum  $J_1$ - $J_1'$ - $J_2$  spin-1 Heisenberg model: Influence of the interchain coupling on the ground-state magnetic ordering in 2D", Europhysics Letters **83**, 47004 (2008)



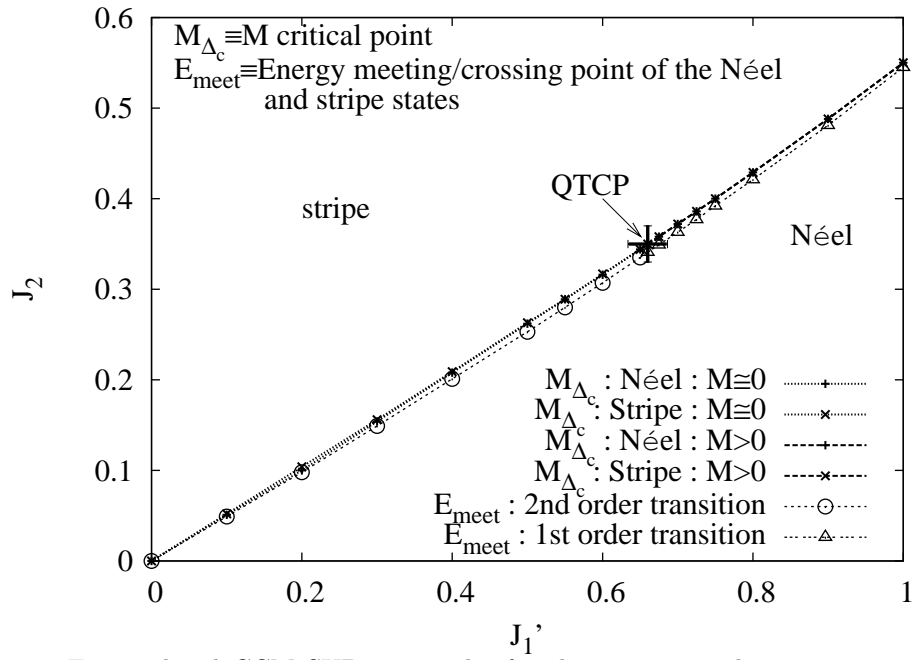


**Figure 8.8.:** Extrapolated CCM  $\text{SUB}_{n-n}$  results for the gs staggered magnetisation,  $M$ , of the spin-1  $J_1-J_1'-J_2$  model, for  $J_1' = 0.2, 0.4, 0.6, 0.7, 0.8, 0.9, 1.0$ . The  $\text{SUB}_{n-n}$  results are extrapolated in the limit  $n \rightarrow \infty$  using the set  $n = \{2, 4, 6, 8\}$ .



EFFECT OF ANISOTROPY ON THE GROUND-STATE  
MAGNETIC ORDERING OF THE SPIN-1/2 AND SPIN-1  
FRUSTRATED  $J_1$ - $J_2$  XXZ MODEL ON THE SQUARE  
LATTICE

9.1. INTRODUCTION

In this chapter we study the zero-temperature phase diagram of the 2D quantum spin-1/2 and spin-1 anisotropic Heisenberg model on the square lattice. In particular, the effects of the anisotropy  $\Delta$  on the  $z$ -aligned Néel and (collinear) stripe states, as well as on the  $xy$ -planar-aligned Néel and collinear stripe states, are examined. We generalize the spin-1/2 and spin-1  $J_1$ - $J_2$  model on the 2D square lattice in a different direction by allowing the bonds to become anisotropic in spin space rather than in real space. Such spin anisotropy is relevant experimentally as well as theoretically, since it is likely to be present, if only weakly, in any real material. Furthermore, the intermediate magnetically-disordered phase is likely to be particularly sensitive to *any* tuning of the quantum fluctuations, as we have seen above in the case of spatial anisotropy. Indeed, other evidence indicates that the intermediate phase might even disappear altogether in certain situations, such as increasing the dimensionality or the spin quantum number.

Thus, for example, the influence of frustration and quantum fluctuations on the magnetic ordering in the GS of the spin-1/2  $J_1$ - $J_2$  model on the body-centered cubic (bcc) lattice has been studied using linked-cluster series expansions [168], and also by using exact diagonalization of small lattices and linear spin-wave theory [167]. Contrary to the results for the corresponding model on the square lattice, it was found for the bcc lattice that frustration and quantum fluctuations do not lead to a quantum disordered phase for strong frustration. Rather, the results of all approaches suggest a first-order quantum phase transition at a value  $J_2/J_1 \approx 0.70$  from the quasiclassical Néel phase at low  $J_2$  to a quasiclassical collinear phase at large  $J_2$ . Similarly, the intermediate phase can also disappear when the spin quantum number  $s$  is increased for the  $J_1$ - $J_2$  model on the 2D square lattice. Thus, we found no evidence for a magnetically disordered state (for larger values of  $J_2/J_1$ ) for the spin-1 case, in contrast with the spin-1/2 case (see Chapter. 8).

As in previous work (see Chap. 8) involving the effect of spatial anisotropy on the spin-1/2 and spin-1  $J_1$ - $J_2$  models on the 2D square lattice, we again employ the

coupled cluster method (CCM) to investigate now the effect on the same model of spin anisotropy.

### 9.2. THE MODEL

The spin-1/2 and spin-1  $J_1$ - $J_2$  model is an isotropic Heisenberg model on a square lattice with two kinds of exchange bonds, with strength  $J_1$  for the NN bonds along both the row and the column directions, and with strength  $J_2$  for the NNN bonds along the diagonals, as shown in Fig. 9.1(a). Here we generalize the model by including an

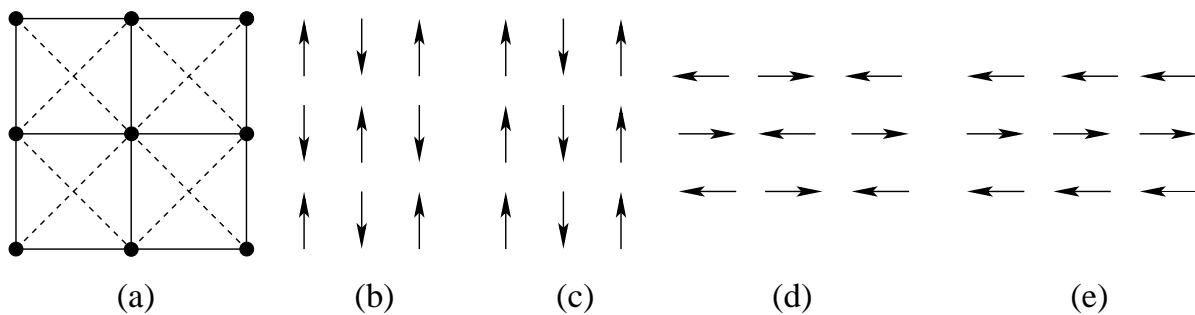


**Figure 9.1.:** (a) The  $J_1$ - $J_2$  XXZ Heisenberg model; —  $J_1$ ; - - -  $J_2$ ; (b) and (c)  $z$ -aligned states for the Néel and stripe columnar phases respectively; (d) and (e) planar  $x$ -aligned states for the Néel and stripe columnar phases respectively. Arrows in (b), (c), (d) and (e) represent spins situated on the sites of the square lattice [symbolized by  $\bullet$  in (a)].

anisotropy in spin space in both the NN and NNN bonds. We are aware of only a very few earlier investigations with a similar goal [41,173,180]. The two most detailed have studied the extreme limits where either the frustrating NNN interaction becomes anisotropic but the NN interaction remains isotropic [41] (viz., the  $J_1$ - $J_2^{XXZ}$  model) and the opposite case where the NN interaction becomes anisotropic but the NNN interaction remains isotropic [173] (viz., the  $J_1^{XXZ}$ - $J_2$  model). In real materials one might expect both exchange interactions to become anisotropic. To our knowledge the only study of this case [180] (viz., the  $J_1^{XXZ}$ - $J_2^{XXZ}$  model) has been done using the rather crude tool of linear spin-wave theory (LSWT), from which it is notoriously difficult to draw any firm quantitative conclusions about the positions of the gs phase boundaries of a system. It is equally difficult to use LSWT to predict with confidence either the number of phases present in the gs phase diagram or the nature of the quantum phase transitions between them. We comment further on the application of spin-wave theory to the  $J_1$ - $J_2$  model and its generalizations in Sec. 9.4. In order to keep the size of the parameter space manageable the anisotropy parameter  $\Delta$  is assumed to be the same in both exchange terms, thus yielding the so-called  $J_1^{XXZ}$ - $J_2^{XXZ}$  model,

whose Hamiltonian is described by

$$H = J_1 \sum_{\langle i,j \rangle} (s_i^x s_j^x + s_i^y s_j^y + \Delta s_i^z s_j^z) + J_2 \sum_{\langle\langle i,k \rangle\rangle} (s_i^x s_k^x + s_i^y s_k^y + \Delta s_i^z s_k^z), \quad (9.1)$$

where the sums over  $\langle i, j \rangle$  and  $\langle\langle i, k \rangle\rangle$  run over all NN and NNN pairs respectively, counting each bond once and once only. We are interested only in the case of competing antiferromagnetic bonds,  $J_1 > 0$  and  $J_2 > 0$ , and henceforth, for all of the results shown in Sec. 9.3, we set  $J_1 = 1$ . Similarly, we shall be interested essentially only in the region  $\Delta > 0$  (although for reasons discussed below in Sec. 9.3 we shall show results also for small negative values of  $\Delta$ ). This model has two types of classical antiferromagnetic ground states, namely a  $z$ -aligned state for  $\Delta > 1$  and an  $xy$ -planar-aligned state for  $0 < \Delta < 1$ . Since all directions in the  $xy$ -plane in spin space are equivalent, we may choose the direction arbitrarily to be the  $x$ -direction, say. Both of these  $z$ -aligned and  $x$ -aligned states further divide into a Néel  $(\pi, \pi)$  state and stripe states (columnar stripe  $(\pi, 0)$  and row stripe  $(0, \pi)$ ), the spin orientations of which are shown in Figs. 9.1(b,c,d,e) accordingly. There is clearly a symmetry under the interchange of rows and columns, which implies that we need only consider the columnar stripe states. The (first-order) classical phase transition occurs at  $J_2^c = J_1/2$ , with the Néel states being the classical GS for  $J_2 < J_1/2$ , and the columnar stripe states being the classical GS for  $J_2 > J_1/2$ .

For the CCM treatment of the model of Eq. (9.1), we use the classical GS (Néel at small  $J_2$  and collinear-columnar (CC) state at large  $J_2$ ) as reference state  $|\Phi\rangle$ . Starting from these reference states the CCM employs the exponential parametrization  $|\Psi\rangle = e^S |\Phi\rangle$  of the quantum GS  $|\Psi\rangle$  where the correlation operator  $S$  contains all possible multi-spin-flip correlations present in the true GS. Naturally,  $S$  has to be approximated. We use the well-elaborated CCM-LSUB $n$  and CCM-SUB $n-m$  approximation [18, 22, 42, 88, 92, 93, 113] for spin-1/2 and spin-1 respectively to calculate the GS energy per spin  $E$  and the sublattice magnetization per spin  $M$ . We note again that the number of fundamental LSUB $n$  configurations for  $s = 1$  becomes appreciably higher than for  $s = \frac{1}{2}$ , since each spin on each site  $j$  can now be flipped twice by the spin-raising operators, so that in this case the multi-configurational creation operators,  $C_I^+$  can contain up to two spin-raising operator  $s_j^+$  for each lattice site  $j$ . Thus, for systems with  $s > \frac{1}{2}$  it is more practical to use the SUB $n-m$  scheme (see e.g., Subsec. 2.2.3). Clearly, for spins with spin-1, the SUB $2n-n$  scheme is fully equivalent to the LSUB $n$  scheme. More generally for spins with arbitrary spin quantum number  $s$ , SUB $2sn-n \equiv$  LSUB $n$ . In order to keep the number of fundamental configurations from growing too quickly with increasing level of approximation we set  $m = n$ , and thus we have the SUB $n-n$  scheme. Clearly, as  $n \rightarrow \infty$ , the approximation becomes exact.

Table 9.1 and 9.2 show the number of fundamental LSUB $n$  and SUB $n-n$  configurations for the  $z$ -aligned and planar  $x$ -aligned states in the Néel and striped phases. We see that the number of fundamental configurations for the planar model state at

**Table 9.1.:** Numbers of fundamental configurations ( $N_f$ ) for spin-1/2 and spin-1 in various CCM approximations for the  $z$ -aligned states of the spin-1/2 and spin-1  $J_1^{XXZ}$ - $J_2^{XXZ}$  model on the square lattice.

$s = 1/2$			$s = 1$		
Scheme	$N_f$		Scheme	$N_f$	
	Néel	stripe		Néel	stripe
LSUB2	1	1	SUB2-2	1	1
LSUB4	7	9	SUB4-4	15	21
LSUB6	75	106	SUB6-6	375	585
LSUB8	1287	1922	SUB8-8	17864	29411
LSUB10	29605	45825	-	-	-

**Table 9.2.:** Numbers of fundamental configurations ( $N_f$ ) for spin-1/2 and spin-1 in various CCM approximations for the planar  $x$ -aligned states of the spin-1/2 and spin-1  $J_1^{XXZ}$ - $J_2^{XXZ}$  model on the square lattice.

$s = 1/2$			$s = 1$		
Scheme	$N_f$		Scheme	$N_f$	
	Néel	stripe		Néel	stripe
LSUB2	1	2	SUB2-2	2	3
LSUB4	10	18	SUB4-4	31	57
LSUB6	131	252	SUB6-6	1085	2131
LSUB8	2793	5532	SUB8-8	61904	123471
LSUB10	74206	148127	-	-	-

the LSUB10(SUB8-8) level of approximation is 74206(61904) for the Néel phase and 148127(123471) for the stripe phase. The intensive calculations required at even this very high order of approximation are easily practicable with relatively modest super-computing resources. Thus, for example, we employed 600(200) processors simultaneously to execute the LSUB10(SUB8-8) calculations using the planar  $x$ -aligned collinear stripe state as model state, and with this number of processors it took approximately

six hours to solve the CCM equations (2.7) and (2.8) at this level of approximation for each value of the anisotropy parameter  $\Delta$  in the Hamiltonian (9.1).

The final step in any CCM calculation is then to extrapolate the approximate LSUB $n$  and SUB $n-n$  results to the exact,  $n \rightarrow \infty$ , limit. We use here for the extrapolations of the raw LSUB $n$  and SUB $n-n$  data the same well-tested scaling laws as we used previously in our studies of the  $J_1-J'_1-J_2$  model for both the  $s = \frac{1}{2}$  and the  $s = 1$  (see e.g., Chap. 8).

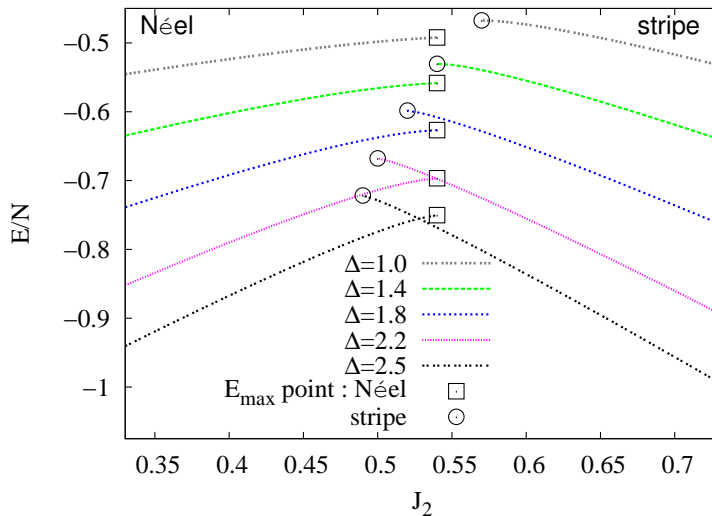
### 9.3. RESULTS

#### 9.3.1. Ground-state energy

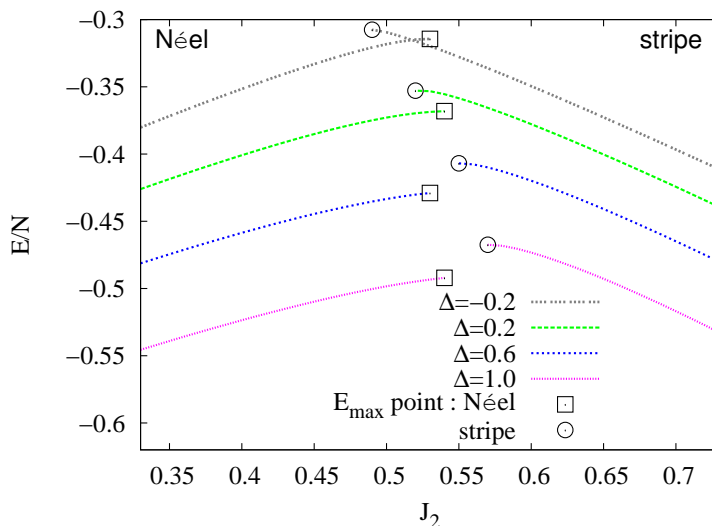
Figure 9.2 shows the extrapolated results for the gs energy per spin as a function of  $J_2$  (with  $J_1 = 1$ ) for various values of  $\Delta$ , for the  $z$ -aligned and planar  $x$ -aligned model states. For each model state, two sets of curves are shown, one (for smaller values of  $J_2$ ) using the Néel state, and the other (for larger values of  $J_2$ ) using the stripe state. As has been discussed in detail elsewhere, [22, 88, 92] the coupled sets of LSUB $n$  equations (2.7) and (2.8) have natural termination points (at least for values  $n > 2$ ) for some critical value of a control parameter (here the anisotropy,  $\Delta$ ), beyond which no real solutions to the equations exist. The extrapolation of such LSUB $n$  termination points for fixed values of  $\Delta$  to the  $n \rightarrow \infty$  limit can sometimes be used as a method to calculate the physical phase boundary for the phase with ordering described by the CCM model state being used. However, since other methods exist to define the phase transition points, which are usually more precise and more robust for extrapolation (as we discuss below), we have not attempted such an analysis here.

Instead, in Fig. 9.2, the  $E_{\max}$  points shown, for each set of calculations based on one of the four CCM model states used, are either those natural termination points described above for the highest (LSUB10) level of approximation we have implemented, or the points where the gs energy becomes a maximum should the latter occur first (i.e., as one approaches the termination point). The advantage of this usage of the  $E_{\max}$  points is that we do not then display gs energy data in any appreciable regimes where LSUB $n$  calculations with very large values of  $n$  (higher than can feasibly be implemented) would not have solutions, by dint of having terminated already.

Curves such as those shown in Fig. 9.2(a) illustrate very clearly that the corresponding pairs of gs energy curves for the  $z$ -aligned Néel and stripe phases cross one another for all values of  $\Delta$  above some critical value,  $\Delta \gtrsim 2.1$ . The crossings occur with a clear discontinuity in slope, as is completely characteristic of a first-order phase transition, exactly as observed in the classical (i.e.,  $s \rightarrow \infty$ ) case. Furthermore, the direct first-order phase transition between the  $z$ -aligned Néel and stripe phases that is thereby indicated for all values of  $\Delta \gtrsim 2.1$ , occurs (for all such values of  $\Delta$ ) very close to the classical phase boundary  $J_2 = \frac{1}{2}$ , the point of maximum (classical) frustration. Conversely, curves such as those shown in Fig. 9.2(a) for values of  $\Delta$  in the range  $1 < \Delta \lesssim 2.1$  also illustrate clearly that the corresponding pairs of gs energy



(a)  $z$ -aligned states

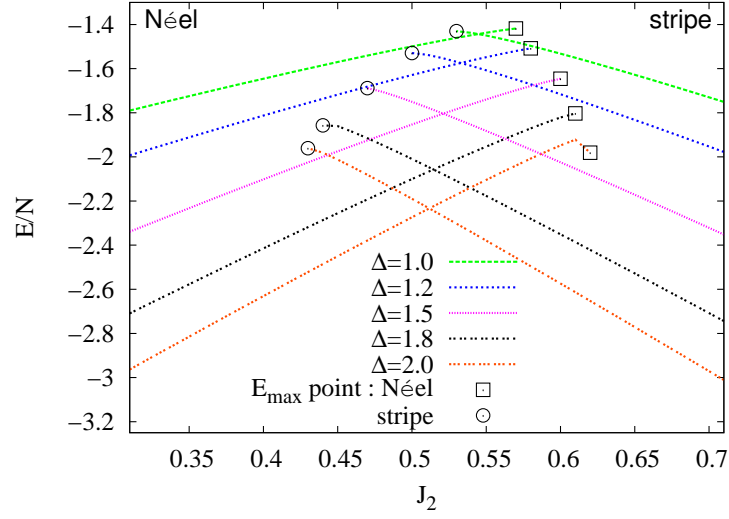
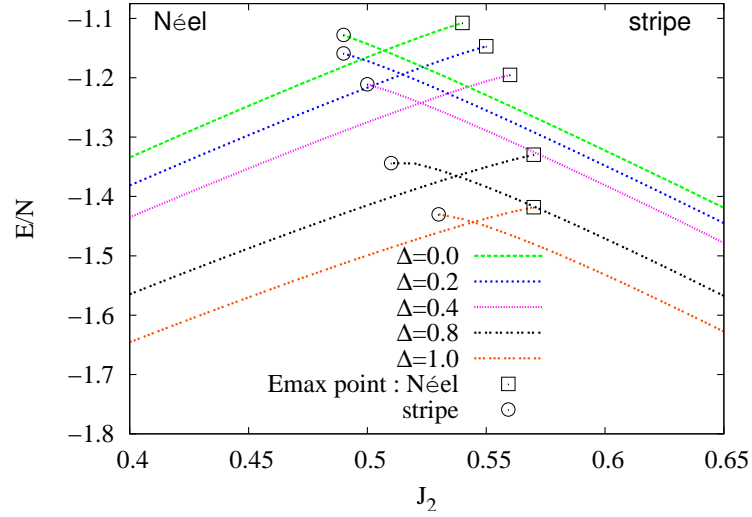


(b) planar  $x$ -aligned states

**Figure 9.2.:** Extrapolated CCM LSUB $n$  results using (a) the  $z$ -aligned and (b) planar  $x$ -aligned states for the gs energy per spin,  $E/N$ , for the Néel and stripe phases of the  $s = 1/2$   $J_1^{XXZ}$ - $J_2^{XXZ}$  model. The LSUB $n$  results are extrapolated in the limit  $n \rightarrow \infty$  using the sets  $n = \{4, 6, 8, 10\}$  for both the  $z$ -aligned states and the planar  $x$ -aligned states. The NN exchange coupling  $J_1 = 1$ . The meaning of the  $E_{\max}$  points shown is described in the text.

curves for the  $z$ -aligned Néel and stripe phases do not intersect one another. In this regime we thus have clear preliminary evidence for the opening up of an intermediate phase between the Néel and stripe phases. The corresponding curves in Fig. 9.2(b)



(a)  $z$ -aligned states(b) planar  $x$ -aligned states

**Figure 9.3.:** Extrapolated CCM  $\text{SUB}_{n-n}$  results using (a) the  $z$ -aligned and (b) planar  $x$ -aligned states for the gs energy,  $E/N$ , for the Néel and stripe phases of the  $s = 1$   $J_1^{XXZ} - J_2^{XXZ}$  model. The  $\text{SUB}_{n-n}$  results are extrapolated to the limit  $n \rightarrow \infty$  using the sets  $n = \{2, 4, 6, 8\}$  for both the  $z$ -aligned and planar  $x$ -aligned states.

for values of  $\Delta < 1$  tell a similar story, with an intermediate phase similarly indicated to exist between the  $xy$ -planar-aligned Néel and stripe phases for values of  $\Delta$  in the range  $-0.1 \lesssim \Delta < 1$ .

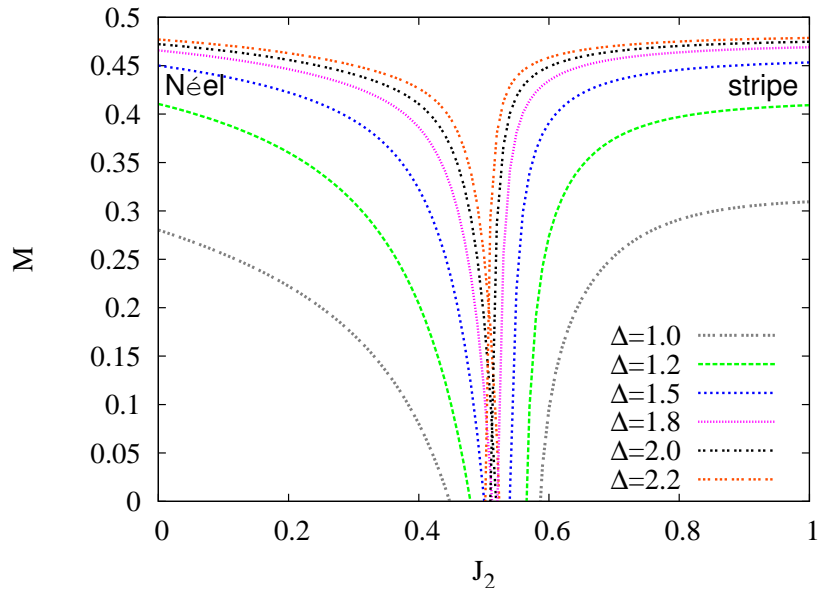
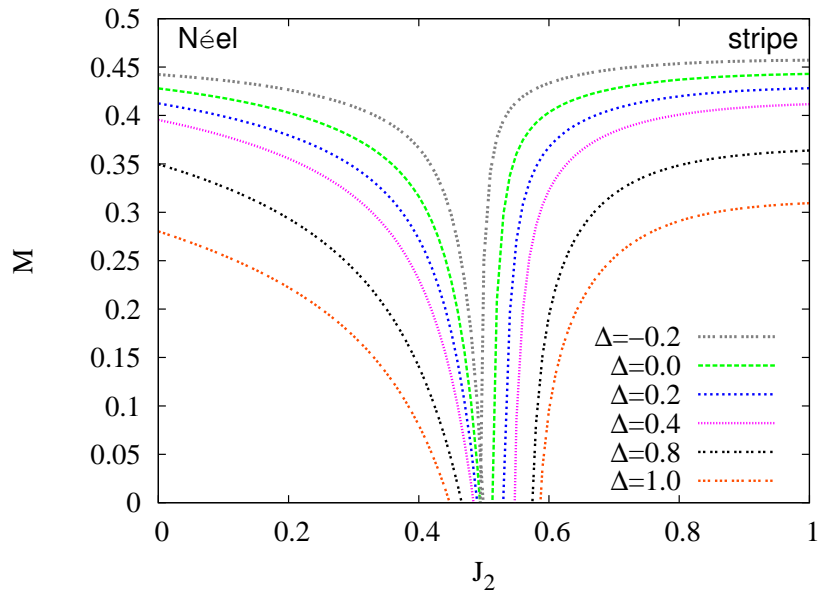
Figure 9.3 shows the extrapolated CCM results for the gs energy per spin,  $E/N$ , as

a function of  $J_2$  for various values of  $\Delta$ , using both the  $z$ -aligned and planar  $x$ -aligned model states. For each value of  $\Delta$  two curves are shown, one (for smaller values of  $J_2$ ) using the Néel state, and the other (for larger values of  $J_2$ ) using the stripe state as CCM model state. All of the curves such as those shown in figure 9.3 illustrate very clearly that the corresponding pairs of gs energy curves (for the same values of  $\Delta$ ) for the Néel and stripe phases cross one another, for both the  $z$ -aligned (figure 9.3(a) for all values  $\Delta > 1$ ) and the  $x$ -aligned (figure 9.3(b) for all values  $0 \leq \Delta < 1$ ) cases. The crossings occur with a clear discontinuity in slope, which is completely characteristic of a first-order phase transition, exactly as observed in the classical (i.e.,  $s \rightarrow \infty$ ) case. Unlike in the  $s = \frac{1}{2}$  version, there is no indication at all in the present spin-1 case of any intermediate paramagnetic phase emerging for any values of the parameters  $J_2$  and  $\Delta$ . Furthermore, the direct first-order phase transition, so indicated by our results for the gs energy, between the quasiclassical Néel-ordered and collinear stripe-ordered phases, in both the  $z$ -aligned and planar  $x$ -aligned cases, occurs for all values of  $\Delta \geq 0$  very close to the classical phase boundary  $J_2^c = \frac{1}{2}$ , the point of maximum (classical) frustration.

### 9.3.2. Magnetic order parameter

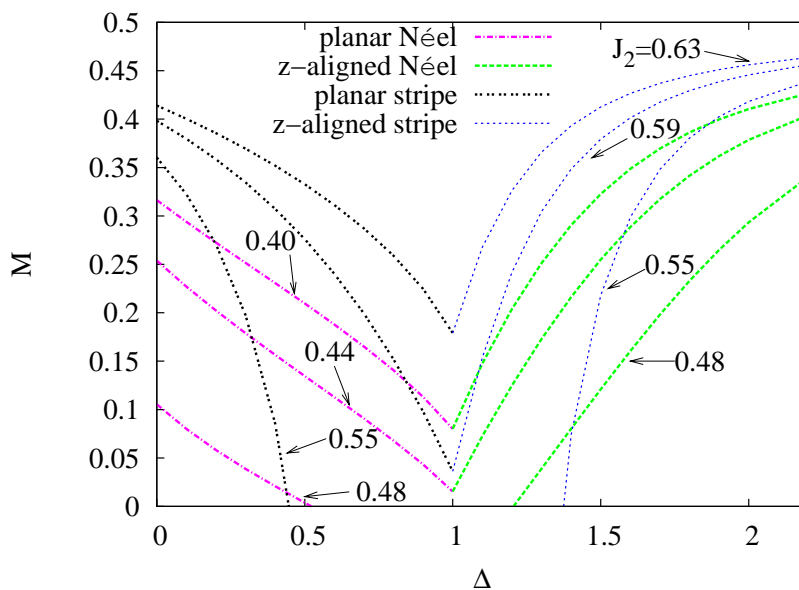
We show in Fig. 9.4 corresponding indicative sets of CCM results, based on the same four model states, for the gs order parameter (viz., the staggered magnetization), to those shown in Fig. 9.3 for the gs energy. The staggered magnetization data completely reinforce the phase structure of the model as deduced above from the gs energy data. Thus, let us now denote by  $M_c$  the quantum phase transition point deduced from curves such as those shown in Fig. 9.4, where  $M_c$  is defined to be either (a) the point where corresponding pairs of CCM staggered magnetization curves (for the same value of  $\Delta$ ), based on the Néel and stripe model states, intersect one another if they do so at a physical value  $M \geq 0$ ; or (b) if they do not so intersect at a value  $M \geq 0$ , the two points where the corresponding values of the staggered magnetization go to zero.

Clearly, case (a) here corresponds to a direct phase transition between the Néel and stripe phases, which will generally be first-order if the intersection point has a value  $M \neq 0$  (and, exceptionally, second-order, if the crossing occurs exactly at  $M = 0$ ). On the other hand, case (b) corresponds to the situation where the points where the LRO vanishes for both quasiclassical (i.e., Néel-ordered and stripe-ordered) phases are, at least naively, indicative of a second-order phase transition from each of these phases to some intermediate magnetically-disordered phase. We return to a discussion of the actual order of such transitions in Sec. 9.4. In summary, we hence define the staggered magnetization criterion for a quantum critical point as the point where there is an indication of a phase transition between the two states by their order parameters becoming equal, or where the order parameter vanishes, whichever occurs first. A detailed discussion of this order parameter criterion and its relation to the stricter energy crossing criterion may be found elsewhere [42].

(a)  $z$ -aligned states(b) planar  $x$ -aligned states

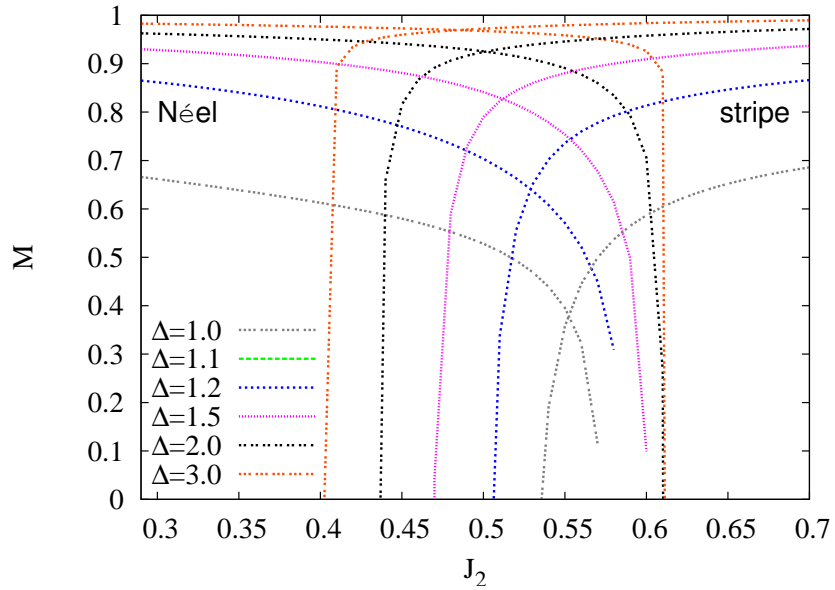
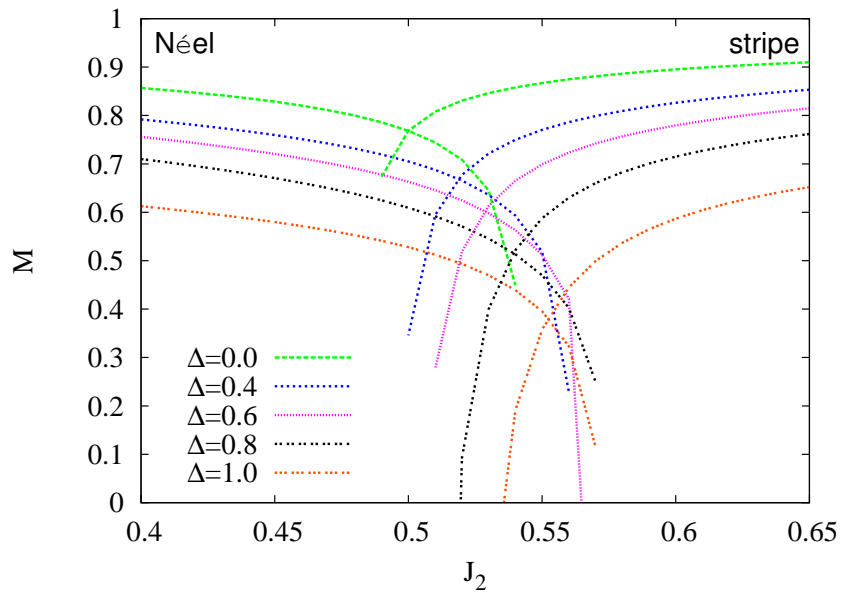
**Figure 9.4.:** Extrapolated CCM LSUB $n$  results using (a) the  $z$ -aligned and (b) planar  $x$ -aligned states for the gs staggered magnetization,  $M$ , for the Néel and stripe phases of the  $s = 1/2$   $J_1^{XXZ} - J_2^{XXZ}$  model. The LSUB $n$  results are extrapolated in the limit  $n \rightarrow \infty$  using the sets  $n = \{4, 6, 8, 10\}$  for both the  $z$ -aligned states and planar  $x$ -aligned states. The NN exchange coupling  $J_1 = 1$ .

From curves such as those shown in Fig. 9.4(a) we see that for  $\Delta \lesssim 1.95$  for the  $z$ -aligned states, there exists an intermediate region between the critical points at which  $M \rightarrow 0$  for the Néel and stripe phases. Conversely, for  $\Delta \gtrsim 1.95$  the two curves for the order parameters  $M$  of the quantum Néel and stripe phases for the same value of  $\Delta$  meet at a finite value,  $M > 0$ , as is typical of a first-order transition. Similarly, Fig. 9.4(b) shows that for the planar  $x$ -aligned states, there exists an intermediate region between the critical points at which  $M \rightarrow 0$  for the Néel and stripe phases for all values of  $\Delta$  in the range  $-0.15 \lesssim \Delta < 1$ . Again, the two curves for the order parameters  $M$  of the Néel and stripe phases for the same value of  $\Delta$  intersect at a value  $M > 0$  for  $\Delta \lesssim -0.15$ . In order to show more explicitly how the quantum phase transitions are driven by anisotropy,  $\Delta$ , we display the same data for the extrapolated results for the order parameter,  $M$ , somewhat differently in Fig. 9.5, where we plot  $M$  as a function of  $\Delta$  for various values of  $J_2$  around the value  $J_2 = 0.5$ , corresponding to the point of maximum (classical) frustration.



**Figure 9.5.:** Extrapolated CCM LSUB $n$  results using the  $z$ -aligned and planar  $x$ -aligned states for the staggered magnetization versus the anisotropy  $\Delta$  for the  $s = 1/2$   $J_1^{XXZ} - J_2^{XXZ}$  model, for the NN exchange coupling  $J_1 = 1$ . The LSUB $n$  results are extrapolated in the limit  $n \rightarrow \infty$  using the sets  $n = \{4, 6, 8, 10\}$  for both the  $z$ -aligned model states and the planar  $x$ -aligned model states.

For spin-1 we present in Fig. 9.6 the gs order parameter  $M$  calculated by CCM for  $N \rightarrow \infty$ , based on the same four model states. It is clear from figures 9.6(a) and (b) that case (b) never occurs for the present spin-1 model for any values of the anisotropy parameter  $\Delta$  or for any values of the NNN exchange coupling  $J_2$ , unlike in the  $s = \frac{1}{2}$  version.

(a)  $z$ -aligned states(b) planar  $x$ -aligned states

**Figure 9.6.:** Extrapolated CCM SUB $n$ - $n$  results using (a) the  $z$ -aligned and (b) planar  $x$ -aligned states for the gs staggered magnetization,  $M$ , for the Néel and stripe phases of the spin-1  $J_1^{XXZ}$ - $J_2^{XXZ}$  model. The SUB $n$ - $n$  results are extrapolated to the limit  $n \rightarrow \infty$  using the sets  $n = \{2, 4, 6, 8\}$  for the  $z$ -aligned states.

9.3.3. Ground-state phase diagrams

By putting together data of the sort shown in Figs. 9.2 and 9.4 of the spin-1/2 we are able to deduce the gs phase diagram of our 2D spin-1/2  $J_1^{XXZ}$ - $J_2^{XXZ}$  model on the square lattice, from our CCM calculations based on the four model states with quasiclassical antiferromagnetic LRO (viz., the Néel and stripe states for both the  $z$ -aligned and planar  $xy$ -aligned cases). We show in Fig. 9.7 the zero-temperature gs phase diagram, as deduced from the order parameter criterion, and using our extrapolated LSUB $n$  data sets with  $n = \{4, 6, 8, 10\}$ , shown as the critical value  $J_2^c$  for the NNN exchange coupling  $J_2$  as a function of anisotropy  $\Delta$  (with NN exchange coupling strength  $J_1 = 1$ ). Very similar results are obtained from using the energy criterion, where it can be applied (viz., along the transition lines between quasiclassical states with magnetic LRO). In order to test the accuracy of our results, particularly the positions of the phase boundaries shown in Fig. 9.7, we have also performed extrapolations using the LSUB $n$  data sets with  $n = \{2, 4, 6, 8, 10\}$  and  $n = \{6, 8, 10\}$  for both the energy criterion and the order parameter criterion. In general terms we find that the results are remarkably robust, and the error bars quoted below are based on such an analysis.

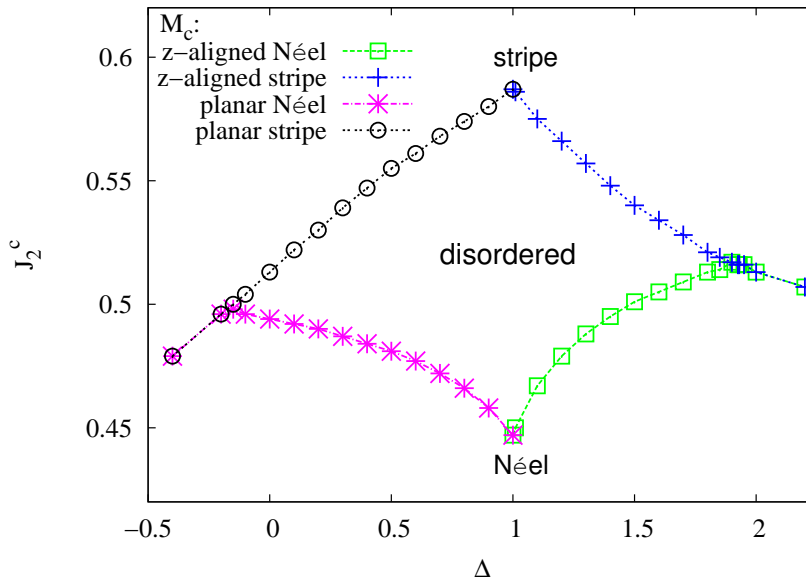


**Figure 9.7.:** Extrapolated CCM LSUB $n$  results using the  $z$ -aligned and planar  $x$ -aligned states for the ground-state phase diagram of the spin-1/2  $J_1^{XXZ}$ - $J_2^{XXZ}$  model, for the NN exchange coupling  $J_1 = 1$ . The LSUB $n$  results for the staggered magnetization are extrapolated to the limit  $n \rightarrow \infty$  using the sets  $n = \{4, 6, 8, 10\}$  for both the  $z$ -aligned model states and the planar  $x$ -aligned model states.  $M_c \equiv$  magnetization critical point, defined in the text.

For the case of the  $z$ -aligned states, all of our results provide clear and consistent evidence for an upper *quantum triple point* (QTP) at  $(\Delta^c = 2.05 \pm 0.15, J_2^c = 0.530 \pm 0.015)$  (for  $J_1 = 1$ ). For  $1 < \Delta \lesssim 2.0$ , there exists an intermediate paramagnetic

(magnetically-disordered) quantum phase, separating the Néel and stripe phases. This intermediate phase disappears for  $\Delta \gtrsim 2.0$ , and both our energy and order parameter criteria give clear and unequivocal evidence for a direct first-order quantum phase transition between the two quasiclassical antiferromagnetic states in this regime, just as in the corresponding classical model (i.e., with  $s \rightarrow \infty$ ). The phase boundary approaches the classical line  $J_2^c = 0.5$  as  $\Delta \rightarrow \infty$ .

Similarly, for the case of the  $xy$ -planar-aligned phases, a second (lower) QTP occurs at ( $\Delta^c = -0.10 \pm 0.15$ ,  $J_2^c = 0.505 \pm 0.015$ ) (for  $J_1 = 1$ ), with an intermediate disordered phase existing in the region  $-0.1 \lesssim \Delta < 1$ . The  $z$ -aligned and  $xy$ -planar-aligned phases meet precisely at  $\Delta = 1$ , just as in the classical case. Exactly at the isotropic point  $\Delta = 1$ , where the model becomes just the original  $J_1$ - $J_2$  model, the disordered phase exists for the largest range of values of  $J_2$ ,  $J_2^{c1} < J_2 < J_2^{c2}$ , as can be clearly seen from Fig. 9.7. For the pure  $J_1$ - $J_2$  model our calculations yield the values  $J_2^{c1}/J_1 = 0.44 \pm 0.01$  and  $J_2^{c2}/J_1 = 0.59 \pm 0.01$  that demarcate the phase boundaries for the disordered phase, in complete agreement with both our own earlier work and that of others that we have already discussed in Chap. 6.

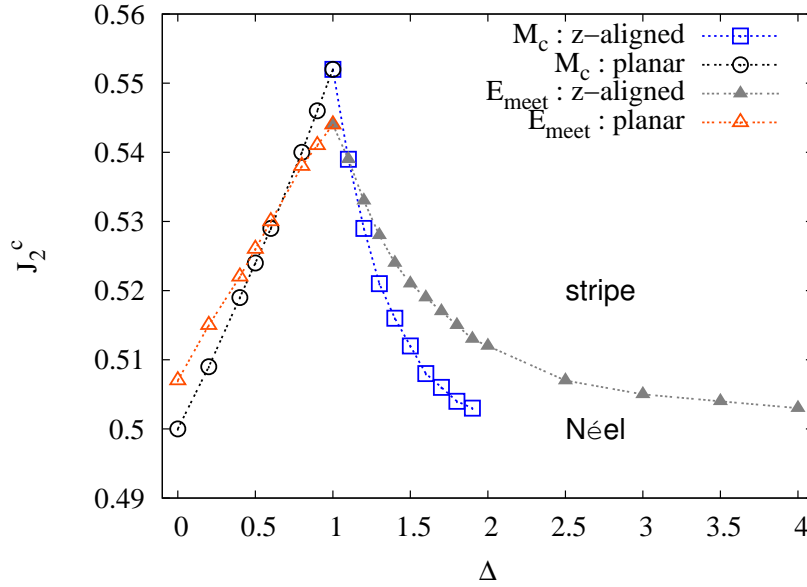


**Figure 9.8.:** Extrapolated CCM SUB $n$ - $n$  results using the  $z$ -aligned and planar  $x$ -aligned states for the ground-state phase diagram of the spin-1  $J_1^{XXZ}$ - $J_2^{XXZ}$  anisotropic Heisenberg model on the square lattice, for the NN exchange coupling  $J_1 = 1$ . The SUB $n$ - $n$  results for the energy per spin and the staggered magnetization are extrapolated to the limit  $n \rightarrow \infty$  using the sets  $n = \{2, 4, 6, 8\}$  for both the  $z$ -aligned and planar  $x$ -aligned model states.  $M_c \equiv$  magnetization critical point, defined in the text.  $E_{\text{meet}}$  denotes the crossing point of the CCM energy curves for the same value of  $\Delta$  based on the Néel-ordered and collinear stripe-ordered model states.

In Fig. 9.8 we present the zero-temperature gs phase diagram of the 2D spin-1  $J_1^{XXZ}$ - $J_2^{XXZ}$  model on the square lattice for the  $z$ -aligned and planar  $x$ -aligned states, as obtained from our extrapolated results for both the gs energy and the gs order

parameter. The completely independent results from both the energy criterion and the order parameter criterion for the phase transition give extremely similar positions for the phase boundary, as one can observe from figure 9.8. Note that the results from using the order parameter criterion become increasingly inaccurate for large values of  $\Delta$ , and this is why we show them in figure 9.8 only out to  $\Delta \lesssim 2$ . The reason for this is simple. Thus, as  $\Delta \rightarrow \infty$ , the order parameters  $M \rightarrow 1$  for both the Néel-ordered and collinear stripe-ordered phases, and it becomes increasingly difficult to determine the point where they cross, since the angle of their crossing becomes vanishingly small. This effect can clearly be seen in figure 9.6(a), where it has clearly become acute even for values of  $\Delta$  as small as about 2. On the other hand, the energy criterion correspondingly becomes *more* accurate as  $\Delta \rightarrow \infty$ , as one may observe from figure 9.3(a). Thus, figure 9.8 clearly shows that the phase boundary approaches the classical line  $J_2^c = 0.5$  as  $\Delta \rightarrow \infty$ , as expected in this Ising-like limit.

Our results certainly provide very clear and consistent evidence that there exists no intermediate phase. Thus, the curves for the order parameters of the Néel and stripe phases always meet at a finite value and the corresponding curves for the gs energies of the two phases intersect with a discontinuity in slope, for both the  $z$ -aligned and planar  $x$ -aligned states, for all values of the anisotropy parameter  $\Delta$ . All of the evidence clearly points towards a first-order phase transition between the two phases.

We note also that the  $z$ -aligned and  $xy$ -planar-aligned phases meet precisely at the isotropic point  $\Delta = 1$ , just as in the classical case, and exactly as expected. However, this does provide a consistency check on our independent numerical calculations for the two phases. The case  $\Delta = 1$  obviously reproduces the usual (isotropic)  $J_1$ - $J_2$  model. Thus, at  $\Delta = 1$ , we find  $J_2^c = 0.55 \pm 0.01$  which, very encouragingly, is the same value we found (see e.g., Chap. 8 and Ref. [113]) for the spin-1  $J_1$ - $J_1'$ - $J_2$  model in the spatially isotropic limiting case when  $J_1'/J_1 = 1$ . We also note that in the present spin-1 quantum model, the isotropic point  $\Delta = 1$  is precisely the point at which the boundary between the two quasiclassical phases deviates most from its classical position at  $J_2^c = \frac{1}{2}$  for all values of  $\Delta \geq 0$ . Our calculations also indicate that at the isotropic  $XY$  point of the model (i.e., where  $\Delta = 0$ ) the phase boundary is at  $J_2^c = 0.50 \pm 0.01$

#### 9.4. DISCUSSION AND CONCLUSIONS

We have shown in detail how, as expected, the quantum fluctuations present in the spin-1/2 and spin-1  $J_1$ - $J_2$  model on the 2D square lattice, that has become an archetypal model for studying the interplay between quantum fluctuations and frustration, can be tuned by the introduction of spin anisotropy. We have clearly confirmed our prior expectation that anisotropy reduces the quantum fluctuations. Thus, for both the cases  $\Delta > 1$  and  $0 < \Delta < 1$ , the intermediate paramagnetic phase present in the pure  $J_1$ - $J_2$  model is observed to shrink to a smaller range of values of  $J_2/J_1$  centered near



to the point of maximal classical frustration,  $J_2^c/J_1 = \frac{1}{2}$ , that marks the classical phase boundary between the Néel-ordered and collinear stripe-ordered phases. However, unlike what would be predicted by lowest-order LSWT [27], for example, we can now conclude with confidence from our results that no such intermediate disordered phase as the one that we observed in the spin-1/2 version of this model between the two quantum triple points at ( $\Delta^c = -0.10 \pm 0.15$ ,  $J_2^c/J_1 = 0.505 \pm 0.015$ ) and ( $\Delta^c = 2.05 \pm 0.15$ ,  $J_2^c/J_1 = 0.530 \pm 0.015$ ), exists for the spin-1 version, for any values of the parameters  $J_2/J_1$  and  $\Delta$ . In the context of a spin-wave theory treatment of the isotropic  $J_1$ - $J_2$  model on the square lattice, LSWT predicts that quantum fluctuations can destabilize the classical GS with LRO, even at large values of the spin quantum number  $s$ , for values of the frustration parameter  $J_2/J_1$  around 0.5. For the spin-1/2 case the range of values,  $\alpha^{c1} < J_2/J_1 < \alpha^{c2}$ , for which a magnetically-disordered phase thereby occurs is predicted by LSWT to be given by  $\alpha^{c1} \approx 0.38$  and  $\alpha^{c2} \approx 0.52$ . These values may be compared to our own predictions of  $\alpha^{c1} = 0.44 \pm 0.01$  and  $\alpha^{c2} = 0.59 \pm 0.01$ . For the spin-1 case LSWT predicts a narrower, but still non-vanishing, strip of disordered intermediate phase in a range with  $\alpha^{c1} \approx 0.47$  and  $\alpha^{c2} \approx 0.501$ , whereas we predict with confidence that the disordered phase simply does not exist as a GS in this case.

The discrepancy between our results and those of LSWT for the spin-1 case are undoubtedly due to the shortcomings of LSWT. Thus, while LSWT can work reasonably well in the absence of frustration (e.g., for the isotropic  $J_1$ - $J_2$  model here when  $J_2 = 0$ , that represents the Heisenberg model with only NN interactions), in the presence of frustration it consistently overestimates the effects of quantum fluctuations. This effect worsens as the frustration (here measured by the ratio  $J_2/J_1$ ) increases.

Thus, Igarashi [33] has shown explicitly for the  $J_1$ - $J_2$  model by going to higher orders in SWT (i.e., by calculating higher-order terms in the  $1/s$  power expansion), that while the series seems to converge for values  $J_2/J_1 \lesssim 0.35$ , the second-order corrections grow so large for values  $J_2/J_1 \gtrsim 0.4$  that no prediction based on LSWT, or even on higher-order SWT, in this region (e.g., about the appearance of an intermediate magnetically-disordered phase near  $J_2/J_1 \approx 0.5$ ) should be relied upon. Furthermore, he showed that the effects of the higher-order correction terms to LSWT make the Néel-ordered state more stable than predicted by LSWT.

We note that the results presented here for the spin-anisotropic spin-1  $J_1^{XXZ}$ - $J_2^{XXZ}$  model are also consistent with our own previous results (see e.g., Chap. 8) and Ref. [113]) for the spatially-anisotropic spin-1  $J_1$ - $J_1'$ - $J_2$  model discussed in Chap. 8, for which we also found no evidence for an intermediate disordered phase between the quasiclassical Néel and collinear stripe phases with LRO. However, whereas for the spin-1  $J_1$ - $J_1'$ - $J_2$  model we found strong evidence for a quantum tricritical point at ( $J_1'/J_1 \approx 0.66$ ,  $J_2/J_1 \approx 0.35$ ) where a line of second-order phase transitions between the Néel-ordered and the collinear stripe-ordered states (for  $J_1'/J_1 \lesssim 0.66$ ) meets a line of first-order phase transitions between the same two states (for  $J_1'/J_1 \gtrsim 0.66$ ), we find for the present spin-1  $J_1^{XXZ}$ - $J_2^{XXZ}$  model that the phase transition between these two states is first-order for all values  $\Delta \geq 0$ . Clearly, these two sets of results are in complete agreement with one another at their common point of overlap, when

$J'_1 = J_1$  and  $\Delta = 1$ .

At the  $XY$  isotropic point ( $\Delta = 0$ ) of the present spin-1  $J_1^{XXZ}$ - $J_2^{XXZ}$  model we predict that the phase boundary occurs at a value  $J_2^c(0) = 0.50 \pm 0.01$ . It is interesting to note that our results for the spin-1/2 version of the model 9.1 showed QTP at ( $\Delta^c = -0.10 \pm 0.015$ ,  $J_2^c = 0.505 \pm 0.015$ ). Clearly our results for this spin-1/2 case are consistent with this lower QTP occurring exactly at the  $XY$  isotropic point ( $\Delta = 0$ ) and also at the point of maximum classical frustration,  $J_2 = \frac{1}{2}$ . Similarly, in the present spin-1 case our results are consistent with the phase boundary at the  $XY$  isotropic point also occurring at the point  $J_2 = \frac{1}{2}$ . It would seem likely, therefore, that for both the cases of spin-1/2 and spin-1 particles the corresponding quantum  $J_1^{XX}$ - $J_2^{XX}$  model has a special behaviour at the point  $J_2/J_1 = \frac{1}{2}$  where the classical frustration is greatest. Our results indicate that a more detailed investigation of this case might, therefore, be worth undertaking for general values of the spin quantum number  $s$ . We note that some of the results presented in this chapter are published in.<sup>1 2</sup>

---

<sup>1</sup>R. F. Bishop, P. H. Y. Li, R. Darradi, J. Schulenburg and J. Richter "Effect of anisotropy on the ground-state magnetic ordering of the spin-half quantum  $J_1^{XXZ}$ - $J_2^{XXZ}$  model on the square lattice", Phys. Rev. B **78**, 054412 (2008)

<sup>2</sup>R. F. Bishop, P. H. Y. Li, R. Darradi, J. Richter and C. E. Campbell "The effect of anisotropy on the ground-state magnetic ordering of the spin-1 quantum  $J_1^{XXZ}$ - $J_2^{XXZ}$  model on the square lattice", J. Phys.: Condens. Matter **20**, 415213 (2008)

## SUMMARY AND OUTLOOK

In this thesis, we have performed a numerical and analytical investigation of the ground state properties on different low dimensional quantum spin models, using the coupled cluster method (CCM) for high orders of approximation, exact diagonalization (ED), and variational mean-field approach (MFA). We discuss the influence of strong quantum fluctuations and frustration on zero-temperature phase transitions, we study competition of magnetic bonds with and without frustration. In Chap. 2 we present new CCM results for the ground-state energy and the sublattice magnetization of the spin-1/2 Heisenberg antiferromagnet (HAFM) on the square lattice and simple cubic lattice which are in excellent agreement with other accurate methods.

In Chap. 3 we investigate the quantum phase transitions in unfrustrated systems using the CCM, ED, and MFA. We consider the square lattice spin-1/2 XXZ Heisenberg antiferromagnet with two different nearest-neighbour coupling  $J$  and  $J'$ . Increasing  $J' > J$  the model shows in the isotropic Heisenberg limit a second-order transition from semi-classical Néel order to a quantum paramagnetic phase with enhanced local dimer correlations on the  $J'$  bonds at about  $J'_c \sim 2.5 \dots 3J$ . This transition is driven by the quantum competition between  $J'$  and  $J$  on the square lattice. We study the influence of Ising anisotropy parameter  $\Delta$  and spin quantum number  $s$  on this phase transition. By increasing the anisotropy parameter  $\Delta > 1$  and quantum number  $s > 1/2$  we diminish the quantum fluctuations and thus the degree of competition. As a result the transition point  $J'_c$  is shifted to larger values. We find that the critical value  $J'_c$  increases with growing  $\Delta > 1$  and  $s$  according to  $J'_c(\Delta) \propto \alpha\Delta$  ( $\Delta \geq 1$ ) with  $\alpha \sim 2.3 \dots 3.0$  and  $J'_c \propto s(s+1)$ , i.e. the transition disappears in the Ising limit  $\Delta \rightarrow \infty$  and in the limit  $s \rightarrow \infty$ .

In Chap. 4 we study the ground state and the magnetization process of the spin-half two-dimensional Shastry-Sutherland antiferromagnet. We find that this model demonstrates various ground-state phases (Néel, magnetically disordered, orthogonal dimer). In particular, we find that orthogonal-dimer state becomes the ground state at  $J_2^d/J_1 \sim 1.477$ . For the critical point  $J_2^c/J_1$  where the semi-classical Néel order disappears we obtain a significantly lower value than  $J_2^d/J_1$ , namely,  $J_2^c/J_1$  in the range 1.14–1.39. We conclude that an intermediate phase exists between the Néel and the dimer phases. An analysis of the energy of a competing spiral phase yields clear evidence that the spiral phase does not become the ground state for any value of  $J_2$ . we also conclude from our CCM data that there exists a valence-bond phase between the Néel -ordered phase and the orthogonal-dimer phase.

In Chap. 5 we present a method for the direct calculation of the spin stiffness by means of the CCM. For the spin-half Heisenberg antiferromagnet on the square, the triangular and the cubic lattices we calculate the stiffness in high orders of approximation. For the square and the cubic lattices our results are in very good agreement with the best results available in the literature. For the triangular lattice our result is more precise than any other result obtained so far by other approximate method.

In Chap. 6 we investigate the phase diagram of the frustrated Heisenberg antiferromagnet, the  $J_1$ - $J_2$  model, in two dimensions. We have found that the quantum critical points for both the Néel and collinear order are  $J_2^{c1} \approx 0.44 \dots 0.45 J_1$  and  $J_2^{c2} \approx 0.58 \dots 0.59 J_1$  respectively, which are in good agreement with the results obtained by other approximations. We use the CCM and ED to analyse the generalized susceptibilities. We find that the phase transition from the Néel to the paramagnetic state at  $J_2^{c1}$  is second order. This result agrees with the deconfined critical point scenario which is suggested by Senthil *et al.*, [72, 73], but contradicts the conclusion of Ref. [47].

In Chap. 7 we also discuss the influence of interlayer coupling ( $J_\perp$ ) on the quantum paramagnetic ground-state phase. We demonstrate that increasing the interlayer coupling  $J_\perp > 0$  the parameter region of this phase decreases, and finally the quantum paramagnetic phase disappears for quite small  $J_\perp \sim 0.2 - 0.3 J_1$ .

In Chap. 8 we use the CCM to investigate the GS phase diagram of the 2D  $J_1$ - $J'_1$ - $J_2$  spin-1/2 and spin-1 Heisenberg model, where the nearest-neighbour bonds have different strengths  $J_1$  and  $J'_1$  in, say, the  $x$  (intrachain) and  $y$  (interchain) directions respectively. In particular, we study the effect of the coupling  $J'_1$  on the Néel and stripe states. We found that for the spin-1/2 case there exists a quantum triple point (QTP) below which there is a second-order phase transition between the quasiclassical Néel and stripe-ordered phase with magnetic LRO, whereas only above this point are these two phases separated by the intermediate magnetically disordered phase seen in the pure spin-1/2  $J_1$ - $J_2$  model ( $J'_1 = J_1$ ). The QTP was found to occur at  $J'_1/J_1 \approx 0.60 \pm 0.03$ ,  $J_2/J_1 \approx 0.33 \pm 0.02$ . Similarly, the intermediate phase can also disappear when the spin quantum number  $s$  is increased for the  $J_1$ - $J_2$  model on the 2D square lattice. By contrast with the  $s = 1/2$  case, we found for the spin-1 no evidence for a magnetically disordered state between the Néel and stripe states. However, for the  $s = 1$  case we found instead strong evidence for the QTP at  $J'_1/J_1 = 0.66 \pm 0.03$ ,  $J_2/J_1 = 0.35 \pm 0.02$ , where a line of second-order phase transitions between the quasiclassical Néel and columnar stripe-ordered phases (for  $J'_1/J_1 \lesssim 0.66$ ) meets a line of first-order phase transitions between the same two phases (for  $J'_1/J_1 \gtrsim 0.66$ ).

In Chap. 9 we discuss the influence of an exchange anisotropy  $\Delta$  on the zero-temperature phase transition of the spin-1/2 and spin-1 frustrated  $J_1$ - $J_2$  XXZ antiferromagnet on the square lattice. We find for spin-1/2 case strong evidence for two QTP's at ( $\Delta^c = -0.10 \pm 0.15$ ,  $J_2^c/J_1 = 0.505 \pm 0.015$ ) and ( $\Delta^c = 2.05 \pm 0.15$ ,  $J_2^c/J_1 = 0.530 \pm 0.015$ ), between which an intermediate magnetically-disordered phase emerges to separate the quasiclassical Néel and stripe collinear phases. Above the upper QTP ( $\Delta \gtrsim 2.0$ ) we find a direct first-order phase transition between the Néel and stripe

phases, exactly as for the classical case. The  $z$ -aligned and  $xy$ -planar-aligned phases meet precisely at  $\Delta = 1$ , also as for the classical case. For all values of the anisotropy parameter between those of the two QTP's there exists a narrow range of values of  $J_2/J_1$ ,  $\alpha^{c1}(\Delta) < J_2/J_1 < \alpha^{c2}(\Delta)$ , centered near the point of maximum classical frustration,  $J_2/J_1 = \frac{1}{2}$ , for which the intermediate phase exists. This range is widest precisely at the isotropic point,  $\Delta = 1$ , where  $\alpha^{c1}(1) = 0.44 \pm 0.01$  and  $\alpha^{c2}(1) = 0.59 \pm 0.01$ . The two QTP's are characterized by values  $\Delta = \Delta^c$  at which  $\alpha^{c1}(\Delta^c) = \alpha^{c2}(\Delta^c)$ .

For spin-1 we predict no intermediate disordered phase between the Néel and collinear stripe phases, for any value of the frustration  $J_2/J_1$ , for either the  $z$ -aligned ( $\Delta > 1$ ) or  $xy$ -planar-aligned ( $0 \leq \Delta < 1$ ) states. The quantum phase transition is determined to be first-order for all values of  $J_2/J_1$  and  $\Delta$ . The position of the phase boundary  $J_2^c(\Delta)$  is determined accurately. It is observed to deviate most from its classical position  $J_2^c = \frac{1}{2}$  (for all values of  $\Delta > 0$ ) at the Heisenberg isotropic point ( $\Delta = 1$ ), where  $J_2^c(1) = 0.55 \pm 0.01$ . By contrast, at the XY isotropic point ( $\Delta = 0$ ), we find  $J_2^c(0) = 0.50 \pm 0.01$ . In the Ising limit ( $\Delta \rightarrow \infty$ )  $J_2^c \rightarrow 0.5$  as expected.

Finally, this thesis has provided a number of interesting results which may serve to understand more about quantum phase transitions in quantum magnetic system. The CCM is universal tool of microscopic quantum many-body theory that has been applied successfully, e.g. in quantum chemistry, nuclear physics and condensed matter physics. Several years ago, a special variant of the CCM has been developed to calculate the ground-state properties of quantum magnets. Recent investigations on quantum magnets have demonstrated that the CCM is able to describe accurately the various zero-temperature phases of quantum spins systems with competing interactions and the quantum phase transitions between them. Unlike the quantum Monte Carlo (QMC) techniques, the CCM does not suffer from the minus sign problem and so can be applied also to the challenging problem of highly frustrated quantum magnets and for lattices of arbitrary spatial dimensionality.

In order to compute a general ground-state physical quantity such as the ground-state energy, the magnetic order parameter, the spin stiffness, and generalized susceptibilities, we need to find and to solve a coupled set of non-linear equations for both the ket and the bra states equations in a certain level of approximation  $n$ . The number of those equations (i.e. the technical complexity of the numerical problem), however, increases with  $n$ . Since the quality and accuracy of the results is the better the higher the level of approximation  $n$  one has to try to increase  $n$  as much as possible. Recently, in collaboration with a group in Manchester the Magdeburg group has developed an open source program package called CCCM [116]. It is written in programming language C++ and uses the MPI library for parallelization. with this CCCM package we can now solve a big number of CCM equations with high level of approximation  $n$ . We can also calculate excitation energy with spins of general spin quantum number  $s$ . Another new application of CCM using CCCM package is to study the frustrated systems in magnetic field. In the future we plan to apply the CCM to quantum spin systems at non-zero temperature.



## BIBLIOGRAPHY

- [1] J. RICHTER, J. SCHULENBURG, A. HONECKER. *Quantum magnetism in two dimensions: From semi-classical Néel order to magnetic disorder*, in: U. Schollwöck, J. Richter, D. J. J. Farnell, R. F. Bishop, (Eds.) *Quantum Magnetism, Lecture Notes in Physics*, vol. **645**. Springer-Verlag, Berlin, 2004. pp. 85-183, <http://www.tu-bs.de/honecker/papers/2dqm.ps.gz>.
- [2] S. SACHDEV. *Quantum Phase Transitions*. Cambridge University Press, Cambridge, 1999.
- [3] J. RICHTER, S. KRÜGER, D. FARNELL, R. BISHOP. *Quantum phase transitions in spin systems*, in *Series on Advances in Quantum Many-Body Theory*, Vol. **5**. Eds. R. F. Bishop, K. A. Gernoth, N. R. Walet. World Scientific, Singapore, 2001. pp 239-246.
- [4] T. BARNES, *Int. J. Mod. Phys. C* **2** (1991) 659.
- [5] E. DAGOTTO, *Rev. Mod. Phys* **66** (1994) 763.
- [6] S. TOMONAGA, *Prog. Theor. Phys* **5** (1950) 544.
- [7] J. LUTTINGER, *J. Math. Phys* **4** (1963) 1154.
- [8] N. MERMIN H. WAGNER, *Phys. Rev. Lett* **17** (1966) 1133.
- [9] H.-J. MIKESKA A. KOLEZHUK. *Quantum magnetism in two dimensions: From semi-classical Néel order to magnetic disorder*, in: U. Schollwöck, J. Richter, D. J. J. Farnell, R. F. Bishop, (Eds.) *Quantum Magnetism, Lecture Notes in Physics*, vol. **645**. Springer-Verlag, Berlin, 2004. pp.1.
- [10] N. MANOUSAKIS, *Rev. Mod. Phys* **63** (1991) 1.
- [11] G. MISGUICH C. LHUILLIER. *Two-dimensional quantum antiferromagnets*, in: *Frustrated spin systems*, edited by H. T. Diep. World-Scientific, 2003.
- [12] S. TANIGUCHI, T. NISHIKAWA, Y. YASUI, Y. KOBAYASHI, M. SATO, T. NISHIOKA, M. KONTANI, K. SANO, *J. Phys. Soc. Jpn* **64** (1995) 2758.
- [13] M. TROYER, H. KONTANI, K. UEDA, *Phys. Rev. Lett* **76** (1996) 3822.
- [14] H. KAGEYAMA, K. YOSHIMURA, R. STERN, N. V. MUSHNIKOV, K. ONIZUKA, M. KATO, K. KOSUGE, C. P. SLICHTER, T. GOTO, Y. UEDA, *Phys. Rev. Lett* **82** (1999) 3168.
- [15] A. KOGA N. KAWAKAMI, *Phys. Rev. Lett* **84** (2000) 4461.

- [16] C. GROS, W. WENZEL, J. RICHTER, *Europhys. Lett.* **32** (1995) 747.
- [17] A. W. SANDVIK D. J. SCALAPINO, *Phys. Rev. Lett.* **72** (1994) 2777.
- [18] S. E. KRÜGER, J. RICHTER, J. SCHULENBURG, D. J. J. FARNELL, R. F. BISHOP, *Phys. Rev. B* **61** (2000) 14607.
- [19] R. R. P. SINGH, M. P. GELF, D. A. HUSE, *Phys. Rev. Lett* **61** (1988) 2484.
- [20] S. KRÜGER J. RICHTER, *Phys. Rev. B* **64** (2001) 024433.
- [21] J.-K. KIM M. TROYAER, *Phys. Rev. Lett* **80** (1998) 2705.
- [22] R. F. BISHOP, *Microscopic Quantum-Many-Body Theories and Their Applications*, edited by J. Navarro and A. Polls, *Lecture Notes in Physics* **510** (1998) 1.
- [23] L. CAPRIOTTI, *Int. J. Mod. Phys* **15** (2001) 1799.
- [24] L. CAPRIOTTI, F. BECCA, A. PAROLA, S. SORELLA, *Phys. Rev. Lett* **87** (2001) 097201.
- [25] L. CAPRIOTTI, F. BECCA, A. PAROLA, S. SORELLA, *Phys. Rev. B* **67** (2003) 212402.
- [26] L. CAPRIOTTI S. SORELLA, *Phys. Rev. Lett* **84** (2000) 3173.
- [27] P. CHANDRA B. DOUCOT, *Phys. Rev. B* **38** (1988) 9335.
- [28] E. DAGOTTO A. MOREO, *Phys. Rev. Lett* **63** (1989) 2148.
- [29] A. V. DOTSENKO O. P. SUSHKOV, *Phys. Rev. B* **50** (1994) 3821.
- [30] M. S. L. DU CROO DE JONGH P. J. H. DENTENEER, *Phys. Rev. B* **55** (1997) 2713.
- [31] T. EINARSSON H. J. SCHULZ, *Phys. Rev. B* **51** (1995) 6151.
- [32] F. FIGUEIRIDO, A. KARLHEDE, S. KIVELSON, S. SONDHI, M. ROCEK, D. S. ROKHSAR, *Phys. Rev. B* **41** (1990) 4619.
- [33] J. IGARASHI, *J. Phys. Soc. Jpn* **62** (1993) 4449.
- [34] N. B. IVANOV P. C. IVANOV, *Phys. Rev. B* **46** (1992) 8206.
- [35] M. MAMBRINI, A. LÄUCHLI, D. POILBLANC, F. MILA, *Phys. Rev. B* **74** (2006) 144422.
- [36] T. MUNEHISA Y. MUNEHISA, *J. Phys.: Condens. Matter* **19** (2007) 196202.
- [37] F. KRÜGER S. SCHEIDL, *Europhys. Lett* **74** (2006) 896.
- [38] N. READ S. SACHDEV, *Phys. Rev. Lett* **66** (1991) 1773.
- [39] J. RICHTER, *Phys. Rev. B* **47** (1993) 5794.
- [40] J. RICHTER, N. B. IVANOV, K. RETZLAFF, *Europhys. Lett* **25** (1994) 545.



- [41] T. ROSCILDE, A. FEIGUIN, A. L. CHERNYSHEV, S. LIU, S. HAAS, Phys. Rev. Lett **93** (2004) 017203.
- [42] D. SCHMALFUSS, R. DARRADI, J. RICHTER, J. SCHULENBURG, D. IHLE, Phys. Rev. Lett **97** (2006) 157201.
- [43] H. J. SCHULZ T. A. L. ZIMAN, Europhys. Lett **18** (1992) 355.
- [44] H. J. SCHULZ T. A. L. ZIMAN, J. Phys. I **6** (1996) 675.
- [45] R. R. P. SINGH, Z. WEIHONG, C. J. HAMER, J. OITMAA, Phys. Rev. B **60** (1999) 7278.
- [46] R. R. P. SINGH, Z. WEIHONG, J. OITMAA, O. P. SUSHKOV, C. J. HAMER, Phys. Rev. Lett **91** (2003) 017201.
- [47] J. SIRKER, Z. WEIHONG, O. P. SUSHKOV, J. OITMAA, Phys. Rev. B **73** (2006) 184420.
- [48] L. SIURAKSHINA, D. IHLE, R. HAYN, Phys. Rev. B **64** (2001) 104406.
- [49] O. P. SUSHKOV, J. OITMAA, Z. WEIHONG, Phys. Rev. B **63** (2001) 104420.
- [50] O. P. SUSHKOV, J. OITMAA, Z. WEIHONG, Phys. Rev. B **66** (2002) 054401.
- [51] G. M. ZHANG, H. HU, L. YU, Phys. Rev. Lett **91** (2003) 067201.
- [52] M. E. ZHITOMIRSKY K. UEDA, Phys. Rev. B **54** (1996) 9007.
- [53] G. BASKARAN P. W. ANDERSON, Phys. Rev. B **37** (1988) 580.
- [54] R. MELZI, P. CARETTA, A. LASCIALFARI, M. MAMBRINI, M. TROYER, P. MILLET, F. MILA, Phys. Rev. Lett **85** (2000) 1318.
- [55] R. MELZI, S. ALDROVANDI, F. TEDOLDI, P. CARRETTA, P. MILLET, F. MILA, Phys. Rev. B **64** (2001) 024409.
- [56] P. CARRETTA, N. PAPINUTTO, C. B. AZZONI, M. C. MOZZATI, E. PAVARINI, S. GONTHIER, O. MILLE, Phys. Rev. B **66** (2002) 094420.
- [57] E. E. KAUL, H. ROSNER, N. SHANNON, R. V. SHPANCHENKO, C. GEIBEL, J. Magn. Mater **272-276** (2004) 922.
- [58] M. STEINER, K. KAKURAI, J. K. KJEMS, D. PETITGRAND, R. PYNNE, J. Appl. Phys **61** (1987) 3953.
- [59] B. DORNER, D. VISSER, U. STEIGENBERGER, K. KAKURAI, M. STEINER, Z. Phys. B **72** (1988) 487.
- [60] J. P. RENARD, M. VERDAGUER, L. P. REGNAULT, W. A. C. ERKELENS, J. ROSSAT-MIGNOD, J. Appl. Phys **63** (1988) 3538.

- [61] M. ORENDÁČ, A. ORENDÁČOVÁ, J. ČERNÁK, A. F. P. J. G. SIGNORE, M. W. MEISEL, S. MERAH, M. VERDAGUER, *Phys. Rev. B* **52** (1995) 3435.
- [62] R. J. BIRGENEAU, J. S. JR, G. SHIRANE, *J. Appl. Phys* **41** (1970) 1303.
- [63] F. D. M. HALDANE, *Phys. Lett. A* **93** (1983) 464.
- [64] F. D. M. HALDANE, *Phys. Rev. Lett* **50** (1983) 1153.
- [65] S. NAKATSUJI, Y. NAMBU, H. TONOMURA, O. SAKAI, S. JONAS, C. BROHOLM, H. TSUNETSUGA, Y. M. QIU, Y. MAENO, *Science* **309** (2005) 1697.
- [66] H. TSUNETSUGU M. ARIKAWA, *J. Phys. Soc. Japan* **75** (2006) 083701.
- [67] S. BHATTACHARJEE, V. B. SHENOY, T. SENTHIL, *Phys. Rev. B* **74** (2006) 092406.
- [68] P. CHANDRA P. COLEMAN, *Phys. Rev. Lett* **66** (1991) 100.
- [69] Y. KAMIHARA, T. WATANABE, M. HIRANO, H. HOSONO, *J. Am. Chem. Soc* **130** (2008) 3296.
- [70] F. MA, Z.-Y. LU, T. XIANG, *Phys. Rev. B* **78** (2008) 224517.
- [71] Q. SI E. ABRAHAMS, arXiv:0804.2480v2 [cond-mat.mtrl-sci].
- [72] T. SENTHIL, A. VISHWANATH, L. BALENTS, S. SACHDEV, M. P. A. FISHER, *Science* **303** (2004) 1490.
- [73] T. SENTHIL, L. BALENTS, S. SACHDEV, A. VISHWANATH, M. P. A. FISHER, *Phys. Rev. B* **70** (2004) 144407.
- [74] B. S. SHASTRY B. SUTHERLAND, *Physica B* **108** (1981) 1069.
- [75] S. MIYAHARA K. UEDA, *Phys. Rev. Lett.* **82** (1999) 3701.
- [76] S. E. SEBASTIAN, N. HARRISON, P. SENGUPTA, C. D. BATISTA, S. FRANCOUAL, E. PALM, T. MURPHY, H. A. DABKOWSKA, B. D. GAULIN, arXiv:0707.2075v2 [cond-mat.str-el].
- [77] C. K. MAJUMDAR D. K. GOSH, *J. Math. Phys* **10** (1969) 1388.
- [78] J. SCHULENBURG, A. HONECKER, J. SCHNACK, J. RICHTER, H.-J. SCHMIDT, *Phys. Rev. Lett* **88** (2002) 167207.
- [79] J. RICHTER, J. SCHULENBURG, A. HONECKER, J. SCHNACK, H.-J. SCHMIDT, *J. Phys.: Condens. Matter* **16** (2004) 779.
- [80] F. COESTER, *Nucl. Phys* **7** (1958) 421.
- [81] F. COESTER H. KÜMMEL, *Nucl. Phys* **17** (1960) 477.
- [82] M. ROGER J. H. HETHERINGTON, *Phys. Rev. B* **44** (1990) 200.

- [83] R. F. BISHOP, J. B. PARKINSON, Y. XIAN, Phys. Rev. B **43** (1991) 13782.
- [84] R. F. BISHOP, J. B. PARKINSON, Y. XIAN, Phys. Rev. B **44** (1991) 9425.
- [85] R. F. BISHOP, R. G. HALE, Y. XIAN, Phys. Rev. Lett. **73** (1994) 3157.
- [86] R. BURSILL, G. A. GEHRING, D. J. J. FARNELL, J. B. PARKINSON, T. XIANG, C. ZENG, J. Phys. Condens. Matter **7** (1995) 8605.
- [87] R. F. BISHOP, D. J. J. FARNELL, J. B. PARKINSON, Phys. Rev. B **58** (1998) 6394.
- [88] C. ZENG, D. J. J. FARNELL, R. F. BISHOP, J. stat. Phys **90** (1998) 327.
- [89] R. F. BISHOP, D. J. J. FARNELL, S. KRÜGER, J. B. PARKINSON, J. RICHTER, C. ZENG, J. Phys. Condens. Matter **12** (2000) 6887.
- [90] N. B. IVANOV, J. RICHTER, D. J. J. FARNELL, Phys. Rev. B **66** (2002) 014421.
- [91] R. DARRADI, J. RICHTER, S. E. KRÜGER, J. Phys.: Condens. Matter **16** (2004) 2681.
- [92] D. J. J. FARNELL R. F. BISHOP. *Quantum magnetism in two dimensions: From semi-classical Néel order to magnetic disorder, in: U. Schollwöck, J. Richter, D. J. J. Farnell, R. F. Bishop, (Eds.) Quantum Magnetism, Lecture Notes in Physics, vol. 645.* Springer-Verlag, Berlin, 2004. pp 307.
- [93] R. DARRADI, J. RICHTER, D. FARNELL, Phys. Rev. B **72** (2005) 104425.
- [94] D. J. J. FARNELL, J. SCHULENBURG, J. RICHTER, K. A. GERNOETH, Phys. Rev. B **72** (2005) 172408.
- [95] S. E. KRÜGER, R. DARRADI, J. RICHTER, D. FARNELL, Phys. Rev. B **73** (2006) 094404.
- [96] R. F. BISHOP, Y. XIAN, C. ZENG, Int. J. Quantum Chem **55** (1995) 181.
- [97] R. F. BISHOP, Theor. Chim. Acta **80** (1991) 95.
- [98] D. J. J. FARNELL, R. F. BISHOP, K. A. GERNOETH, J. stat. Phys **108** (2002) 401.
- [99] K. EMRICH, Nucl. Phys. A **351** (1981) pages 379, 397.
- [100] J. BONCA, J. P. RODRIGUEZ, J. FERRER, K. S. BEDELL, Phys. Rev. B **50** (1994) 3415.
- [101] S. CHAKRAVARTY, B. I. HALPERIN, D. R. NELSON, Phys. Rev. B **39** (1989) 2344.
- [102] A. V. CHUBUKOV, S. SACHDEV, T. SENTHIL, J. Phys. Condens. Matte **6** (1994) 8891.
- [103] A. V. CHUBUKOV, S. SACHDEV, J. YE, Phys. Rev. B **49** (1994) 11919.
- [104] B. I. HALPERIN P. C. HOHENBERG, Phys. Rev. B **188** (1969) 898.

- [105] C. J. HAMER, Z. WEIHONG, J. OITMAA, Phys. Rev. B **50** (1994) 6877.
- [106] J. IGARASHI, Phys. Rev. B **46** (1992) 10763.
- [107] J. IGARASHI A. WATABE, Phys. Rev. B **44** (1991) 5057.
- [108] P. LECHEMINANT, B. BERNU, C. LHUILLIER, L. PIERRE, Phys. Rev. B **52** (1995) 9162.
- [109] M. RACZKOWSKI A. OLES, Phys. Rev. B **66** (2002) 094431.
- [110] R. R. P. SINGH D. A. HUSE, Phys. Rev. B **40** (1989) 7247.
- [111] R. F. BISHOP, P. H. Y. LI, R. DARRADI, J. RICHTER, J. Phys. Condens. Matter **20** (2008) 255251.
- [112] R. F. BISHOP, P. H. Y. LI, R. DARRADI, J. SCHULENBURG, J. RICHTER, Phys. Rev. B **78** (2008) 054412.
- [113] R. F. BISHOP, P. H. Y. LI, R. DARRADI, J. RICHTER, Europhys. Lett. **83** (2008) 47004.
- [114] R. F. BISHOP, P. H. Y. LI, R. DARRADI, J. RICHTER, C. E. CAMPBELL, J. Phys.: Condens. Matter **20** (2008) 415213.
- [115] R. DARRADI, O. DERZHKO, R. ZINKE, J. SCHULENBURG, S. KRÜGER, J. RICHTER, Phys. Rev. B **78** (2008) pages 214415–1–10.
- [116] For the numerical calculation we use the program package *CCCM* (D.J.J. Farnell and J. Schulenburg).
- [117] J. K. KIM M. TROYER, Phys. Rev. Lett **43** (1998) 2705.
- [118] M. S. MAKIVIC H. Q. DING, Phys. Rev. B **43** (1991) 3562.
- [119] N. B. IVANOV, S. E. KRÜGER, J. RICHTER, Phys. Rev. B **53** (1996) 2633.
- [120] M. MATSUMOTO, C. YASUDA, S. TODO, H. TAKAYAMA, Phys. Rev. B **66** (2001) 014407.
- [121] P. TOMCZAK J. RICHTER, J. Phys. A: Math. Gen. **34** (2001) L461.
- [122] S. WENZEL, L. BOGACZ, W. JANKE, Phys. Rev. Lett. **101** (2008) 127202.
- [123] D. YOSHIOKA, G. ARAKAWA, I. ICHINOSE, T. MATSUI, Phys. Rev. B **70** (2004) 174407.
- [124] M. MATSUMOTO, S. TODO, C. YASUDA, H. TAKAYAMA, arXiv: 0310619 [cond-mat.supr-con].
- [125] J. RICHTER, S. E. KRÜGER, N. B. IVANOV, Physica B **230-232** (1997) 1028.
- [126] P. HASENFRATZ F. NIEDERMAYER, Z. Phys. B **92** (1993) 91.

- [127] H. NEUBERGER T. ZIMAN, Phys. Rev. B **39** (1989) 2608.
- [128] J. OITMAA, C. J. HAMER, W. ZHENG, Phys. Rev. B **50** (1994) 3877.
- [129] A. W. SANDVIK, Phys. Rev. B **56** (1997) 11678.
- [130] J. RICHTER, J. SCHULENBURG, A. HONECKER, D. SCHMALFUSS, Phys. Rev. B **70** (2004) 174454.
- [131] C. J. HAMER, W. H. ZHENG, P. ARNDT, Phys. Rev. B **46** (1992) 6276.
- [132] D. J. J. FARNELL, K. A. GERNOETH, R. F. BISHOP, Phys. Rev. B **64** (2001) 172409.
- [133] M. ALBRECHT F. MILA, Europhys. Lett. **34** (1996) 145.
- [134] A. LÄUCHLI, S. WESSEL, M. SIGRIST, Phys. Rev. B **65** (2001) 014408.
- [135] E. MÜLLER HARTMANN R. SINGH, Phys. Rev. Lett. **84** (2000) 1808.
- [136] Z. WEIHONG, C. J. HAMER, J. OITMAA, Phys. Rev. B **60** (1999) 6608.
- [137] Z. WEIHONG, J. OITMAA, C. J. HAMER, Phys. Rev. B **65** (2001) 014408.
- [138] M. A. HAJII, N. GUIHERY, J. P. MALRIEU, B. BOUQUILLON, Eur. Phys. J. B **41** (2004) 11.
- [139] C. H. CHUNG, J. B. MARSTON, S. SACHDEV, Phys. Rev. B **64** (2001) 134407.
- [140] S. MIYAHARA K. UEDA, J. Phys. Condens. Matter **15** (2003) R327.
- [141] N. B. IVANOV J. RICHTER, Phys. Lett. A **232** (1997) 308.
- [142] A. KOGA N. KAWAKAMI, Phys. Rev. B **65** (2002) 214415.
- [143] J. RICHTER, N. B. IVANOV, J. SCHULENBURG, J. Phys. Condens. Matter **10** (1998) 3635.
- [144] J. SCHULENBURG J. RICHTER, Phys. Rev. B **65** (2002) 054420.
- [145] K. UEDA S. MIYAHARA, J. Phys. Condens. Matter **11** (1999) L175.
- [146] E. SHENDER, Zh. Eksp. Teor. Fiz. **83** (1982) 326.
- [147] E. SHENDER, Sov. Phys. JET **56** (1982) 178.
- [148] J. VILLAIN, R. BIDAUX, J. P. CARTON, R. CONTE, J. Phys. **41** (1980) 1263.
- [149] Y. XIAN, J. Phys. Condens. Matter **6** (1994) 5965.
- [150] M. MAKIVIC H. DING, Phys. Rev. B **43** (1991) 3562.
- [151] L. O. MANUEL, A. E. TRUMPER, H. A. CECATTO, Phys. Rev. B **57** (1998) 8358.
- [152] L. SPANU A. PAROLA, Phys. Rev. B **72** (2005) 174418.

- [153] A. AUERBACH D. P. AROVAS, Phys. Rev. Lett **61** (1988) 617.
- [154] S. J. MIYAKE, J. Phys. Soc. Jpn **61** (1992) 983.
- [155] L. CAPRIOTTI, A. E. TRUMPER, S. SORELLA, Phys. Rev. Lett **82** (1999) 3899.
- [156] A. BOMBARDI, J. RODRIGUEZ-CARVAJAL, S. D. MATTEO, F. DE BERGEVIN, L. PAOLASINI, P. CARRETTA, P. MILLET, R. CACIUFFO, Phys. Rev. Lett **93** (2004) 027202.
- [157] P. CARRETTA, R. MELZI, N. PAPINUTTO, P. MILLET, Phys. Rev. Lett **88** (2002) 047601.
- [158] R. NATH, A. A. TSIRLIN, H. ROSNER, C. GEIBEL, Phys. Rev. B **78** (2008) 064422.
- [159] H. ROSNER, R. R. P. SINGH, Z. WEIHONG, J. OITMAA, S.-L. DRECHSLER, W. PICKET, Phys. Rev. Lett **88** (2002) 186405.
- [160] T. YILDIRIM, Phys. Rev. Lett **101** (2007) 057010.
- [161] R. KUMAR B. KUMAR, Phys. Rev. B **77** (2008) 144413.
- [162] A. GELLÉ, A. M. LÄUCHLI, B. KUMAR, F. MILA, Phys. Rev. B **77** (2008) 014419.
- [163] A. W. SANDVIK, Phys. Rev. Lett **98** (2007) 227202.
- [164] A. B. KUKLOV, M. MATSUMOTO, N. V. PROKOF'EV, B. V. SVISTUNOV, M. TROYER, arXiv:0805.4334v1 [cond-mat.stat-mech].
- [165] F. ALET, G. MISGUICH, V. PASQUIER, R. MOESSNER, J. L. JACOBSEN, Phys. Rev. Lett **97** (2006) 030403.
- [166] S. POWELL J. T. CHALKER, Phys. Rev. Lett **101** (2008) 155702.
- [167] R. SCHMIDT, J. SCHULENBURG, J. RICHTER, D. D. BETTS, Phys. Rev. B **66** (2002) 224406.
- [168] J. OITMAA Z. WEIHONG, Phys. Rev. B **69** (2004) 064416.
- [169] A. A. NERSESYAN A. M. TSVELIK, Phys. Rev. B **67** (2003) 024422.
- [170] P. SINDZINGRE, Phys. Rev. B **69** (2004) 094418.
- [171] O. A. STARYKH L. BALENTS, Phys. Rev. Lett **93** (2004) 127202.
- [172] S. MOUKOURI, J. Stat. Mech (2006) P02002.
- [173] J. R. VIANA J. R. DE SOUSA, Phys. Rev. B **75** (2007) 052403.
- [174] R. GUIDA J. ZINN-JUSTIN, J. Phys. A **31** (1998) 8103.
- [175] A. E. TRUMPER, L. O. MANUEL, C. J. GAZZA, H. A. CECCATTO, Phys. Rev. Lett **78** (1997) 2216.

- 
- [176] D. U. SCHOLLWÖCK , J. RICHTER R. F. BISHOP. *Quantum Magnetism*. Springer-Verlag, Berlin, 2004.
- [177] B. CANALS C. LACROIX, Phys. Rev. Lett **80** (1998) 2933.
- [178] D. SCHMALFUSS, J. RICHTER, D. IHLE, Phys. Rev. B **70** (2004) 184412.
- [179] S. MOUKOURI, Phys. Lett **A352** (2006) 256.
- [180] A. BENYOUSSEF, A. BOUBEKRI, H. EZ-ZAHRAOUI, Phys. Lett. A **238** (1998) 398.

# Lebenslauf

Darradi Rachid  
Breiter Weg 259  
39104 Magdeburg

## Persönliche Angaben

Geburtsdatum: 25.11.1970  
Geburtsort: Khouribga (Marokko)  
Familienstand: Verheiratet seit 2001, ein Sohn, eine Tochter  
Staatsangehörigkeit: Marokko

## Bildungsweg

06/1992: Abitur an der Schule Ibn Abdoune (Khouribga) mit einer Spezialisierung in Mathematik und Naturwissenschaften  
09/1993–06/1999: Studium der Physik an der staatlichen Kharkov Universität  
Abschluß Diplom "Kernphysik und Plasmaphysik",  
Note: mit Auszeichnung  
03/2002–12/2008: Promotion an der Otto-von-Guericke-Universität Magdeburg

## Berufliche Tätigkeit

09/1999–01/2001: Lehrer für Physik an einer privaten Schule in Casa-blanca (Marokko)  
04/2001–10/2001: wissenschaftlicher Mitarbeiter an der staatlichen Kharkov Universität für Luft- und Raumfahrt  
08/2004–12/2008: wissenschaftlicher Mitarbeiter am Institut für Theoretische Physik der Otto-von-Guericke-Universität Magdeburg in der Arbeitsgruppe "Theorie der kondensierten Materie II" von Prof. Dr. J. Richter